AD737787

SUN PUMPED LASER
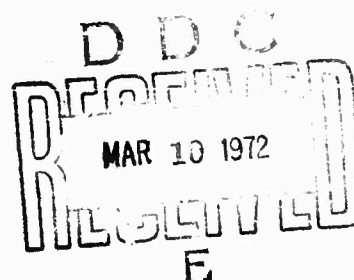
by

Lloyd Huff

GTE Sylvania, Inc.
Mountain View, California

FINAL TECHNICAL REPORT AFAL-TR-71-315

September 1971

D D C
MAR 10 1972
RECEIVED
E

Approved for Public Release; distribution unlimited

Air Force Avionics Laboratory
Air Force Systems Command
Wright Patterson Air Force Base, Ohio

NOTICE

When Government drawings, specifications, or other data are used for any purpose other than in connection with a definitely related Government procurement operation, the United States Government thereby incurs no responsibility nor any obligation whatsoever; and the fact that the government may have formulated, furnished, or in any way supplied the said drawings, specifications, or other data, is not to be regarded by implication or otherwise as in any manner licensing the holder or any other person or corporation, or conveying any rights or permission to manufacture, use, or sell any patented invention that may in any way be related thereto.

Copies of this report should not be returned unless return is required by security considerations, contractual obligations, or notice on a specific document.

DOCUMENT CONTROL DATA - R & D

(Security classification of title, body of abstract and indexing annotation must be entered when the overall report is classified)

1 ORIGINATING ACTIVITY *(Corporate author)*	2a. REPORT SECURITY CLASSIFICATION
GTE Sylvania Inc. - Electronic Systems Group Western Division, Electro-Optics Organization Mountain View, California 94040	2b. GROUP

3 REPORT TITLE

SUN PUMPED LASER

4 DESCRIPTIVE NOTES *(Type of report and inclusive dates)*

Final Report January 1, 1970 to September 1, 1971

5 AUTHOR(S) *(First name, middle initial, last name)*

Lloyd Huff

6 REPORT DATE	7a. TOTAL NO. OF PAGES	7b. NO. OF REFS
September 1, 1971	144	

8a. CONTRACT OR GRANT NO. F33615-70-C-1255	9a. ORIGINATOR'S REPORT NUMBER(S)
b. PROJECT NO 5244	
c.	9b. OTHER REPORT NO(S) *(Any other numbers that may be assigned this report)* AFAL-TR-71-315
d.	

10 DISTRIBUTION STATEMENT

Approved for Public Release; distribution unlimited

11 SUPPLEMENTARY NOTES	12. SPONSORING MILITARY ACTIVITY
	AF Avionics Laboratory (AVTL) Wright-Patterson AFB, Ohio 45433

13 ABSTRACT

Results of an experimental program to determine the practicality of solar pumping a spaceborne optical communication laser are described. A feasibility model sun pumped Nd:YAG laser utilizing techniques compatible with space operation was built and successfully operated. Using a 24" diameter sun collecting mirror and an optical system which rejected the sun's IR radiation a power output of 1.6 watts was obtained from the laser. Without the IR filting (which also rejected some useful pump light) an output power of 1.2 watts was achieved with half of the telescope aperture area. Mode locked operation of the device at a rate of 500 MHz was also demonstrated. Based on sun pumped laser performance achieved during the program it is projected that a laser output power of 1.6 watts can be obtained outside the earth's atmosphere with a 12" diameter mirror.

DD FORM 1473 (1 NOV 65)

14 KEY WORDS	LINK A		LINK B		LINK C	
	ROLE	WT	ROLE	WT	ROLE	WT
Laser, sun, space communications, conductive laser cooling						

SUN PUMPED LASER

by

Lloyd Huff
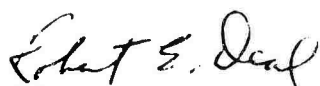
FOREWORD

This Final Technical Report on the "Sun Pumped Laser" was prepared by GTE Sylvania, Inc., Electronic Systems Group - Western Division, Mountain View, California, under contract No. F33615-70-C-1255 for the Air Force Avionics Laboratory, Wright-Patterson Air Force Base, Ohio. Mr. Donald D. Matulka was the program monitor. This study covered the period January 1970 to August 1971 and the report was submitted September 1971.

Dr. L. Huff was the project engineer for the program. Other principal contributors to the program were Dr. J. D. Foster, Mr. R. F. Kirk, Dr. L. M. Osterink and Mr. C. B. Hitz.

This report has been reviewed and is approved for publication.

ROBERT E. DEAL, Actg Chief
Laser and Electro-Optics Technology Branch
Electronic Technology Division

ABSTRACT

Results of an experimental program to determine the practicality
of solar pumping a spaceborne optical communication laser are described.
A feasibility model sun pumped Nd:YAG laser utilizing techniques compatible
with space operation was built and successfully operated. Using a 24" diameter
sun collecting mirror and an optical system which rejected the sun's IR radia-
tion a power output of 1.6 watts was obtained from the laser. Without the IR
filtering (which also rejected some useful pump light) an output power of 1.2
watts was achieved with half of the telescope aperture area. Mode locked opera-
tion of the device at a rate of 500 MHz was also demonstrated. Based on sun
pumped laser performance achieved during the program it is projected that a
laser output power of 1.6 watts can be obtained outside the earth's atmosphere
with a 12" diameter mirror.

TABLE OF CONTENTS

LIST OF ILLUSTRATIONS

LIST OF TABLES

Section I

INTRODUCTION

Optical communication in space using the Nd:YAG laser as a source has several advantages over conventional millimeter wave links. Higher data rates are possible with a mode-locked laser in a PCM system, improved communication link security is possible with reasonably small optics and smaller, lighter weight transmission and reception equipment is required by an optical link. The lifetimes of conventional optical sources which may be used to power the laser (lamps or light emitting diodes) are not as yet sufficient to meet the needs of space use, however. Solar pumping is a very attractive alternative means of operating a solid state laser employed in a space optical communication system because of the long lifetimes possible. Ruby, glass, and Nd:YAG lasers have all been powered by direct use of solar radiation[1-7]. None of this previous sun pumped laser work, however, has demonstrated that it is practical to utilize the concept in a spaceborne system.

The basic objective of the current sun pumped laser program has been to determine the practicality of applying the concept in a space satellite optical communication system. In order to meet this objective, the primary portion of the program was to build and demonstrate a working feasibility model of a sun pumped laser using techniques compatible with spacecraft application. Operating characteristics of the laser were specified to be as representative as possible of actual device requirements envisioned for future space communication needs. The laser was specified to operate mode locked at a pulse rate of 200 MHz or higher with a power output of 1 watt in a low order mode and with a pulse amplitude variation of less than 2.5%. There are three distinctive features of the approach selected to fulfill the objectives of the sun pumped laser program - a Coude optical relay system which separates sun tracking from laser pointing, end pumping of the laser rod, and exclusive use of conductive cooling techniques. A collection and relay system of the Coude type has advantages in terms of practical implementation of the concept on a satellite. Solar end pumping of the Nd:YAG laser rod was chosen for two reasons: (1) it should be more efficient than side pumping because of the longer crystal absorption length presented to the pump light and (2) it is compatible with conventional side pumping of the laser rod with a lamp or diode array during solar eclipse portions of the satellite orbit. The possibility of such a dual pumping scheme allows continuous operation of the communication system while still taking advantage of the long lifetime afforded by solar pumping. Direct conductive cooling of the laser rod and removal of the heat from the laser by conductive means (such as with heat pipes) is a must in a space craft application because of the complexity and low reliability of liquid cooling methods.

Successful operation of the feasibility laser, which employed end pumping and conductive cooling techniques, was realized. A multimode output power of 1.6 watts was obtained using the 24" diameter collector with dielectric filtering to reject the sun's IR radiation. Without the IR filtering (which also rejected some useful pump light) an output of 1.2 watts was achieved with just under one half the telescope collecting area. A mode locked laser output of 0.35 watts was demonstrated at a rate of 500 MHz. Stable mode-locked operation of the device in the fundamental mode was not realized;

1

however, the feasibility of using electrooptic techniques to mode lock the low gain sun pumped laser was demonstrated with the performance obtained. The significance of these results is the conclusive demonstration that it is feasible to end pump, conductively cool, and mode lock the sun pumped Nd:YAG laser in a configuration which is compatible with space operation. Furthermore, based on performance obtained during this program, it is projected that a sun pumped laser output power of 1.6 watts can be obtained outside the earth's atmosphere with a 12" diameter collector.

Sections II and III of this report describe the design of the solar collection and relay system and the laser. Experimental results of the program are presented and discussed in Sections IV and V. A prediction of laser performance attainable outside the earth's atmosphere is derived in Section VI and a discussion of how the performance of the laser can be improved is presented in Section VII. Detailed consideration to the design of and difficulties associated with two end pumping condigurations is given in Appendices I and II. Mode locking the sun pumped laser is thoroughly discussed in Appendix III and a theoretical model of the CW Nd:YAG laser is presented in Appendix IV.

Section II

SOLAR COLLECTION AND RELAY SYSTEM

Figures 1 and 2 show schematically the Coude optical collection and relay system which was designed to separate the sun tracking and laser p inting functions. This system bends the light path from the telescope mirror to the laser in such a manner that the beam entering the laser remains fixed as the mirror tracks the sun. A 24" diameter sun collecting telescope used in previous sun pumped laser studies was provided to GTE Sylvania by the Air Force to perform this program. Unfortunately it turned out not to be practical to make the modifications to the telescope necessary to implement the Coude system. Instead the simpler scheme shown in Figure 3 was designed and built. This is a Cassegranian system which produces a final solar image at the entrance of a light concentrating trumpet. The trumpet reduces the solar image and channels the light into the end of the laser rod.

A description of the elements of the optical system and their positions with respect to the primary mirror are given in Table I. Both the secondary mirror and the toroidal mirror were deposited with evaporated silver and a dielectric overcoating. The reflectivity of these mirrors was greater than 97% above 0.5μ. The aluminized primary, which was not recoated, had a measured reflectivity of 88% at 6328Å. The field lens was antireflection coated with single layer MgF. The coating was designed to reflect the U.V. and to have greater than 90% transmission from 0.4μ to 0.7μ and greater than 98% transmission from 0.7μ to 0.9μ. The secondary mirror forms a virtual image of the primary at a position 3.16" behind the secondary. The field lens, located 21" from the secondary, forms a real image of the primary at the position of the toroidal mirror, 19" from the lens. The object for the field lens is the virtual image of the primary formed by the secondary mirror. The toroidal mirror bends the light path $90°$ and forms the final solar image at a distance of 4.7" from the toroid. The off axis toroidal mirror was used to make the $90°$ bend instead of a plane mirror followed by a lens since it was felt that the spherical and chromatic abberations of the lens would be excessive. The toroid was observed, however, to display rather severe coma; the solar images formed by different portions of the mirror occurred at different spatial positions. Because a distinct solar image was not formed by the mirror, the trumpet could not be placed to accept all the incoming rays. The mirror was expected to have a certain amount of coma, since this element should be a section of an ellipsoid rather than a torus. Laser experiments were performed both with the toroidal mirror and with this mirror replaced by a 100 mm focal length plano-convex lens which was antireflection coated. The coating was single layer MgF centered at 7000Å. In spite of the abberations of this lens a more distinct solar image resulted than was obtained with the toroid. The performance of the laser was improved by about 10% with the use of the lens. In addition, because of the physical position of the laser, it was more convenient to operate the laser in the absence of the $90°$ bend of the light path.

3

COLLECTOR PRIMARY

ELEVATION DRIVE ± 23°

SUN

SECONDARY

MIRROR A

MIRROR B
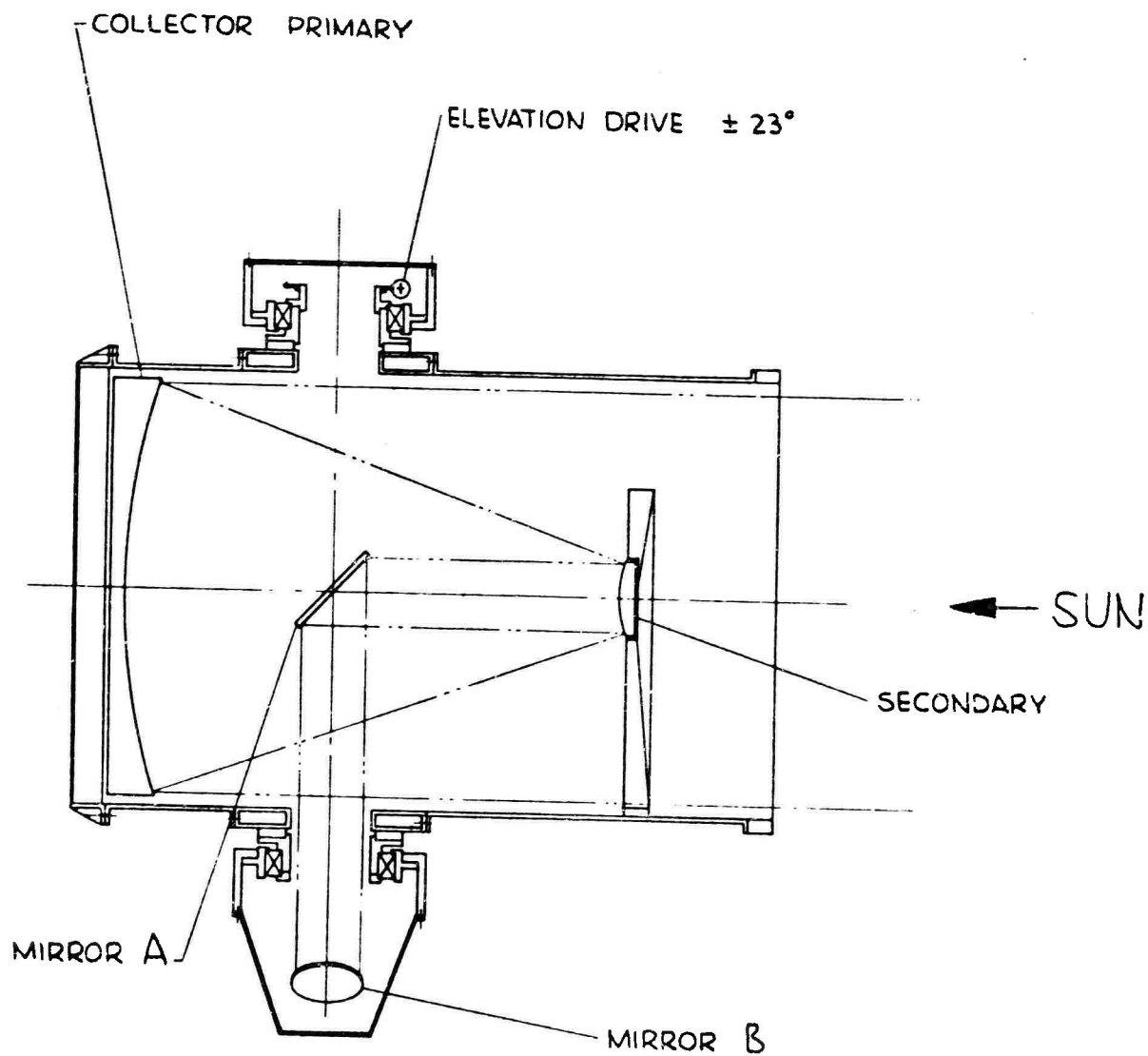
Figure 1   Sun Pumped Laser Collection System Design

4

MIRROR B

YOKE

MIRROR C

AZIMUTH DRIVE 360°

MIRROR D (OFF AXIS TOROIDAL MIRROR)

LASER MIRROR

CONE FRUSTUM 'TRUMPET' LIGHT CONCENTRATOR

LASER - SPACE QUALIFIED

MODULATOR AND POLARIZER

LASER MIRROR

HEAT PIPE
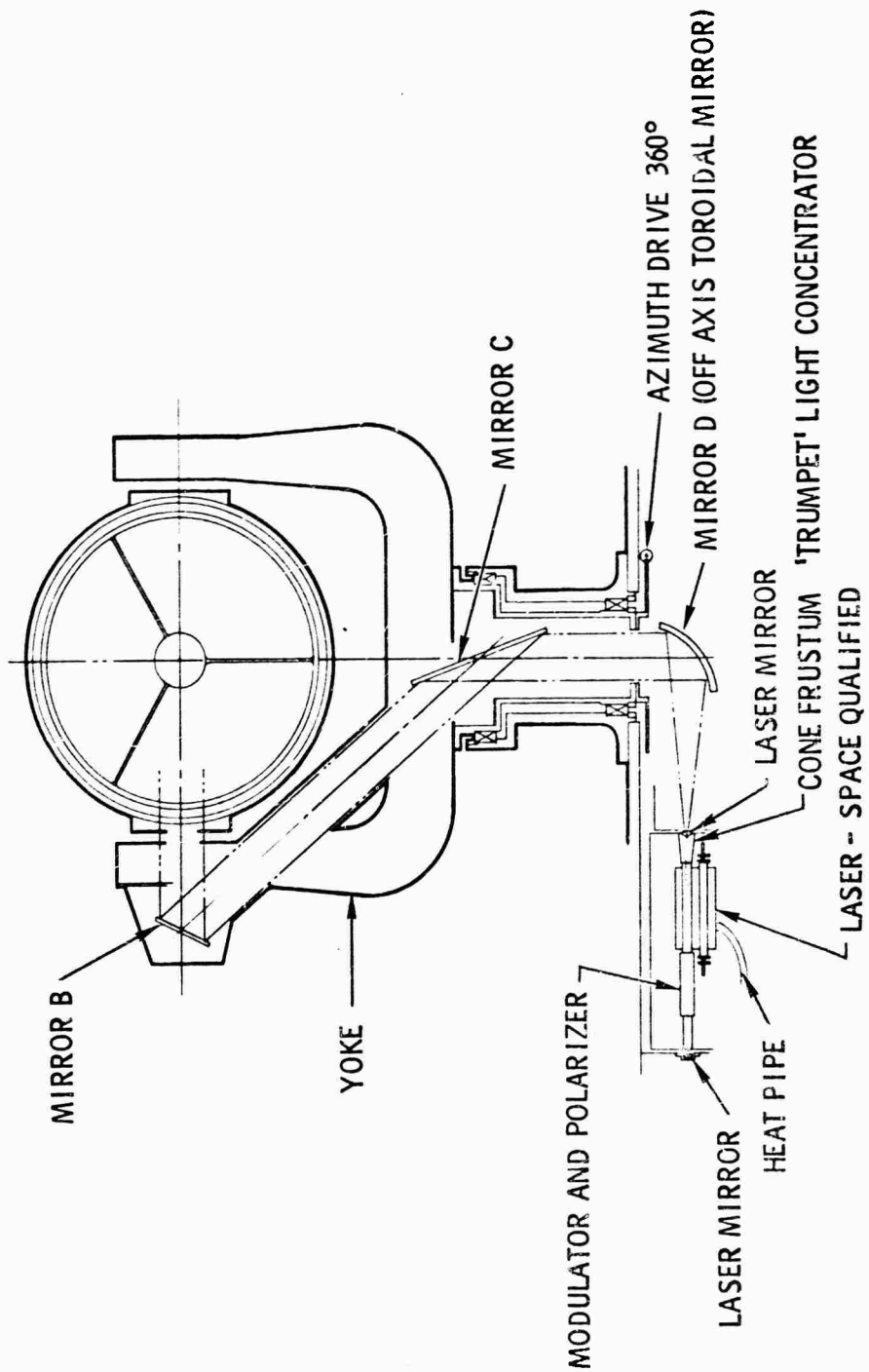
Figure 2. Sun Pumped Laser Design Employing Coude Optical Relay System

5

SOLAR COLLECTION AND RELAY OPTICS
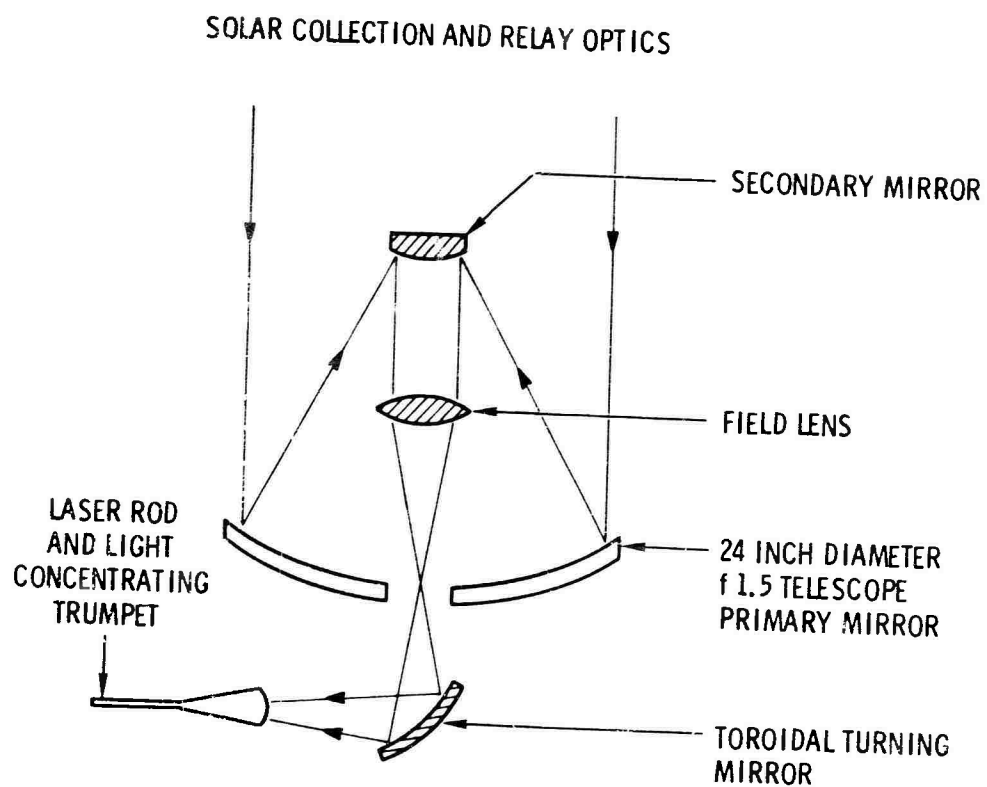
Figure 3   Solar Collection and Relay Optics

Table I

Collection System Elements and Positions

Element	Description	Position
Primary Mirror	24" diameter paraboloid Focal length – 35.4"	
Secondary Mirror	3" 1dameter Focal length = -3.51"	33" from primary
Field Lens	3" diameter Quartz Focal length = 10.6" Antireflection Coated	12" from primary
Toroidal Mirror	3.3" diameter Normal plane radius of curvature – 5.211". Meridial plane radius of curvature – 10.424". On axis focal length –3.7"	7" from primary

The laser was operated with two types of secondary mirrors: the silver coated mirror and one deposited with a dielectric or "cold mirror" coating designed to reject the I.R. radiation. Since a substantial portion of the solar energy is in spectral regions where the laser rod is not pumped, especially above 0.9μ, filtering to reject the non useful light can reduce the amount of heat which must be dissipated by the rod cooling structure without decreasing the laser output. The cold mirror secondary was designed to perform this function by reflecting the sunlight in the pumping spectral regions and transmitting or rejecting the light outside these regions. Figure 4 shows the transmission of the cold mirror coating as a function of wavelength. The coating has a high reflectivity in the region of the primary Nd:YAG pump bands from 0.6μ to 0.85μ and transmits most of the energy above one micron. Unfortunately the coating also transmits or rejects a substantial portion of the sun energy below 0.6μ. This is a disadvantage because the chromium pumping bands of the Nd:Cr:YAG rod used in the sun pumped laser are strongly absorbing from 0.35μ to .7μ (see Figure 14). In addition the sun energy peaks at a wavelength of 0.5μ (Figure 5). This particular mirror thus rejects a significant amount of useful pump light in the laser rod co-doped with chromium. The silver coated mirror reflects or accepts all the useful pump light in the solar spectrum; however, the rod cooling system must dissipate the additional unwanted energy and as a result the rod operates at a higher temperature. A more desirable filter would, of course, be one which rejects everything above 0.85μ and below 0.3μ and passes the energy which lies in between. In principle such filtering could be effected with one or more elements; however, it was not practical to pursue this on this program; the cold mirror coating obtained was available as a fairly standard item.

An important consideration in the use of dielectric filtering with the secondary mirror is the reflectivity characteristics of the mirror as a function of incident angle. Since the light collected by the primary is incident on the secondary over a range of angles $(0 - 30^{\circ})$ it is important that the high reflectivity band of the mirror not shift or change reflectivity appreciably with angle. The transmission of a reference sample coated with the secondary mirror was measured as a function of wavelength for several different angles of incidence. The spectra, shown in Figures 6 through 9 show that, indeed, the reflectivity characteristics do not appreciably change over the range of incident angle corresponding to the optical system.

An attempt was made to determine the efficiency of the collection and relay system by measuring the solar power transmitted by the optical system (at the output of the toroid) and the power incident on a 0.5" aperture using a CRL Model 201 calorimetric type power meter. An incident solar intensity at midday of 0.087 watts/cm^2 was measured in this manner. The fraction of sunlight that is transmitted through the atmosphere on a clear day with the sun at the zenith is given by Threlkeld[8] to be 0.633. This atmospheric transmission factor is defined as the integrated solar intensity at sea level divided by the integrated solar intensity just outside the earth's atmosphere. The solar constant[8] (solar radiation intensity incident upon a surface normal to the sun's rays and at the outer limit of the atmosphere) is 444.7 Btu·hr^{-1}· ft^{-2} or 0.139 watts·cm^{-2}. Multiplying the solar constant by the atmospheric transmission factor gives a sea-level solar intensity of 0.088 watts/cm^2 which agrees well with our measured result. All of the sunlight transmitted by the optical system could not be collected by the power meter detector head;

8
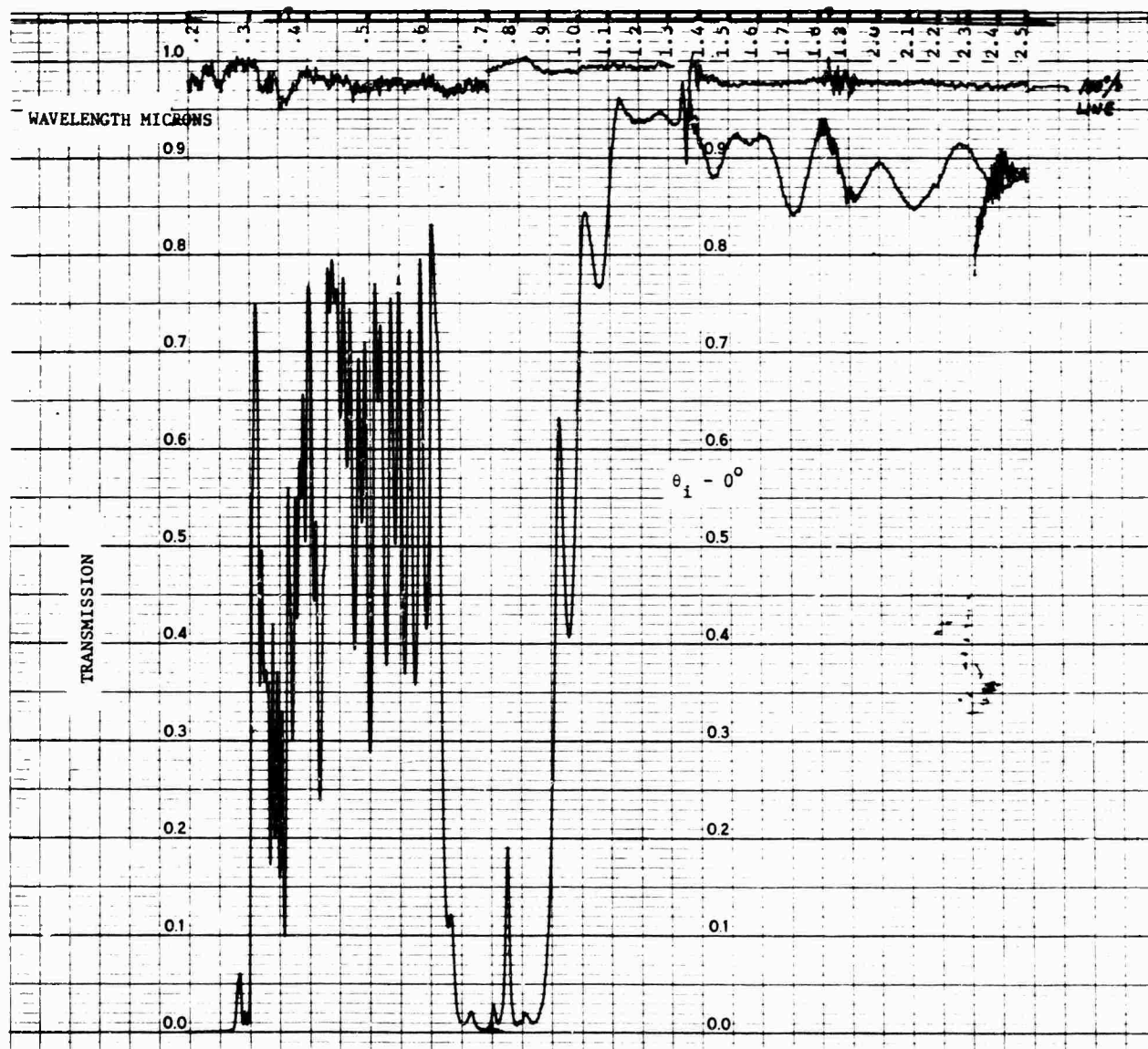
Figure 4   Transmission Spectrum of the Cold Mirror Dielectric
Coating from 0.2 to 2.5 microns

Figure 5   Spectral Distribution of Solar Radiation Outside the Earth's Atmosphere
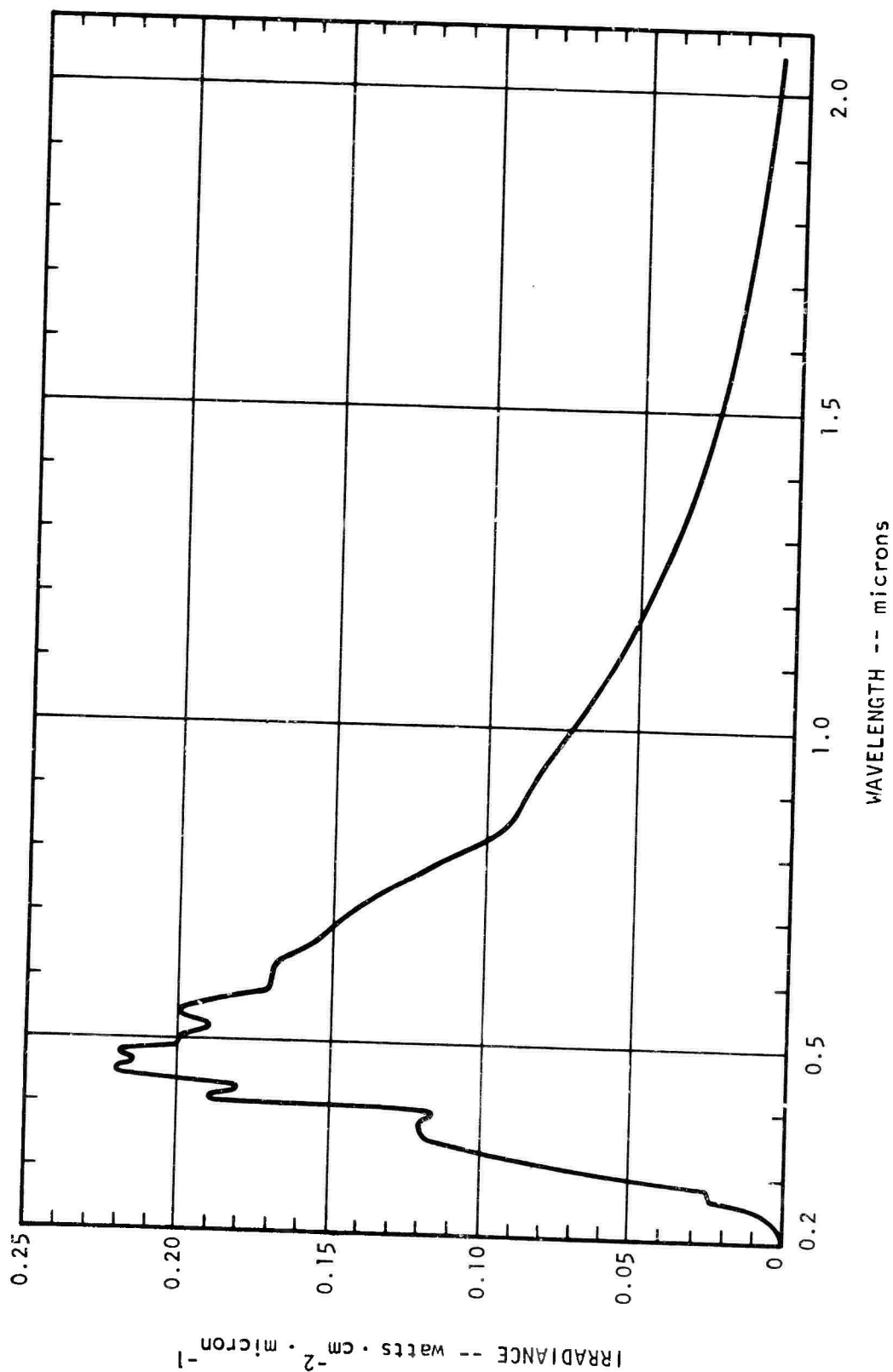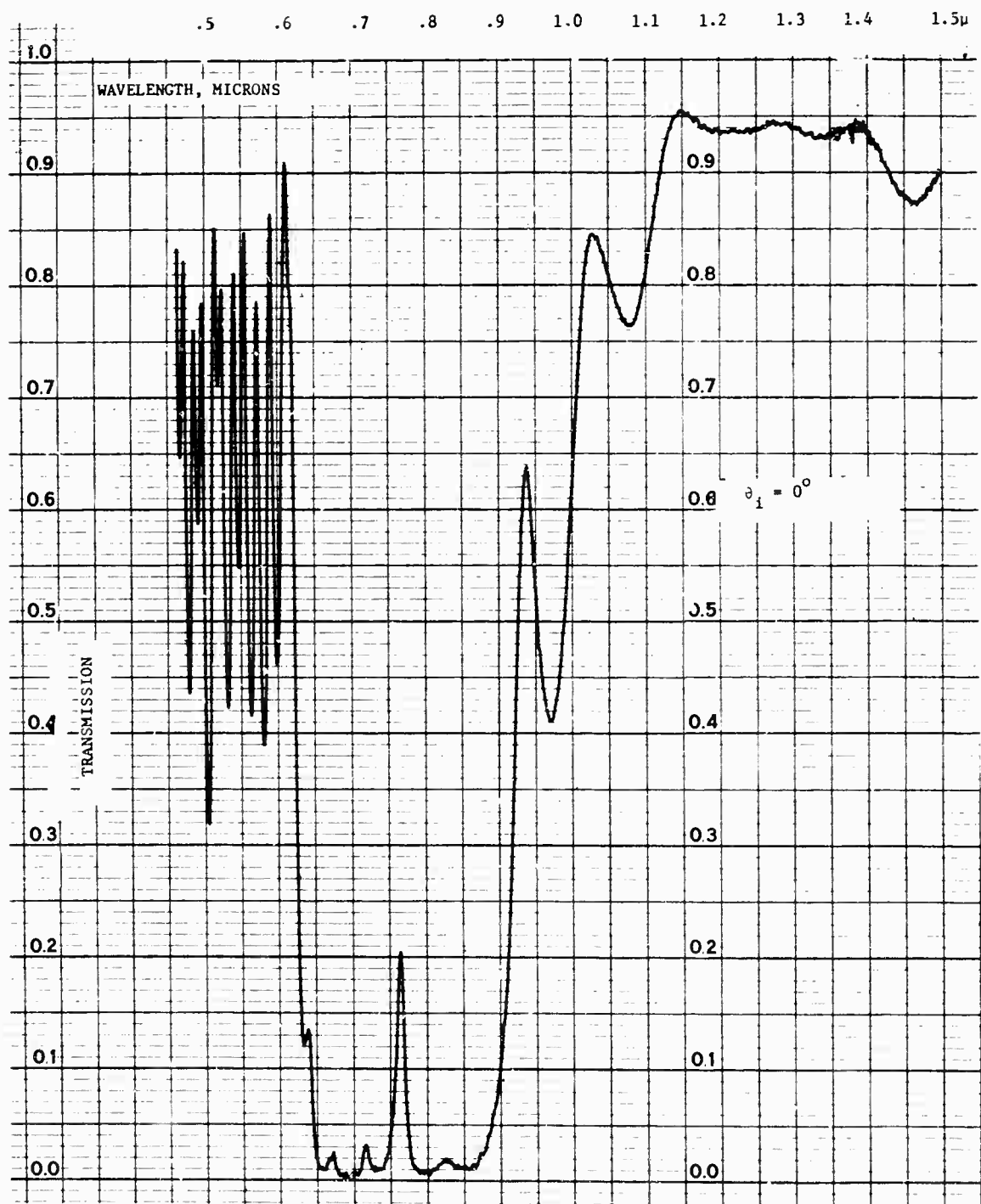
Figure 6   Transmission Spectrum of Cold Mirror Coating $\theta_i - 0^o$
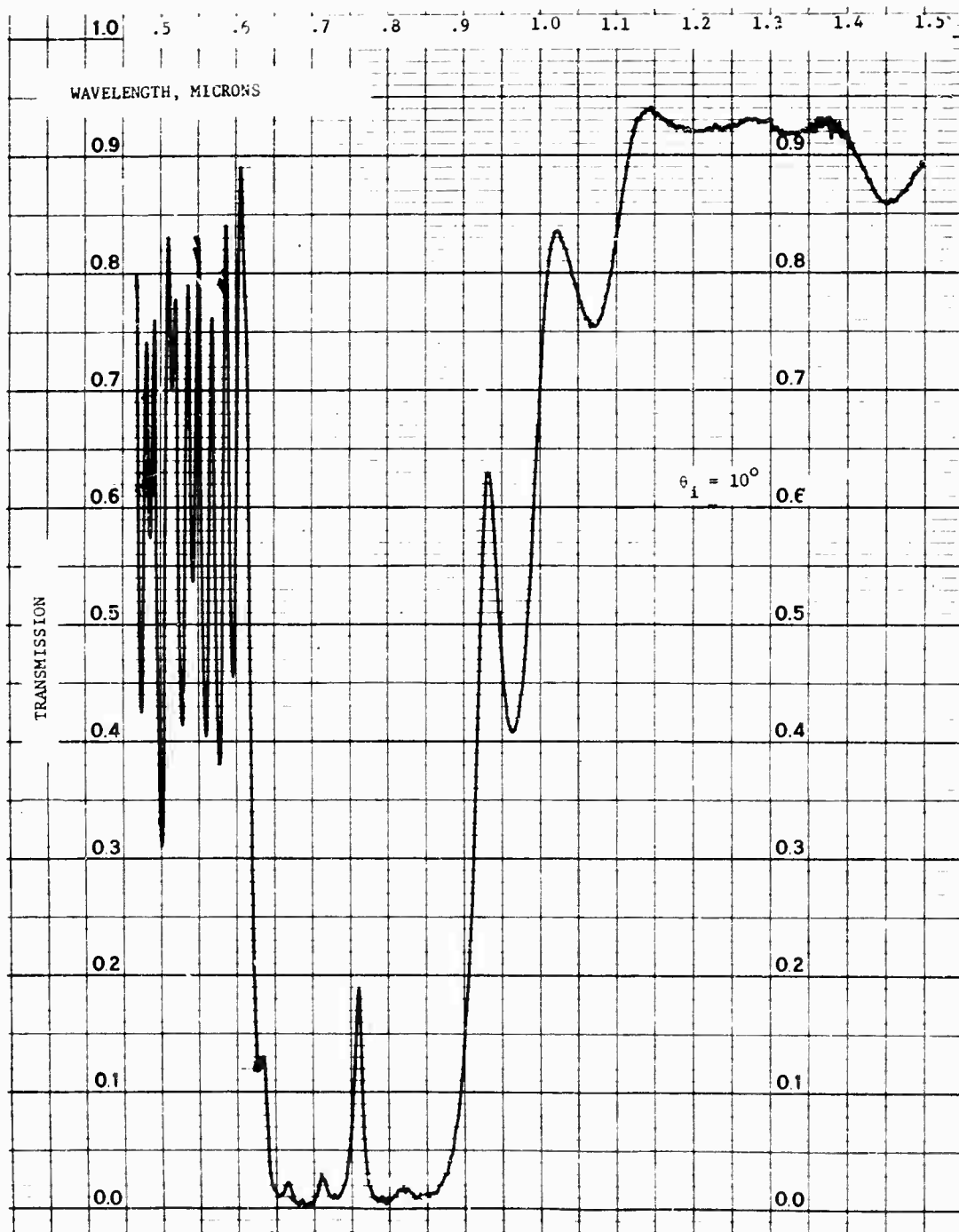
Figure 7   Transmission Spectrum of Cold Mirror Coating, $\theta_i = 10^o$
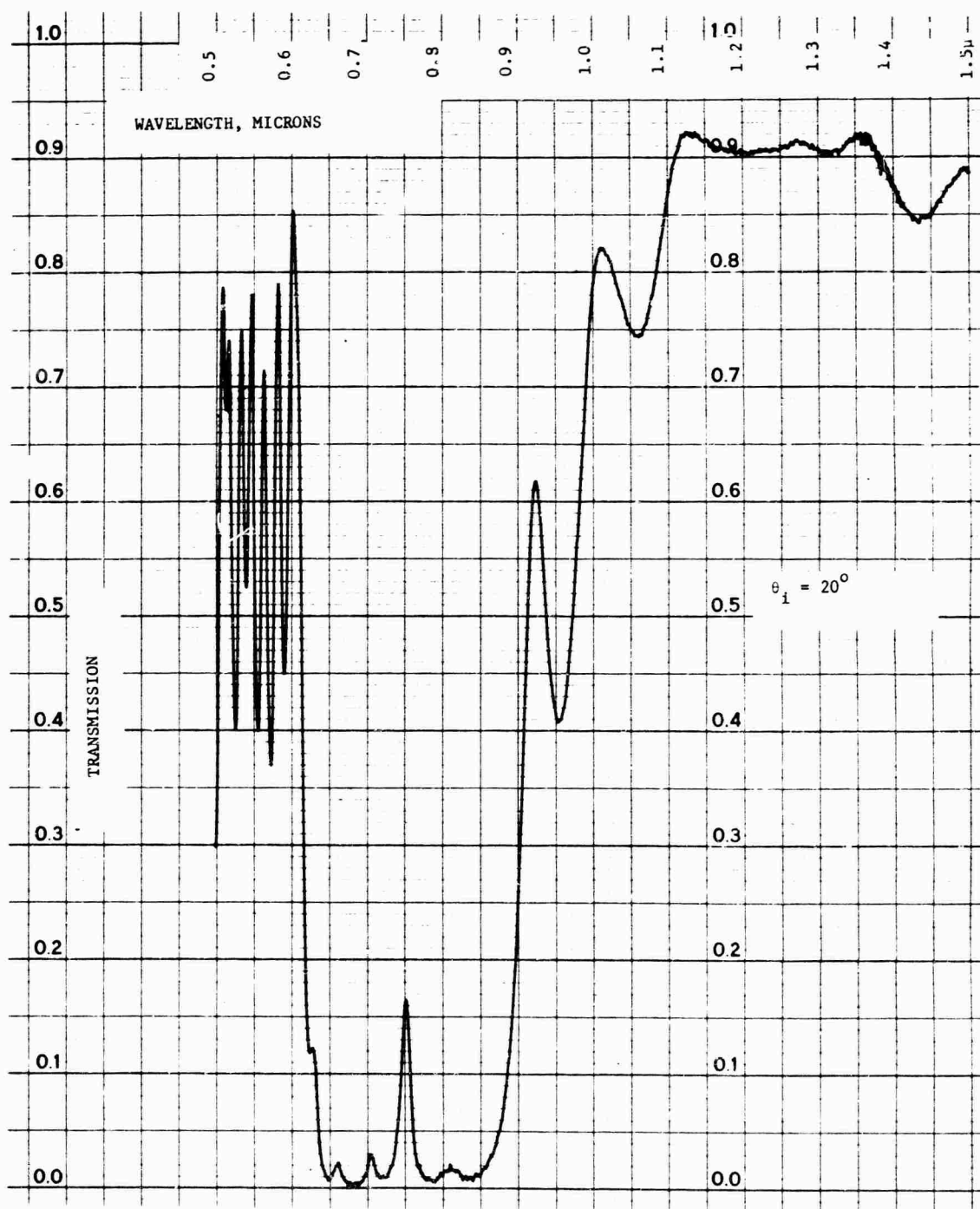
Transmission Spectrum of Cold Mirror Coating $\theta_i = 20^o$
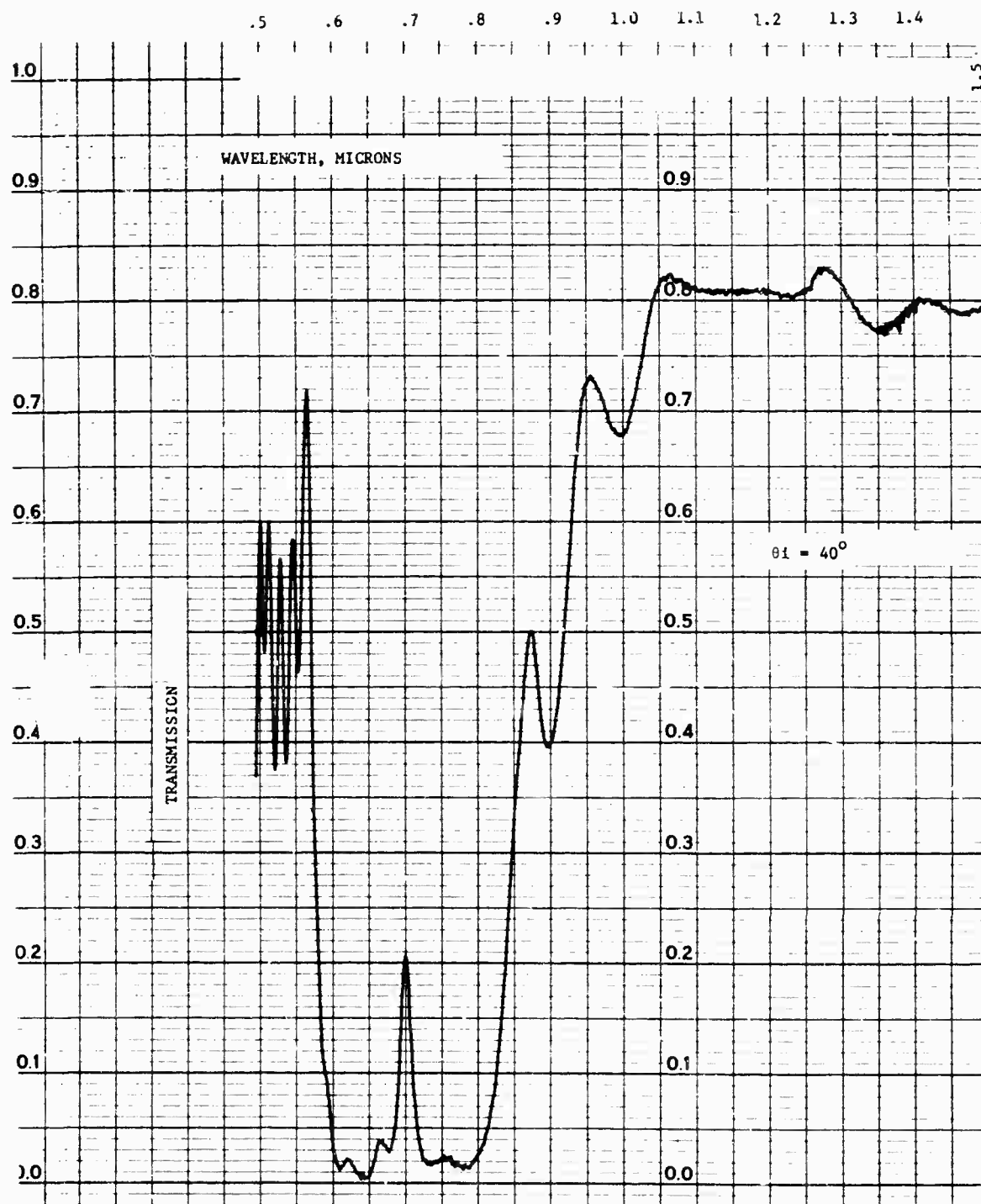
Figure 9   Transmission Spectrum of Cold Mirror Coating, $\theta_i = 40^\circ$

14

therefore, it was not possible to directly measure the efficiency of the system. It was determined from these measurements, however, that the full spectrum reflectivity of the cold mirror secondary was about 45%, i.e., 45% of the total solar energy incident on the mirror was reflected. An estimate of the collection efficiency is readily obtained by multiplying the reflec- tivities and transmission of the various elements. The approximate average values over the solar spectral range are:

Primary mirror	–	R = .88
Secondary mirror	–	R = .98
Toroidal mirror	–	R = .98
Field Lens	–	T = .95

These values result in a collection and relay efficiency of $\sim$ 60%. Therefore, the optical system with the full aperture of the 24" diameter mirror trans- mits $\sim$ 200 watts with the silver secondary and $\sim$ 115 watts with the cold mirror secondary. These numbers should be reduced by 9% to account for the central obscuration of the secondary mirror and mount.

A summary of useful solar data ia present in Table II. Spectra of the sun's radiation[8] outside the earth's atmosphere and at sea level and a clear day, are shown in Figure 10. The sea level spectra are for a precipit- able water depth of 30 mm and a dust scale of 400 (moderately dusty atmosphere) and for air mass values of 1 and 5. The air mass is the ratio of the length of the path of the sun's rays through the atmosphere to the length of the path if the sun were at the zenith. Figure 10 is reproduced from Threlkeld's book.
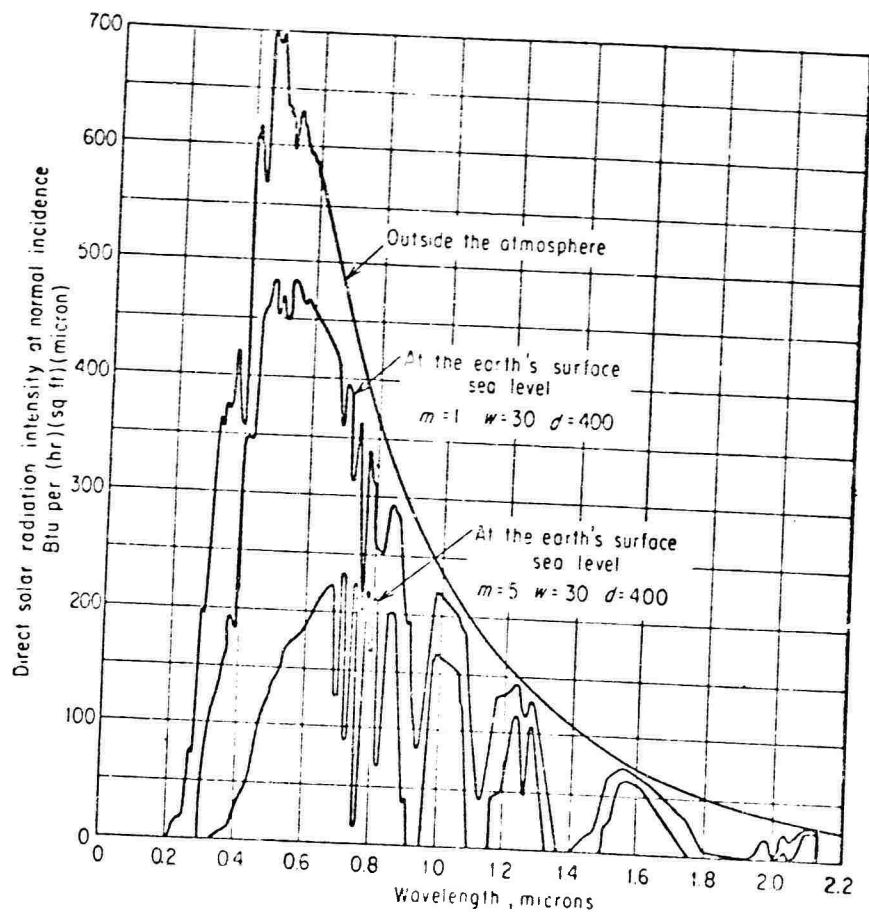
Figure 10 Spectral Distribution of Direct Solar Radiation Outside
the Earth's Atmosphere and at Sea Level

Table II

Summary of Useful Solar Quantities

1.	Solar intensity at the outer limit of the earth's atmosphere (solar constant)	— 0.139 watts/cm^2
2.	Solar power collected by a 24" diameter mirror at the outer limit of the earth's atmosphere	— 406 watts
3.	Atmospheric transmission factor at sea level with sun at the zenith on a clear day	— 0.633
4.	Fraction of solar energy above 1μ	— 27%
	Fraction of solar energy below .4μ	— 13%
5.	Distance of sun from the earth	— 9.29 x 10^7 miles
	Diameter of the sun	— 8.64 x 10^5 miles
	Angular subtense of the sun	— 9 mrad ∿0.5°

Section III

SUN PUMPED LASER DESIGN

1. END PUMPING OPTICS

Two end pumping configurations were investigated during the course of the program, one using an undoped YAG concentrating cone and another using an open silver reflective cone. The original sun pumped laser design which utilized the YAG trumpet is shown schematically in Figure 11. Sunlight enters the large end of the trumpet and is channeled into the end of the laser rod through total internal reflection at the YAG cone air interface. The 2 mm x 50 mm laser rod is held in a niobium heat sink which removes the heat from the rod by direct conduction. The optical resonator is formed by a totally reflecting laser mirror deposited on the central 5 mm dia. of the large end of the YAG trumpet and by an external output mirror. The mode locking modulator is inserted in the cavity near the output end.

The YAG trumpet approach has two advantages over the open air reflective cone. First, there is no reflective loss in the cone; there is only scattering loss which may be much smaller than the reflective loss at a silvered surface. Secondly, because of the sine condition[9] the image size reduction power of the YAG cone is 1.82 (the refractive index of YAG) times greater than that of the open air cone. This means that for a given telescope aperture diameter a laser rod with a smaller diameter can be used with the YAG cone. A smaller laser rod gives higher gain for equivalent pumping levels[10] and is more easily filled with the fundamental mode.[11] Making the gain as large as possible is important in low power lasers where intracavity losses seriously degrade the laser output.[10]

The main difficulty with the YAG cone is in making the optical-mechanical connection to the YAG rod. Several techniques for doing this including optical contacting, grown junction, diffusion, and clear epoxy were considered. Optical contacting was rejected as being mechanically impractical. The growth of a single YAG boule with one end doped and the other undoped is feasible according to crystal vendors; however, it has never been done and a considerable crystal growth development effort was required to pursue this technique. Efforts were made to obtain samples of fused clear and doped YAG plates; however, the vendor (Airtron) was never successful at producing these. The opinion of all the crystal vendors contacted was that it is not possible to obtain a good optical junction between two pieces of YAG by fusion. The method which was decided upon was to bond the YAG trumpet to the rod at Brewster's angle using a clear epoxy. The laser beam undergoes a very low loss at the Brewster junction. Incident sunlight coming into the junction over a wide range of angles undergoes only slight reflective loss because of the index matching effect of the epoxy. An air Brewster interface of the trumpet to the rod cannot be used because of the severe reflective loss of incident sunlight in the absence of the epoxy.

A photo of the rod and trumpet assembly is shown in Figure 12. Since the junction formed at the 2 mm dia. laser rod and the long tapered trumpet is rather fragile, the trumpet is held by a support yoke attached to the niobium heat sink by an invar rod. For additional support the junction is surrounded

Preceding page blank
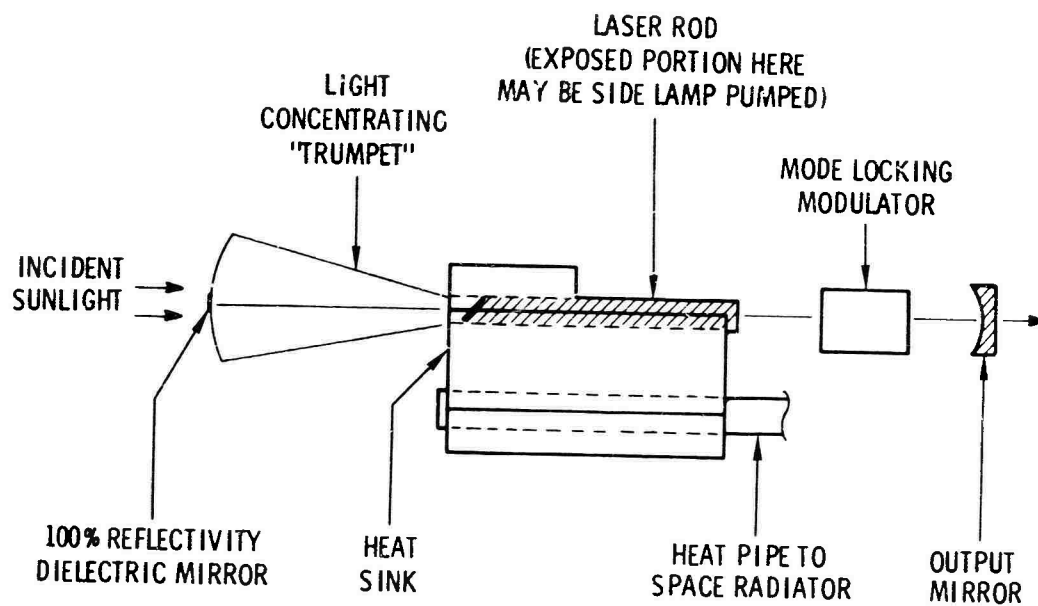
Figure 11.   Sun-Pumped Nd:YAG Laser Cavity Configuration
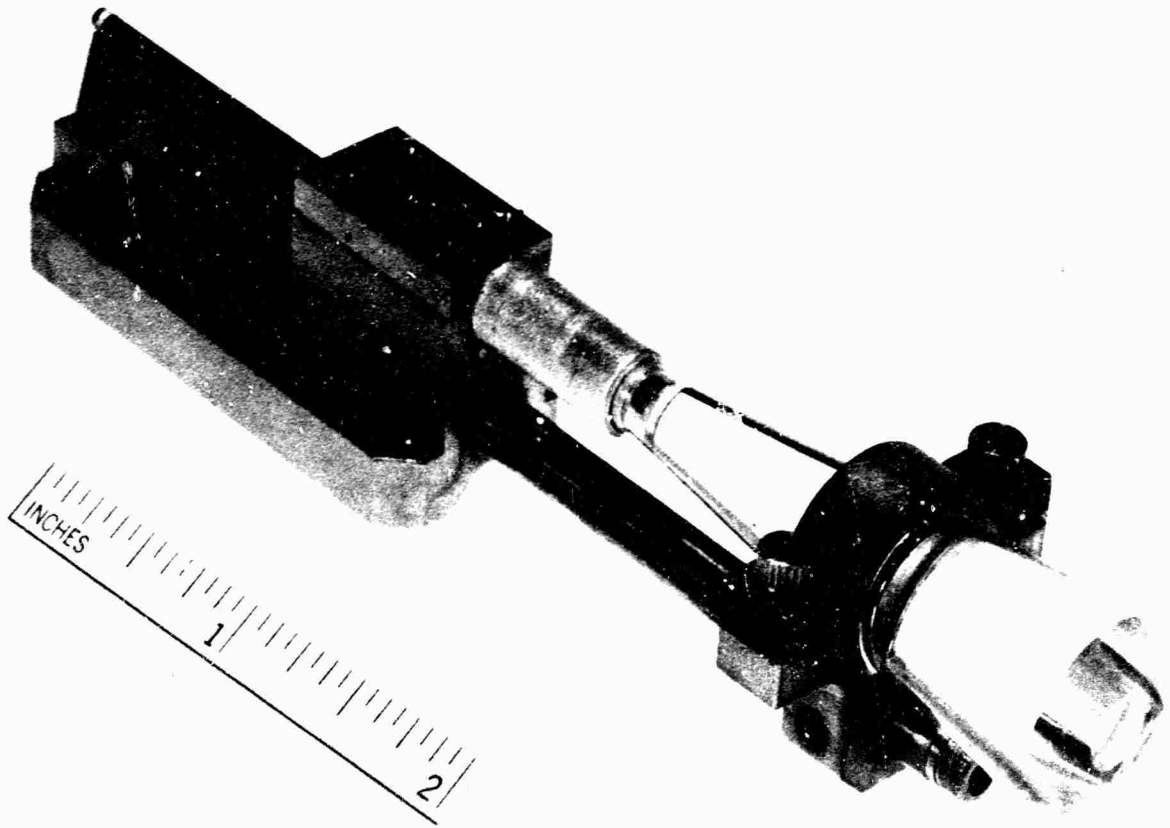
Figure 12.   Solar End Pumped Laser Rod-Trumpet Assembly

by a sleeve which is silvered on the inside. When the trumpet is attached to the rod an epoxy bond is formed between the trumpet and the sleeve as well as between the trumpet and the rod resulting in a mechanically strong joint.

The YAG trumpet end pumping configuration failed in the initial attempt to operate the device. The failure was due primarily to the thermal breakdown of the Epo-Tek 301 epoxy under the intense solar radiation at the junction which led to overheating and cracking of both the rod and trumpet at the joint. Contributing to the problem was the rigid mechanical design of the trumpet mounting yoke and rod which did not allow for the different thermal expansions of the invar rod and trumpet. Following this failure a search was begun for an epoxy or index matching fluid which could withstand the solar flux at the junction. A more detailed consideration of the problem and a discussion of this study are presented in Appendix I. An epoxy, Tra Bond 2114, was found which has a much greater breakdown resistance to the focused sunlight than the Epo-Tek epoxy. An index matching liquid, $SnCl_2 \cdot 2H_2O$ dissolved in glycerol[12] was also found with suitable properties including adequate breakdown resistance. During this study the importance of making the bonding epoxy layer thin was demonstrated with the testing of samples of different thickness. This is another possible contributing factor in the failure during the initial experiments; the epoxy layer at the joint may not have been sufficiently thin. As a result of this investigation it was believed that materials and techniques had been determined which would allow successful implementation of the clear YAG trumpet approach; a second trumpet was therefore ordered and the laser rod refinished. Unfortunately, the second trumpet was received defective; excessive scattering was observed in the bulk of the material near the large end of the cone. Since the laser beam traverses the length of the trumpet, this scattering would have resulted in a severe intracavity loss which would most likely have prevented laser operation. Since the time remaining on the program was not sufficient for the vendor (Airtron) to refabricate the trumpet, this approach was not pursued further.

An alternate end pumping scheme using an open air reflective concentrating cone was conceived during the evaluation of the rod-trumpet bond problem and it was decided to pursue this configuration in parallel with the YAG trumpet approach. A schematic of this scheme is shown in Figure 13. The light concentrating optics consists of a field lens and the reflective cone which is fabricated by electro-forming a thin layer of silver and then a thick backing layer of copper onto a highly polished stainless steel mandrel. The maximum reflectivity laser mirror is deposited on the central 5 mm dia. of the plane side of the plano-convex field lens. Both ends of the rod are anti reflection coated. Consideration was given to placing the maximum reflectivity laser mirror directly on the end of the laser rod; however, this was rejected because the transmission of such a mirror over a broad range of angles and wavelengths is much lower than for an A.R. coating. The smallest area into which the sunlight collected by the 24" diameter mirror may be focused using air optics is 2.84 mm; therefore, a 3 x 30 mm laser rod was used in this configuration. The rod is silvered on its entire OD and soldered into the heat sink with its full length and OD being surrounded by the heat sink. Thus, for simplicity, this configuration was not designed to be capable of dual pumping as was the case with the YAG trumpet scheme. The design of both the YAG trumpet and the air cone is discussed in Appendix II.

22
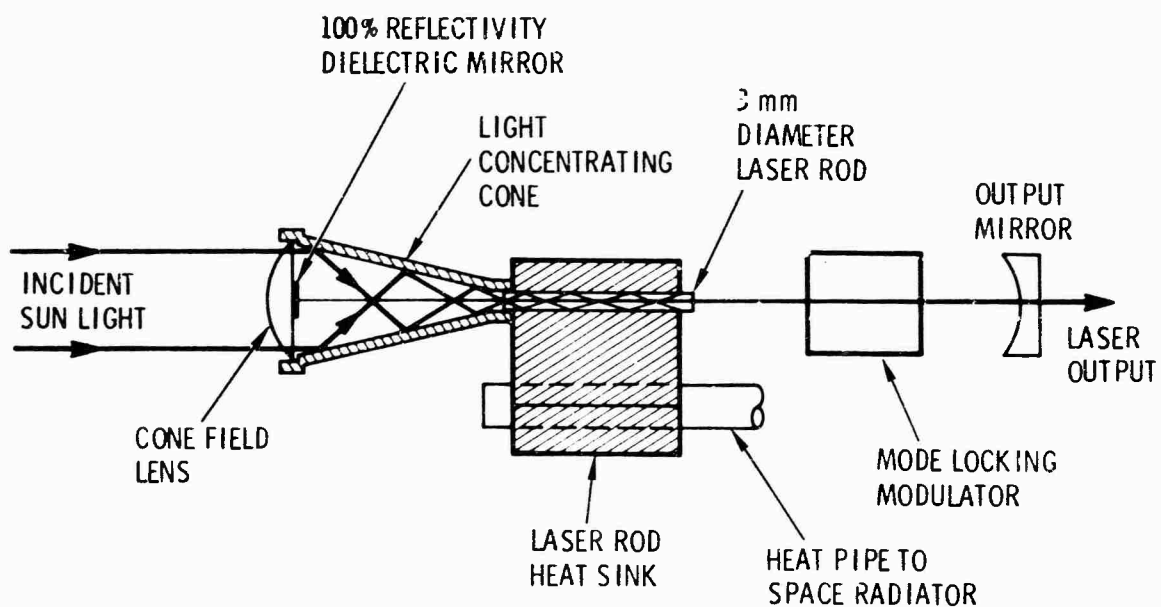
Figure 13   Sun Pumped Laser Configuration Using Open Silver Reflective Cone

The advantages of the open reflective cone are its simplicity, mechanical stability, and reliability. It does have the disadvantages of having a small reflective loss and requiring the use of a larger diameter laser rod than the YAG trumpet. The reflective loss is, however, only a minor consideration. The cone was designed so that the extreme ray from the primary system makes only four reflective bounces before entering the rod. Since the average number of bounces made by all rays is less than four and the reflectivity of silver over the primary pumping range is greater than 98%, the total reflective loss is estimated to be on the order of only 5%. The rod diameter disadvantage of the open cone may also be less a drawback than it first appears. Based on the present sun pumped laser power output it is estimated that the required laser performance will be achievable with an 12" diameter collector. A rod with a diameter of 1.4 mm may be used with this mirror diameter. This is probably about the smallest diameter rod which is practical anyway; in a dual pumping scheme it is increasingly difficult to couple the light from the lamp or diode array into smaller diameter rods. This is an important consideration since it is likely that most applications for the sun pumped laser will require the continuous operating capability afforded by the dual pumping scheme.

2.   LASER ROD MATERIAL

The laser material used in both the YAG trumpet configuration and the open cone configuration which was successfully operated was Nd:Cr:YAG with nominally 1 atomic percent doping of Nd and 0.1 percent chromium. Chromium YAG was chosen because of its broad absorption bands in the spectral region where the sun peaks. It was felt that with the chromium doping level of 0.1 percent the optical quality of the material would be retained and that over the full length of the rod substantial absorption by the chromium ions would take place. Figures 14 through 16 show the transmission spectra in the visible and near IR of a sample (courtesy of Airtron) taken from the same crystal boule used to produce the laser rods in both configurations.

An extremely important consideration in the design of any laser is how much of the incident pump light from a given source is absorbed by the laser crystal. We have made measurements of the absorption of sunlight by samples of Nd:Cr:YAG of varying lengths to determine this quantity for the solar pumping case. Again the samples were from the 1 percent Nd, 0.1 percent Cr doped boule which yielded our laser rods. Using the telescope and optical relay system a beam of sunlight was passed through both the doped samples of varying lengths (L = 0.33, 0.66 and 1.0 cm) and an undoped YAG sample and the power in the transmitted beam was measured using the CRL model 201 calorimetric power meter. In the absorption calculation the incident power is taken as the power transmitted through the undoped YAG sample in order to account for the Fresnel reflections off the faces of the doped samples. These measurements were made with both the silver secondary mirror and the dielectric secondary mirror and the results are shown in Figure 17. The circles represent the experimentally measured values of the fraction 1-T of incident sunlight absorbed by the crystal samples in the two cases. Both sets of data were fitted by the exponential relation

$$1 - T = (1 - T_f)(1 - e^{-<\alpha>x}) \qquad (1)$$

24
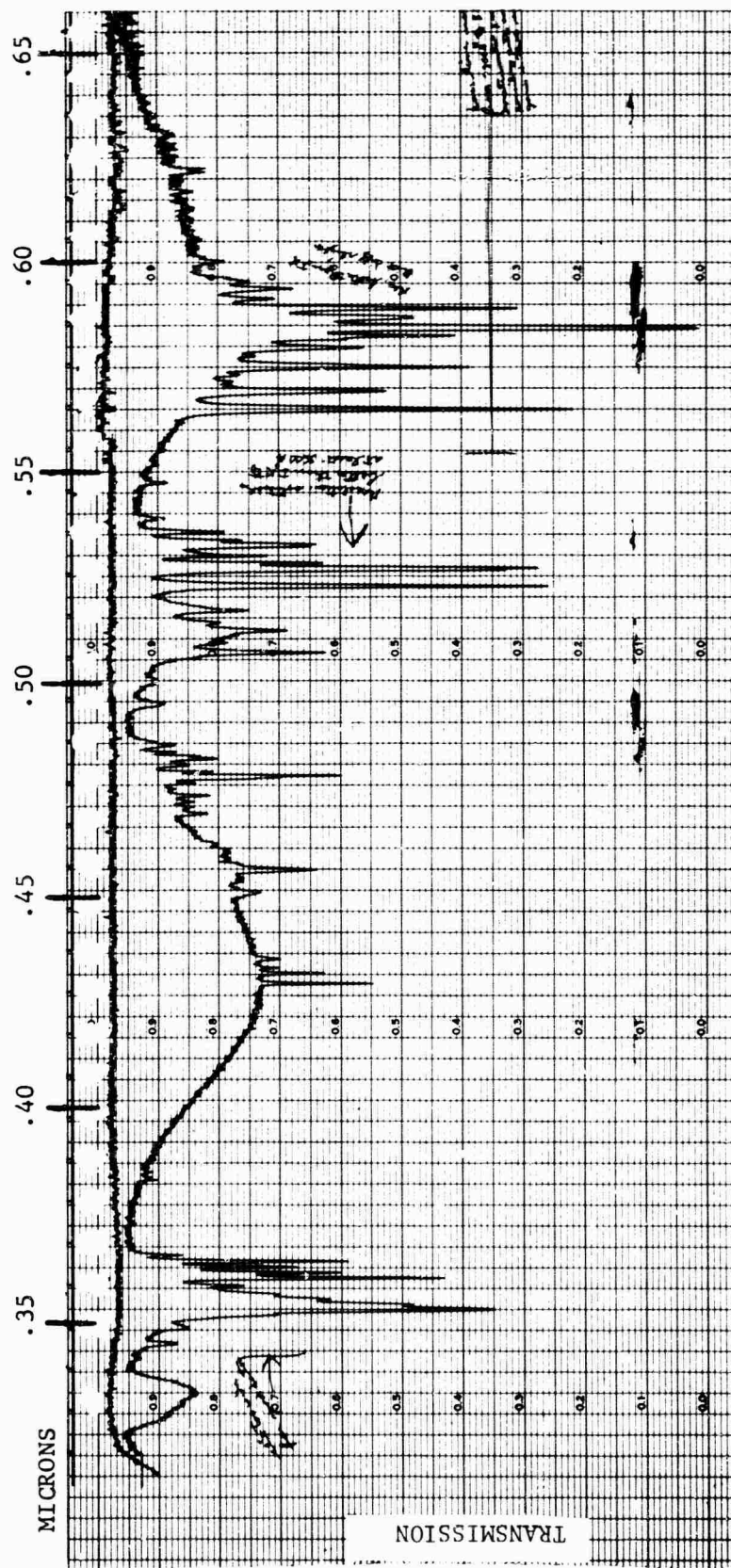
Figure 14 Transmission Spectrum of Nd:Cr:YAG from 0.35 to 0.66 microns

Figure 15   Transmission Spectrum of Nd:Cr:YAG from 0.65 to 1.0 microns

26
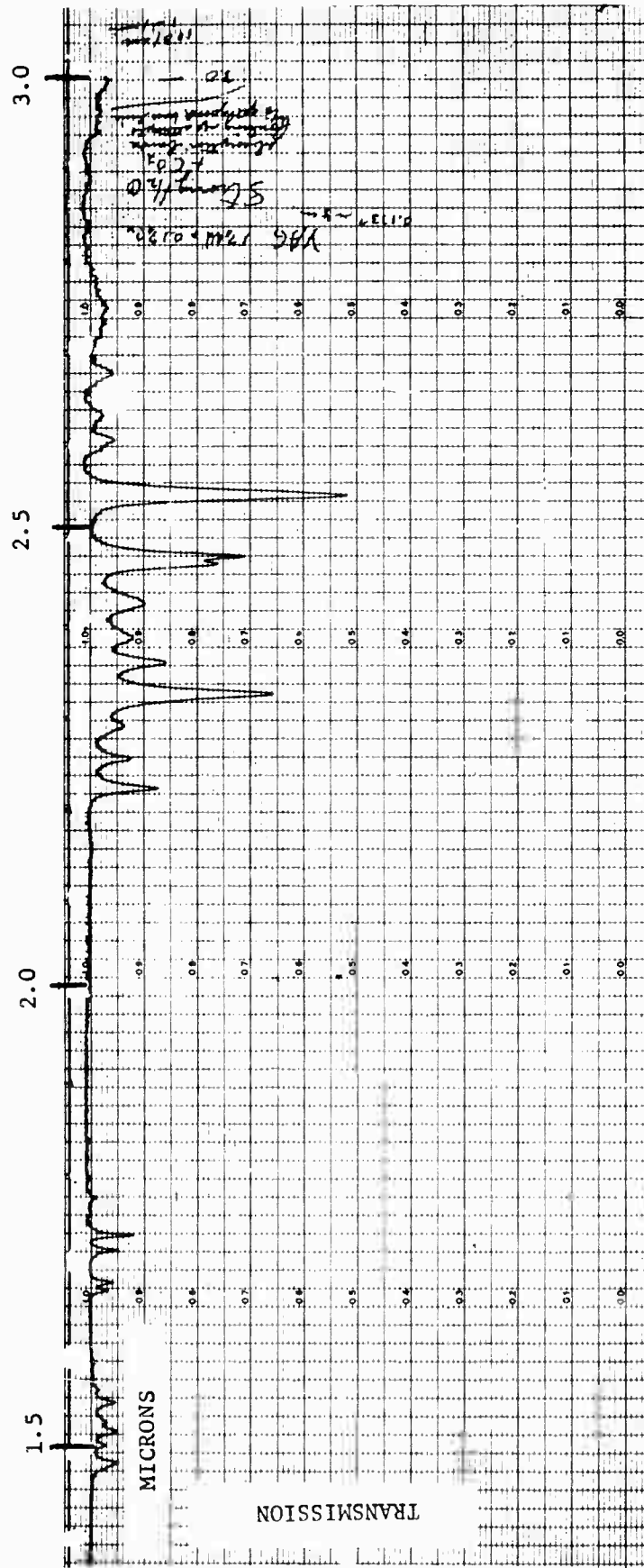
Figure 16   Transmission Spectrum of Nd:Cr:YAG from 1.4 to 3.0 Microns

27
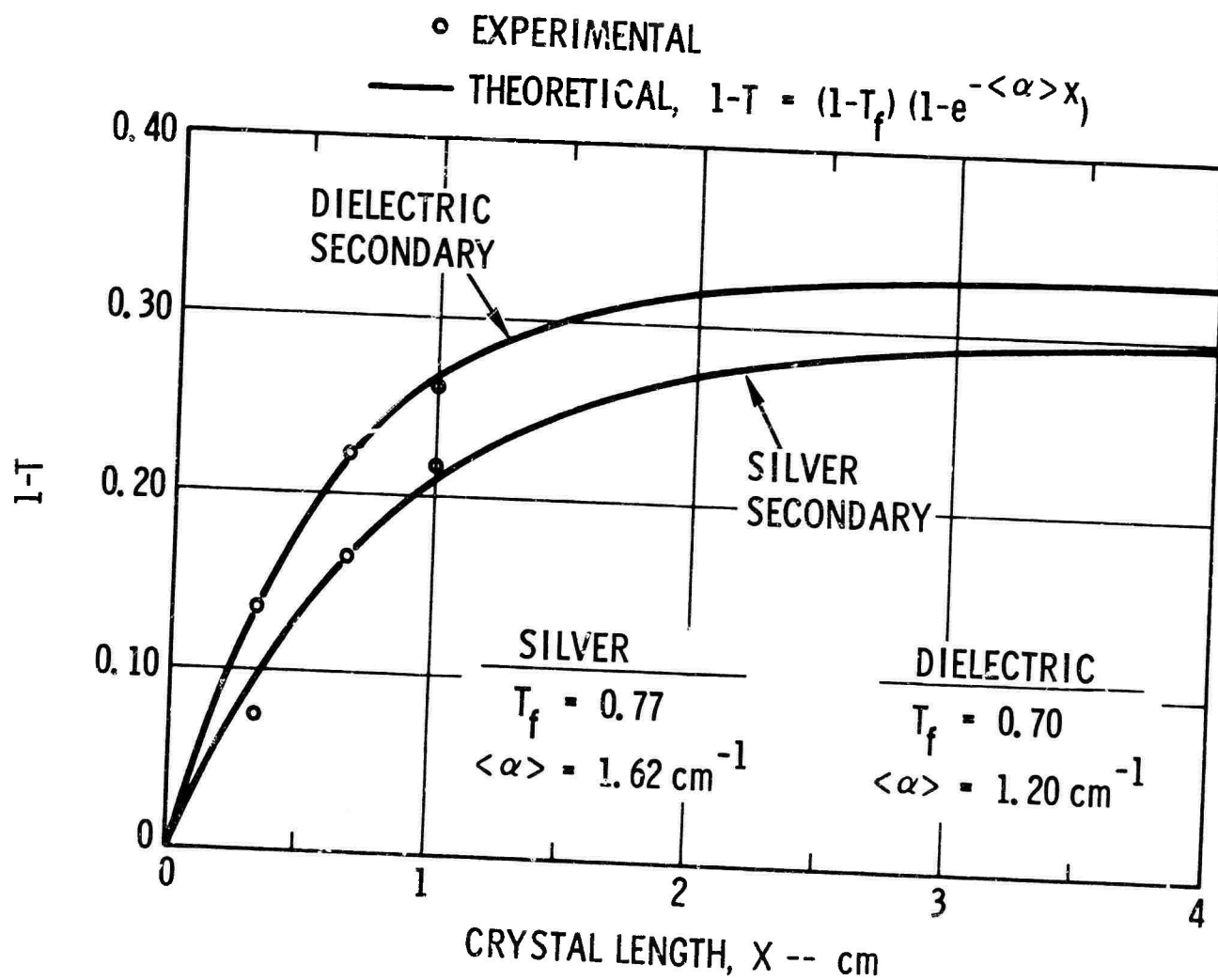
Figure 17   Fraction of Sunlight Absorbed by Nd:Cr:YAG
at the Earth's Surface

where $<\alpha>$ is an average absorption coefficient. It is important to recognize that for a material which displays narrow absorption bands with voids in between the light transmission (whether the light be the spectral emission from an arc lamp or the broad blackbody emission from the sun) of a long length of the material does not approach zero but some asymptotic value. This is the reason for the appearance of T_f in equation (1). Equation (1) is only an approximation to the absorption behavior of the material. The broad spectrum light transmission of an absorber of length x is given by

$$T = \frac{\int_\lambda I_{out}(\lambda) \, d\lambda}{\int_\lambda I_{in}(\lambda) \, d\lambda} \qquad (2)$$

Now $\dfrac{I_{out}(\lambda)}{I_{in}(\lambda)} = e^{-\alpha(\lambda) x}$

so that $I_{out}(\lambda) = I_{in}(\lambda) \, e^{-\alpha(\lambda) x}$ and

$$T = \frac{\int_\lambda I_{in}(\lambda) \, e^{-\alpha(\lambda) x} \, d\lambda}{\int_\lambda I_{in}(\lambda) \, d\lambda} \qquad (3)$$

Thus, in this case T cannot be expressed by a simple exponential relation. It is likely, however, that equation (1) is usually a good approximation and this is indicated by the good fit to the data. The value of T_f is not well defined by this procedure, though, it is likely that more light is absorbed by long crystals than is indicated by the theoretical curves in Figure 17. Unfortunately, longer samples with large enough cross sectional area were not available to check this.

We can use these absorption results to estimate the output power attainable from a sun pumped laser using the Nd:Cr:YAG rod. The absorption results in Figure 17 do not strictly apply to exospheric sunlight because the atmospheric depletion of solar radiation is a function of wavelength (see Figure 10); however, the difference between the amount of sea level sunlight and exospheric sunlight absorbed by the laser material is expected to be small. We will therefore use the above absorption results to predict attainable laser power outside the earth's atmosphere. At the outer limits of the earth's atmosphere a 12" diameter mirror collects 100 watts of solar power. Assume a collection and relay efficiency of 80% and suppose that 50% of the relayed power can be channeled into the laser rod by the end pumping optics. From Figure 17 ~ 30% of the sunlight entering the rod is absorbed; there, of the incident 100 watts, 12 watts

would be absorbed by the rod. If 30% of the absorbed light is converted to 1.06μ fluorescence and the laser is operating for above threshold the laser output would then be $\sim$ 4 watts.

3.   LASER ROD COOLING

Circulating liquid cooling schemes commonly used to remove waste heat from a laser are not appropriate for space application. Their inherent complexity, limited life, and relative unrealiability make them unattractive for this purpose. Failure of pumps and seals, corrosion of coolant piping materials, and photolytic breakdown of cooling liquids are some of the disadvantages of this cooling method. Conductive and liquid-filled heat pipe cooling techniques, which have much longer life and are more reliable, were therefore chosen for use in the operation of the sun pumped laser.

Heat is removed from the laser rod through the heat sink which is constructed of niobium. Niobium was chosen for this purpose because it has a thermal expansion coefficient which closely matches that of YAG and good thermal conductivity. A good match between the thermal expansion coefficients of the laser material and the heat sink is essential. The strain induced in the rod by an expansion mismatch as the rod and heat sink heat up causes the rod to become birefringent. This seriously degrades the optical quality of the rod and laser performance is impaired. If the mismatch were to be severe enough, breaking of the rod could even occur at high input powers. The match between niobium and YAG is adequate to eliminate these difficulties. The coefficient of YAG is 6.9 in/in/$^{\circ}$C and that of niobium is 6.88 to 7.38 in/in/$^{\circ}$C, depending on the melt and manufacturer. Niobium is one of the refractory metal family, having a melting temperature of 4379°F. It has a density of 535 lbs/ft^3, approximately the same as brass, and a reasonably high thermal conductivity of 31 BTU/hr ft^2 $^{\circ}$F/ft about the same as cast iron or tin.

The mounting surface for the rod is a machined-radiused groove into which the rod is soldered providing intimate contact between the rod and heat sink. In the original sun pumped laser configuration which was designed to be compatible with sun and lamp pumping the 20 mm portion of the rod next to the trumpet was contacted on the entire OD and the remaining 30 mm was contacted over only 120° to allow for the side pumping capability (Figure 11). For the configuration using the open cone the ll length of the rod was contacted the full 360°. The rod was laid in t 120° groove and a cap placed over the rod and heat sink to provide the remaining contact. The rod was soldered to both the groove and the cap.

Niobium cannot be wet and soldered with ordinary fluxes due to the inertness of the oxide coating: therefore, the niobium is first nickel plated. The OD of the YAG rod is silver coated to allow it to be soldered into the heat sink. The proprietary techniques of Liberty Mirror Division of Libby Owens Ford produces a vacuum-deposited silver, highly reflective second surface mirror with the best adherence of a number of techniques we have investigated. Layers of nickel and indium are applied over this to provide coating thickness and solder-ability without scavenging. The YAG rod is soldered to the support block using pure indium solder, which has a low melting point, high ductility, low yield strength and scavenge to the nickel and silver during soldering. The high ductility and low yield strength of the indium solder greatly diminish the already small effect of the mismatch between the thermal

30

expansion of the niobium and the YAG. Expansion differences between the two materials are compensated by the ready deformation of the solder layer. The solder bond between the rod and block is maintained at .004 - .005 inch thickness resulting in maximum joint strength and low thermal resistivity.

In space operation of the sun pumped laser heat will be removed from the rod heat sink by a heat pipe clamped to the bottom of the heat sink or by a heat pipe cooled cold plate in the space craft to which the heat sink is bolted. In either case the heat pipes will terminate in a space radiator. The heat pipe was selected as a means to remove heat from the rod-mounting structure because the high thermal conductance (50 or more times better than a solid metallic conductor), low weight, and high anticipated reliability seem ideal for use in spacecraft applications. The heat pipe as used for this purpose consists of an outer circular housing, an inner screen to carry the fluid, and the working fluid. The fluid is vaporized in the evaporator end by heat input and travels down the center of the assembly to the other end which must be cooled in some manner to cause condensation of the fluid which then travels to the evaporator end by surface tension forces in the screen wick. The pipe is completely closed, forming a hermetic seal between the working fluid and the outside environment. For convenience in the laboratory experiments, the heat was removed from the heat sink by a copper tube through which a refrigerated methanol and water mixture was flowing.

4.   DUAL PUMPING

A satellite communication laser transmitter powered by the sun can have much greater versatility if it is equipped with the capability of being driven by an artificial means during solar eclipse periods of the satellite orbit. Such a dual pumping arrangement makes possible continuous operation as well as taking advantage of the long life afforded by solar pumping. Investigation of dual pumping was not a part of the current sun pumped laser contract, however, the approach initially selected was to add the end solar pumping capability to the lamp pumped space qualifiable Nd:YAG laser under development at GTE Sylvania. Much of the preliminary design work on this laser had been conducted for NASA under the Space Qualified Nd:YAG laser contract (Contract No. NAS12-2160). Unfortunately, basic design difficulties prevented the use of the NASA developed laser for this purpose.

Because of the importance of the dual pumping concept it was decided to continue consideration of this scheme; therefore, a new laser design compatible with both lamp and sun pumping was developed. The YAG trumpet configuration discussed above and shown in Figures 11 and 12 was designed to be lamp pumped by placing an elliptical pump cavity over the exposed portion of the laser rod. The laser rod is situated at one focus of the ellipse and the lamp at the other. A cross-sectional view of the lamp pumped laser cavity is shown in Figure 18. The heat shields and ceramic isolators shown in this schematic have the function of reducing the direct thermal flow from the lamp or cavity into the rod heat sink so as to allow the rod to operate at the lowest temperature possible. Ideally, the rod heat sink should have to transport only the heat absorbed in the rod. In practise the heat which leaks through the support structure cannot be entirely eliminated.

31

PUMP CAVITY

LAMP

LASER ROD

HEAT SHIELD

CERAMIC THERMAL
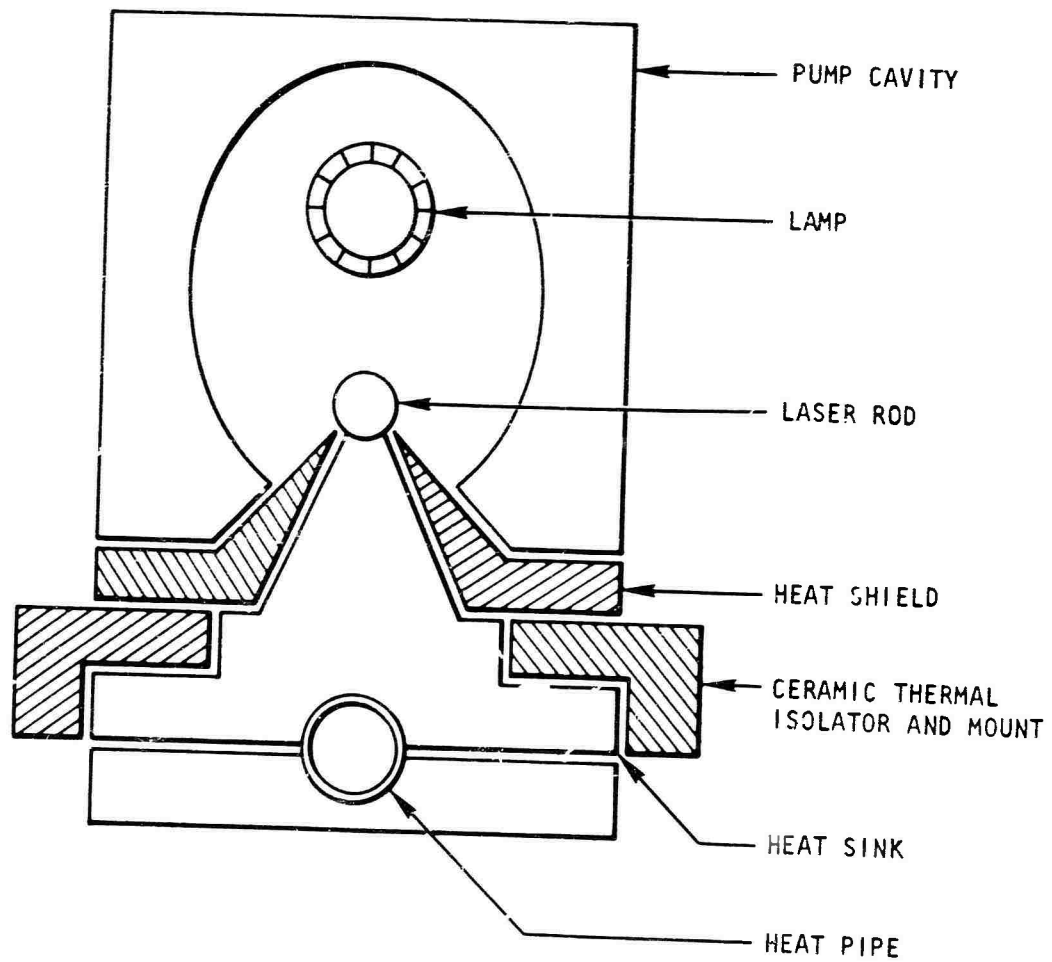ISOLATOR AND MOUNT

HEAT SINK

HEAT PIPE

Figure 18.   Conductively Cooled Laser Head Configuration

The laser was designed to be operated by two different types of lamps: the krypton arc lamp and the alkali metal vapor lamp. Operation of the laser with a krypton arc lamp was desirable as a comparative reference. The potassium-rubidium lamp currently under development at ILC is believed to be the best lamp source for pumping the space qualified Nd:YAG laser[13]. This lamp has a low threshold and high efficiency due to its excellent spectral match to the absorption bands of Nd:YAG, good mechanical stability and it does not require liquid or convective cooling, being cooled only by radiation.

The laboratory model dual sun and lamp pumped laser equipped with a water cooled krypton arc lamp is shown in Figure 19. In this configuration the heat is removed from the laser rod heat sink by a heat pipe; the heat is dispensed by a water jacket surrounding the output end of the pipe. In the lamp pumped experiments with this laser the rod-trumpet assembly was replaced by a 2 x 30 mm round laser rod in its own heat sink mounting. This rod and a rod with a square cross section mounted in this heat sink are shown in Figure 20. Tests were planned using the square cross section rod in order to evaluate the laser performance with a Cartesian thermal profile in the laser rod. Such a geometry leads to thermal strain birefringence with only Cartesian refractive index components. With this birefringent characteristic the entire volume of the rod can support the linearly polarized fundamental mode without polarization rotation into higher modes. This thermal geometry is realized to a degree, of course, even with the round rod since the heat is removed from one side of the rod rather than radially.

Figure 21 shows plots of the power output obtained from this laser as a function of power input to the lamp with the base of the rod heat sink at two different temperatures. A threshold of 260 watts for P_{in} was obtained with a 2% transmitting output mirror. Temperature was measured at the base of the heat sink for convenience. Rod temperature is seen to have a significant effect on the laser performance. This is even more clearly demonstrated in Figure 22 which shows the laser power output as a function of heat sink base temperature at a constant power input to the lamp. The temperature dependence of the laser's performance here results primarily from two effects. The principle effect is the broadening of the 1.06μ fluorescence linewidth which is accompanied by a decrease in the stimulated emission cross section and the laser gain as the rod temperature increases. The second effect is the increase in thermal population of the ground state of the 1.06μ laser transition with increase in temperature. The increased thermal population of this level appears dynamically to the laser as an effective increase in the dissipative loss, α_o. These results clearly indicate that trade-offs will have to be made between laser performance and thermal design for the space qualified Nd:YAG laser. The laser efficiency obtained with the krypton arc lamp as the pump source is poor, as expected. Not only does the krypton lamp have a high threshold and a radiant efficiency which is poorer than that of the alkali metal vapor lamp but in this experiment the 5 mm bore of the lamp (length of arc is 1.2 inches) was a very poor match to the 2 mm rod diameter. Experiments were planned to operate the laser with the alkali vapor lamp in a vacuum enclosure; however, because of the failure of the YAG trumpet assembly in initial solar pumped tests and the need to concentrate on obtaining solar pumped operation of the laser, lamp pumped work was discontinued on this program. The alkali vapor lamp pumped laser effort was continued, however, on a Sylvania funded program with the implementation of a vacuum station to operate the conductively cooled laser with the potassium rubidium lamp under development at ILC. Since this

33
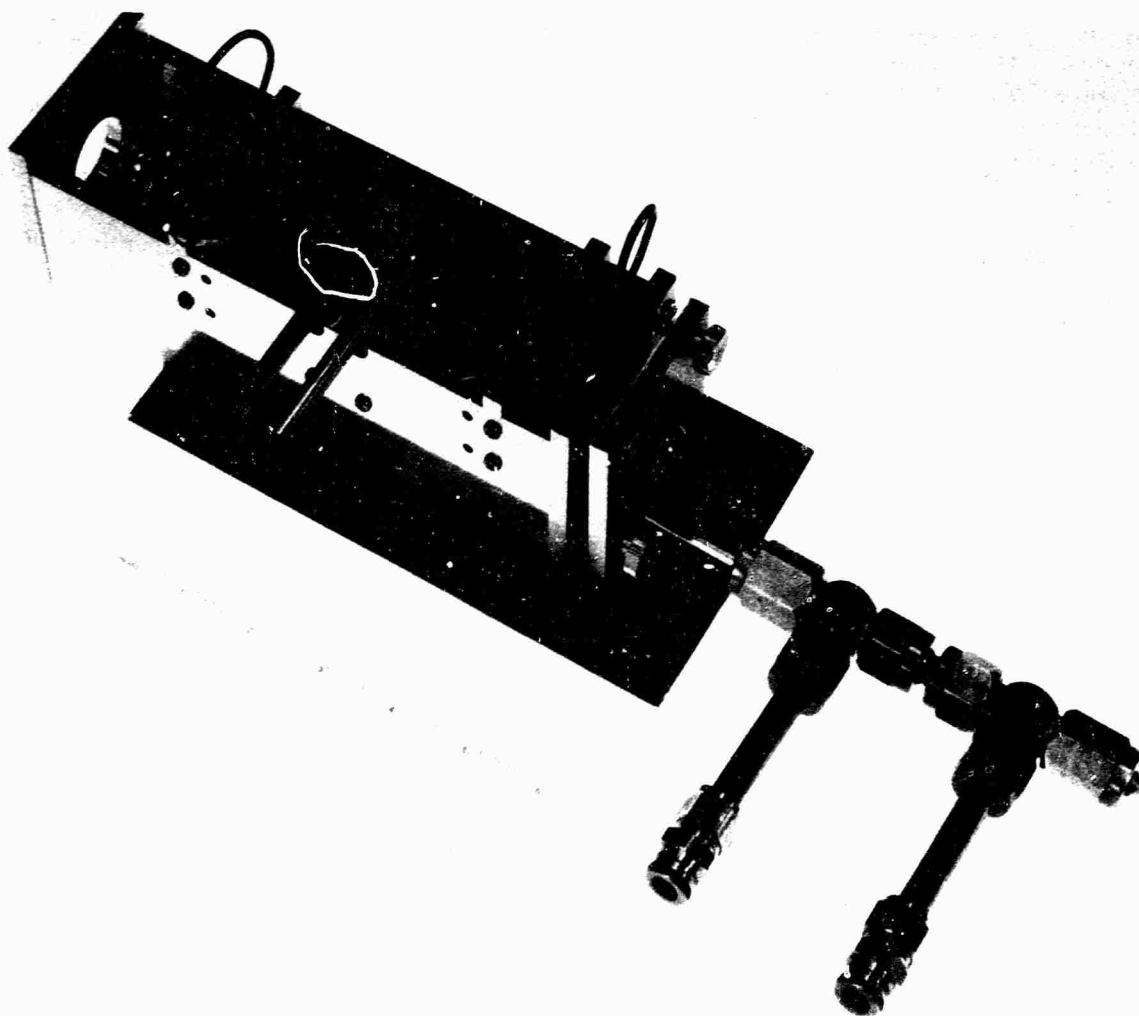
Figure 19.
Conductively Cooled, Dual Solar and Krypton Lamp Pumped Nd:YAG Laser
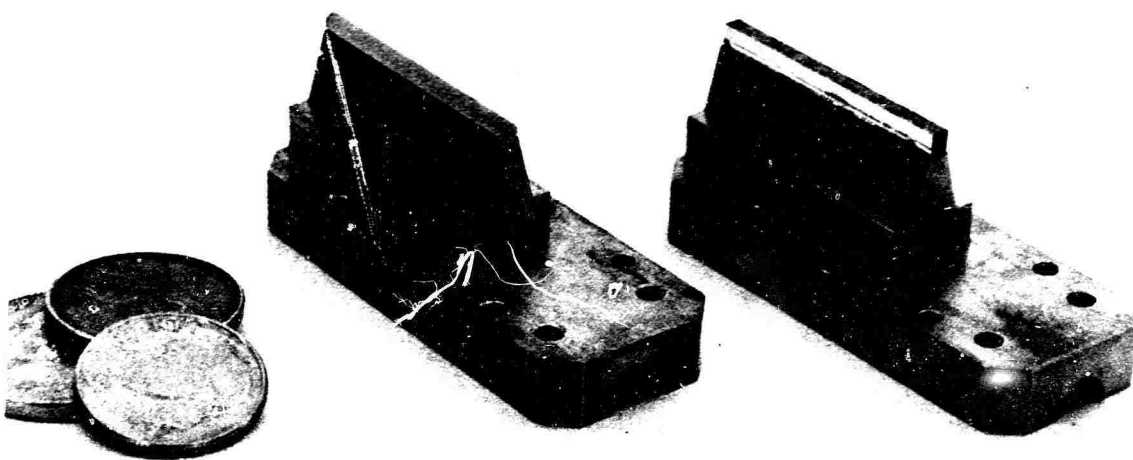
Figure 20.
Laser Rod Heat Sink Mountings for Round and Square Rods
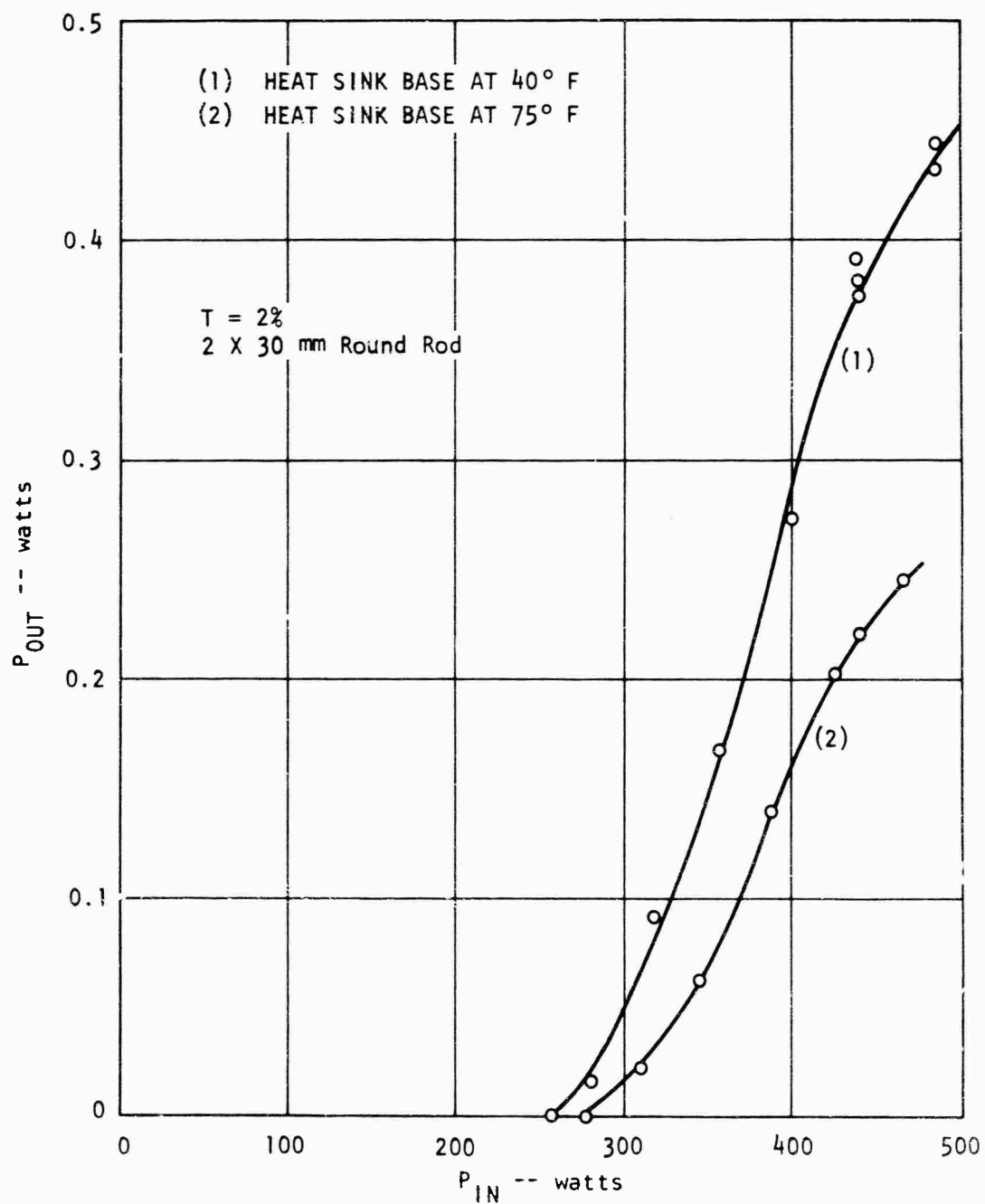
Figure 21.
Conductively Cooled, Krypton Lamp Pumped Laser Performance
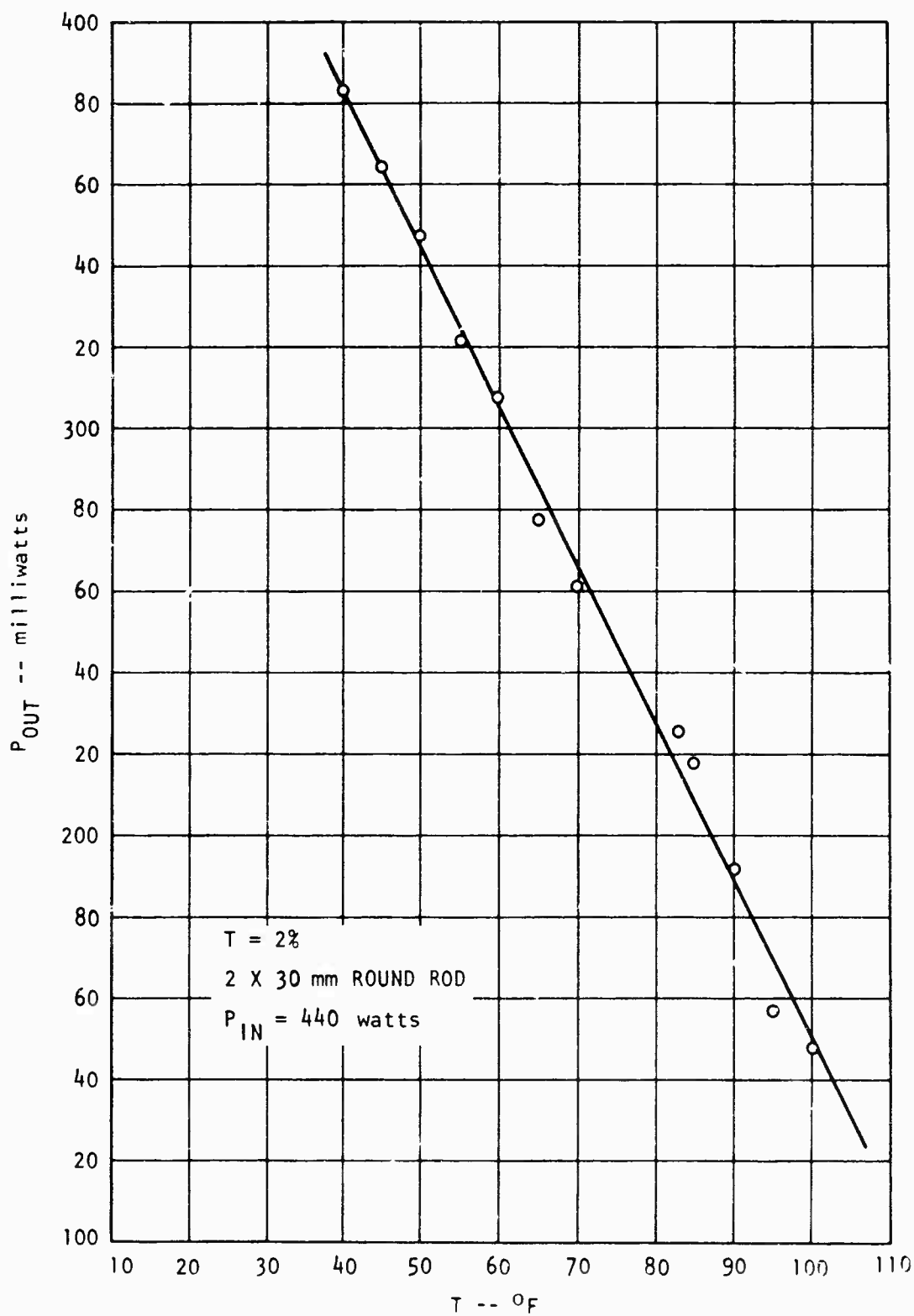
Figure 22.

Laser Output Dependence on Heat Sink (Rod) Temperature

lamp, shown in Figure 23, must be operated in a vacuum to prevent oxidation of the envelope seals, the entire laser is enclosed in the vacuum bell jar apparatus shown in Figure 24 and 25. Alignment of the laser output mirror is accomplished from outside the bell jar during operation with a sealed mirror mount using a flexible stainless steel bellows tube. In this particular configuration, for convenience, heat is removed from the rod heat sink by a water cooled copper pipe rather than with the heat pipe, simplifying the mechanical design of the vacuum bulkhead.

5.   MODE LOCKING

Mode locking the sun pumped laser presents a particularly interesting problem since the laser operates with a low gain. Any additional loss to the laser cavity caused by the insertion of the mode-locking modulator must be minimized or, if possible, eliminated altogether in order to minimize the degradation in the laser power output. The lower the operating gain of the laser the more stringent this requirement becomes. This consideration makes the conventional electro-optic modulator appear somewhat unattractive because the insertion of a polarizer and an electro-optic crystal into the laser cavity usually results in a severe increase of intracavity loss. Several possible alternative techniques of mode locking the sun pumped laser were considered and it was concluded that the most promising technique was the use of a special intra-cavity electro-optic modulator. These various approaches and the reasons for selecting this particular method are discussed in Appendix III.

The mode locking modulator, which is shown in Figure 26, was fabricated using the design considerations presented in Appendix III and tested in a laboratory model Nd:YAG laser. With this device in the laboratory laser, mode locked pulses of less than 100 psec duration (Figure 27) were produced at a rate of 400 MHz. Only 0.2 watts of RF power were required to drive the modulators. The modulator was also used to mode lock the sun pumped laser to produce pulses at a rate of 500 MHz. These results are discussed in section IV.

Figure 23.   One-Inch Arc Length Potassium-Rubidium Lamp
            (Lamp Manufactured by ILC)
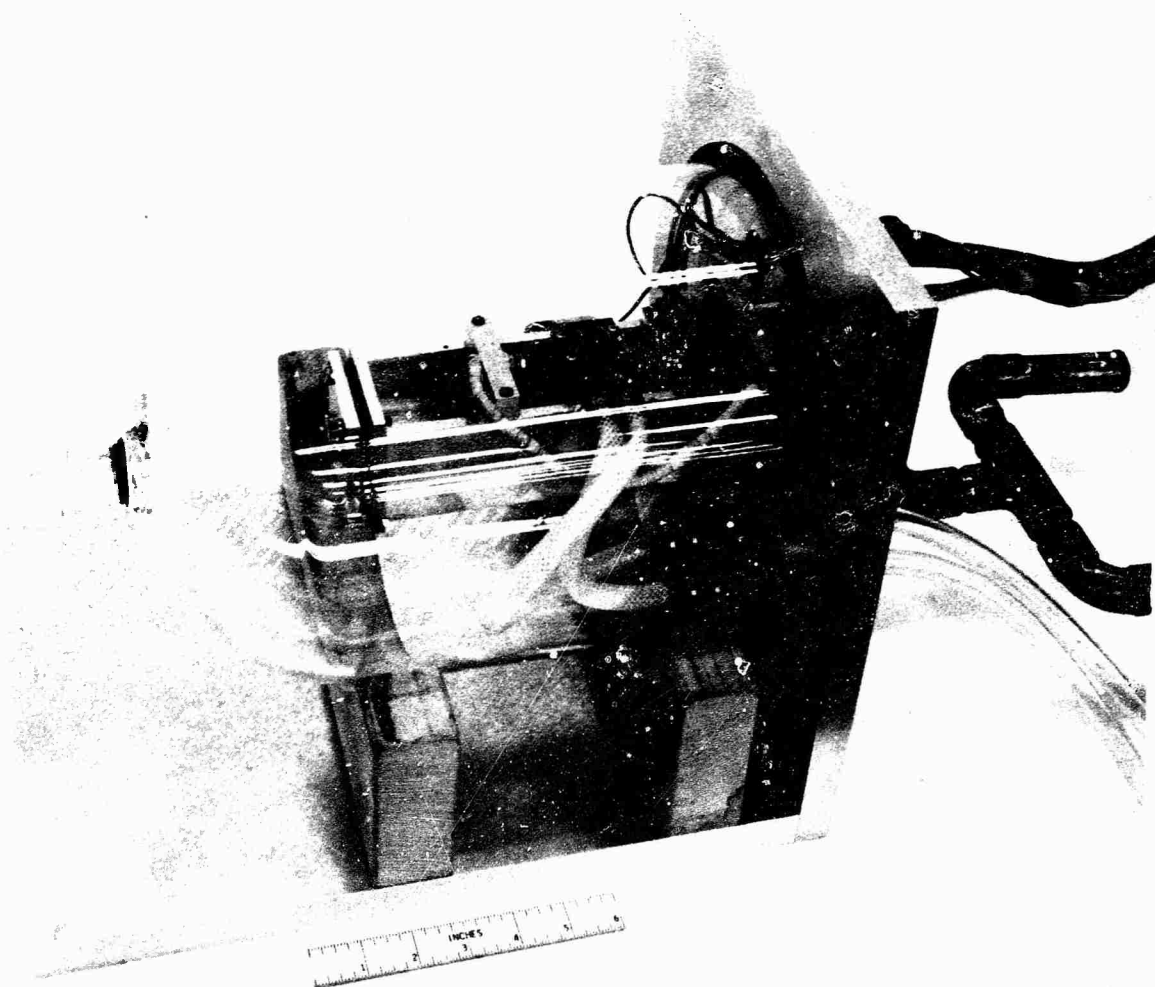
Figure 24.
Conductively Cooled, Potassium-Rubidium Lamp Pumped Nd:YAG Laser in Vacuum Belljar

40
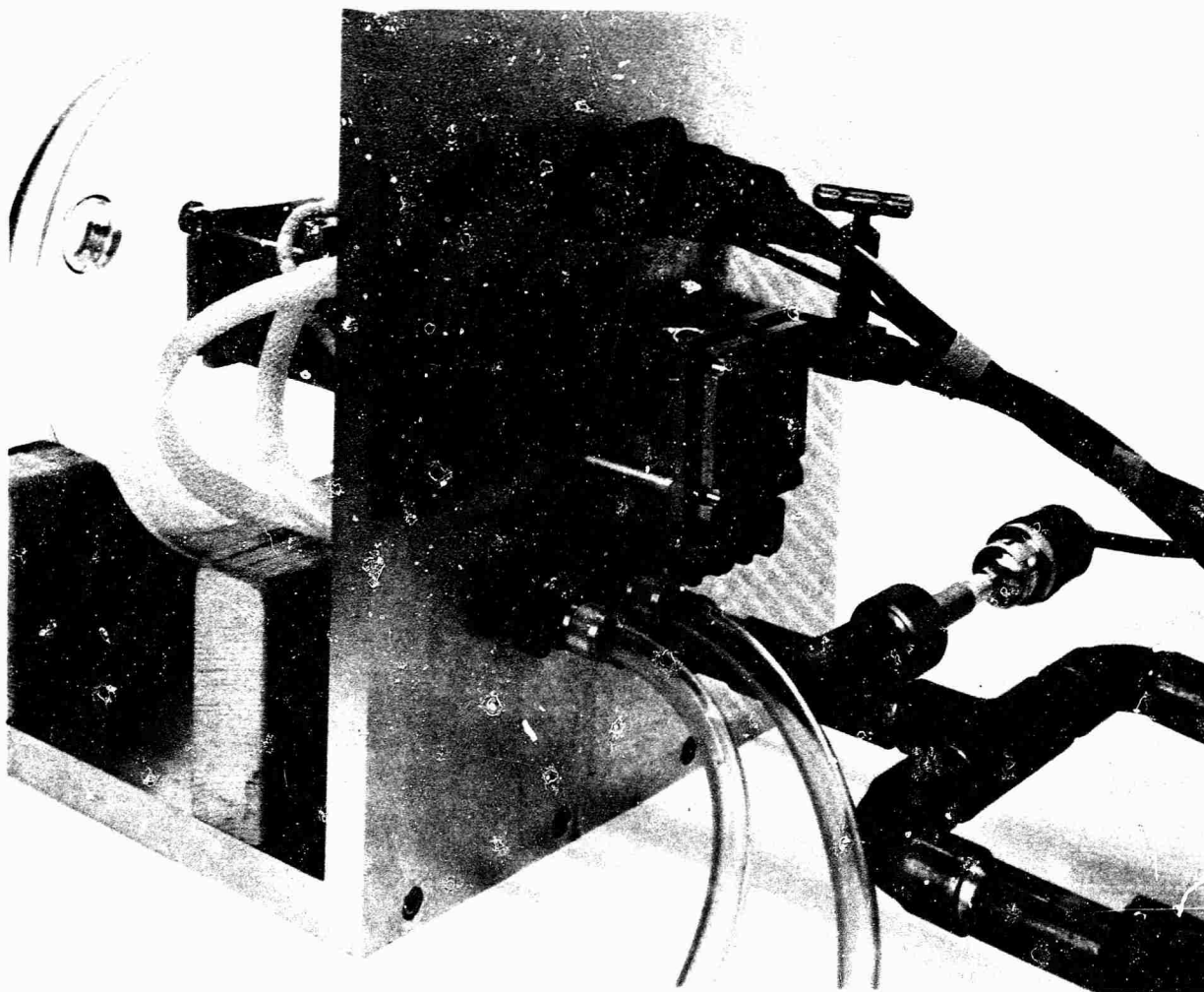
Figure 25.

Vacuum Belljar for Laser Apparatus showing Externally Adjustable Mirror Mount
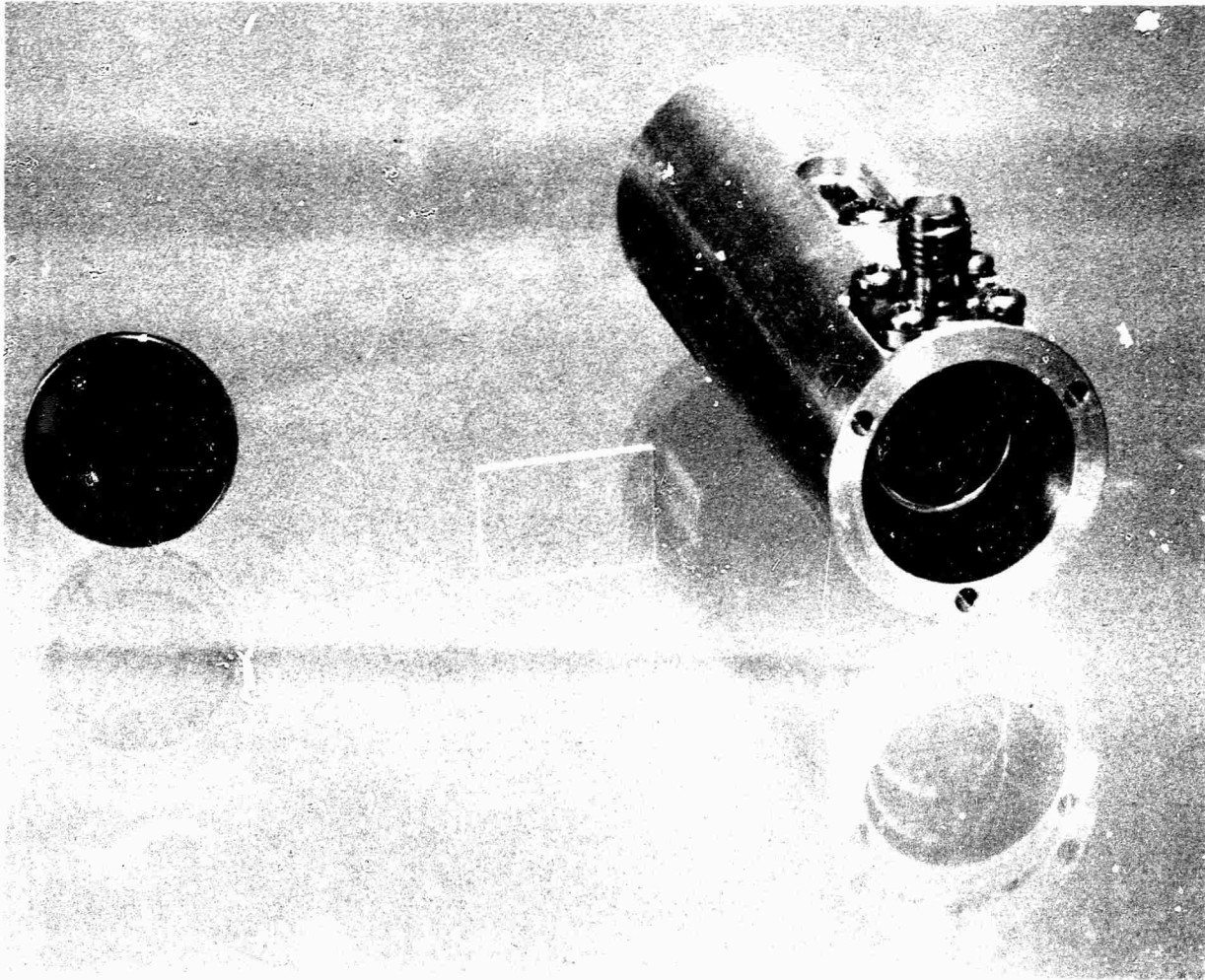
Figure 26.   Mode-Locking Modulator for Sun Pumped Nd:YAG Laser
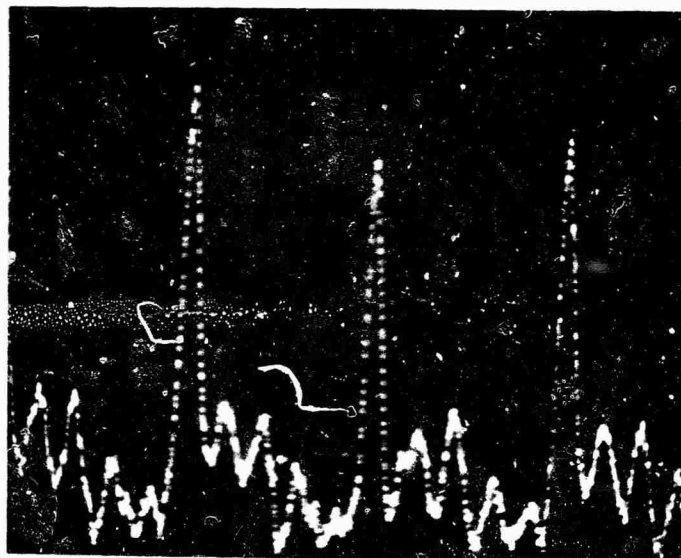
Figure 27.   Mode-Locked Pulses from a Laboratory Laser Produced
by Modulator for the Sun Pumped Laser (Time scale is
1 μsec per major division, instrumental rise time is
approx. 200 psec, jagged peaks between pulses are
instrumental)

PERFORMANCE CHARACTERISTICS OF THE SUN PUMPED LASER

A multimode power output of 1.6 watts was obtained with the laser configuration using the open reflective cone and the 3 mm diameter laser rod, (Figure 12). A photograph of the laser is shown in Figure 28. This output power was achieved using the cold mirror dielectric coated secondary with the full telescope aperture uncovered. The output mirror had a transmission of 2% and a 60 cm radius of curvature. The maximum reflectivity mirror on the cone field lens was flat. In these solar pumped laser tests the toroidal turning mirror shown in Figure 2 was replaced by an A.R. coated plano convex lens which formed the final solar image at the trumpet. As we mentioned earlier, the toroidal mirror was used in the design of the optics because of the spherical and chromatic abberations of a lens; nonetheless, the A.R. coated lens turned out to yield better performance.

The rod temperature was maintained at a temperature of about $100^{\circ}F$ by flowing refrigerated methanol and water through the copper cooling tube clamped to the heat sink. The base of the heat sink operated at about $30^{\circ}F$. This large ΔT between the rod and heat sink base was due in part to the relatively low reflectivity of the silver coating on the laser rod. A sample slide coated with the rod had a reflectivity of 93% at $6328\overset{o}{A}$; the reflectivity should have been 99%. Since the solar energy enters the rod at various angles depending on where the rays originate from on the primary mirror, a substantial portion of the incident solar power makes multiple reflections off the silver coated rod surface as it traverses the rod. With a reflective loss of 7% at each bounce much of the sunlight is absorbed into and dissipated by the rod heat sink rather than being absorbed in the rod or transmitted out the end of the rod. Ideally, all of the solar energy which does not coincide with the rod absorption bands and not selectively rejected by the collection and relay system should be transmitted through the rod rather than being dissipated by the heat sink. This would result in lower temperature operation of the rod than realized in the experiment and improved performance of the laser. (Recall from Figure 22 the effect of rod temperature on the output of the lamp pumped laser.) It is obvious also that absorption loss of useful pump light at the rod silver coating impaired the laser's performance.

From the cone construction diagram (see Appendix II, Figure 45) it is easily determined that the extremal ray makes 6 reflective bounces as it traverses the 30 mm long rod. The power weighted average number of reflections should be about 4. Assuming this weighted average number of reflections to be distributed equally along the length of the rod we can use Figure 17 to estimate how much of the incident solar power is transmitted through the silver coating. Based on data presented later it appears that about 50% of the 100 watts collected by the telescope and relayed by the cold mirror enters the rod. Using an incident power of 50 watts and Figure 17, we calculate that roughly 10 watts are transmitted through the silver coating. About 30% of the power entering the rod is absorbed by the rod; thus, of the 50 watts which enter the rod roughly 25 watts must be dissipated by the heat sink. The thermal resistance between the rod and the base of the heat was calculated

Preceding page blank
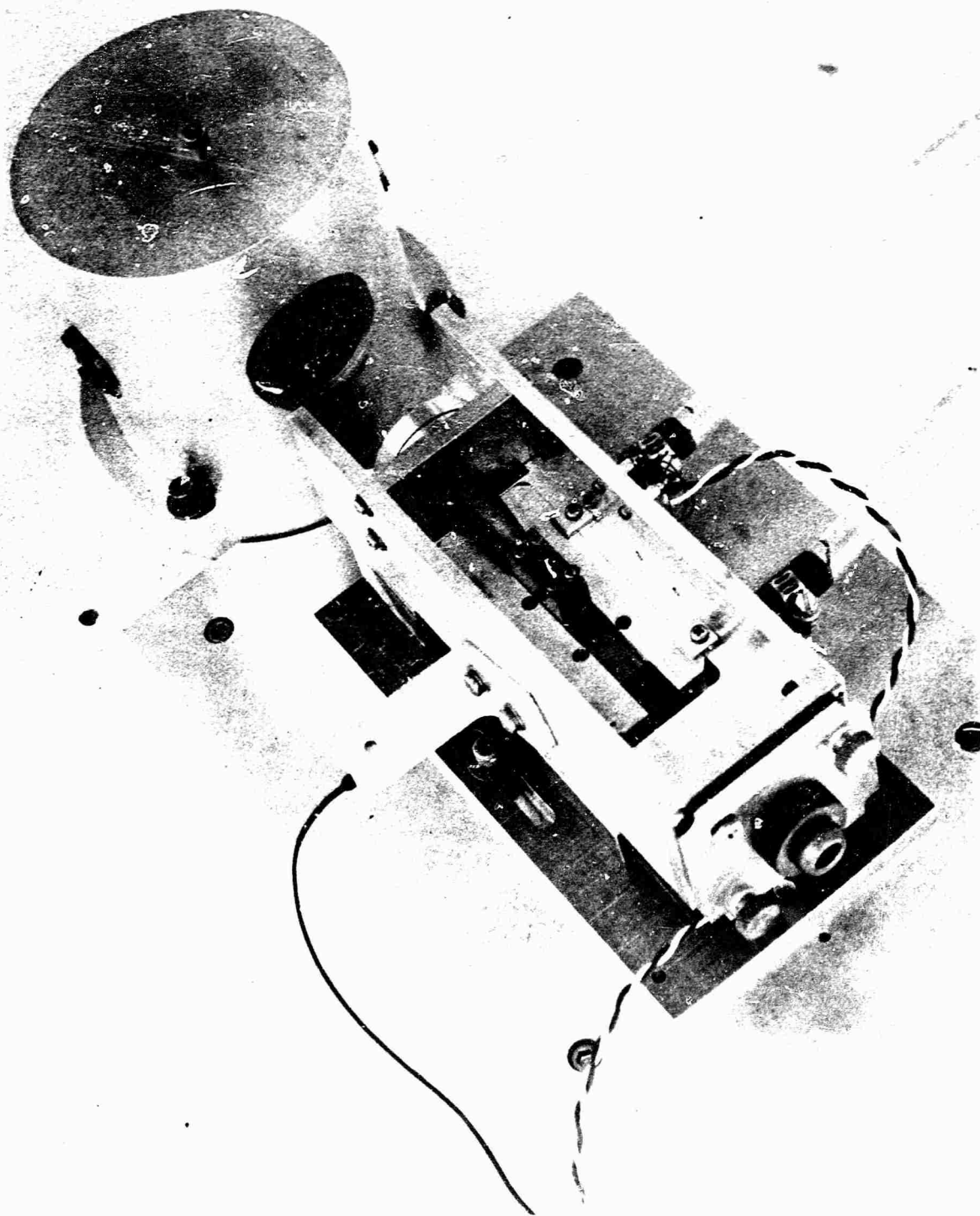
Figure 28.   Photograph of the Conductively Cooled
Sun Pumped Laser

to be about 3°F/watt. Using this value of thermal resistance and the power dissipated we calculate a ΔT of 75°F. This roughly calculated estimate is consistent with the measured value of 70°F.

A characteristic of all the loss mechanisms associated with the end pumping configuration using the open reflective cone is that the losses increase with increasing angles of incidence of rays entering the cone (or increasing primary mirror diameter). These losses are reflection losses at the cone field lens, the surfaces of the cone and the A.R. coated entrance face of the rod and absorption by the silver coating on the OD of the rod. In order to evaluate the effectiveness of the end pumping scheme in utilizing the full 24" diameter of the collecting mirror and to determine how the pumping efficiency varies with primary mirror diameter the laser output as a function of telescope aperture was measured by varying the opening both sectorially and radially. Sectorial variation removes the angle dependence of the pumping scheme and should reveal the laser's input-output characteristics for linear variation of the pumping power.
Radial variation of the aperture includes the angle effects and a comparison of the results for the two cases then indicates how the pumping efficiency depends on mirror diameter. Figure 29 shows the results of these measurements. The abscissa variable A/A_T is the fraction of the total aperture area exposed. The last data point is for $A/A_T = 0.915$ rather than 1 because of the central obscuration of the secondary mirror assembly. The rod temperature was maintained at the same value, $\sim 100^{\circ}$F, for all values of A/A_T in order to remove temperature-dependent effects. The dashed curve is a replot of the sectorial variation input-output curve with the abscissa values normalized so that threshold for the two cases occurs at the same value of A/A_T. The pumping flux in the rod at threshold should be roughly equivalent for the two cases irrespective of how much aperture area was required to produce it or what portion of the mirror was used. The dashed curve thus represents the laser performance that would have been obtained had the pumping efficiency at $A/A_T = 0.27$ (mirror diameter = 14.5" with 7" obscuration) been maintained as the telescope aperture was opened. Extending the dashed curve to the full telescope aperture indicates that an output power of 6 watts could have been obtained had the pumping efficiency at $A/A_T = 0.27$ been maintained. Definite quantitative conclusions should not be drawn from these experimental curves; however, it is clear that significant improvement in laser performance is possible by minimizing the angle dependent loss mechanisms. The pumping efficiency for the full 24" aperture relative to the efficiency at $A/A_T = 0.27$ is found from the ratio of the A/A_T values at $P_{out} = 1.5$ watts for the dashed curve and the solid curves. This value is 0.53; the pumping efficiency is significantly decreased as the mirror diameter increases due to the angle dependent loss mechanisms. These results are important in predicting the mirror diameter required outside the earth's atmosphere for a given laser performance.

The sun pumped laser performance described above was obtained using the cold mirror dielectric coated secondary. This mirror, in addition to rejecting IR radiation above 0.9μ and U.V. radiation rejects about 60% of the solar energy coinciding with the laser rod's chromium pumping bands. Since the sun spectrum peaks in this region at 0.5μ t' mirror rejects a substantial amount of useful pump light. The laser was also operated with a silver coated secondary mirror, which is highly reflecting over the entire sun spectrum, in

47
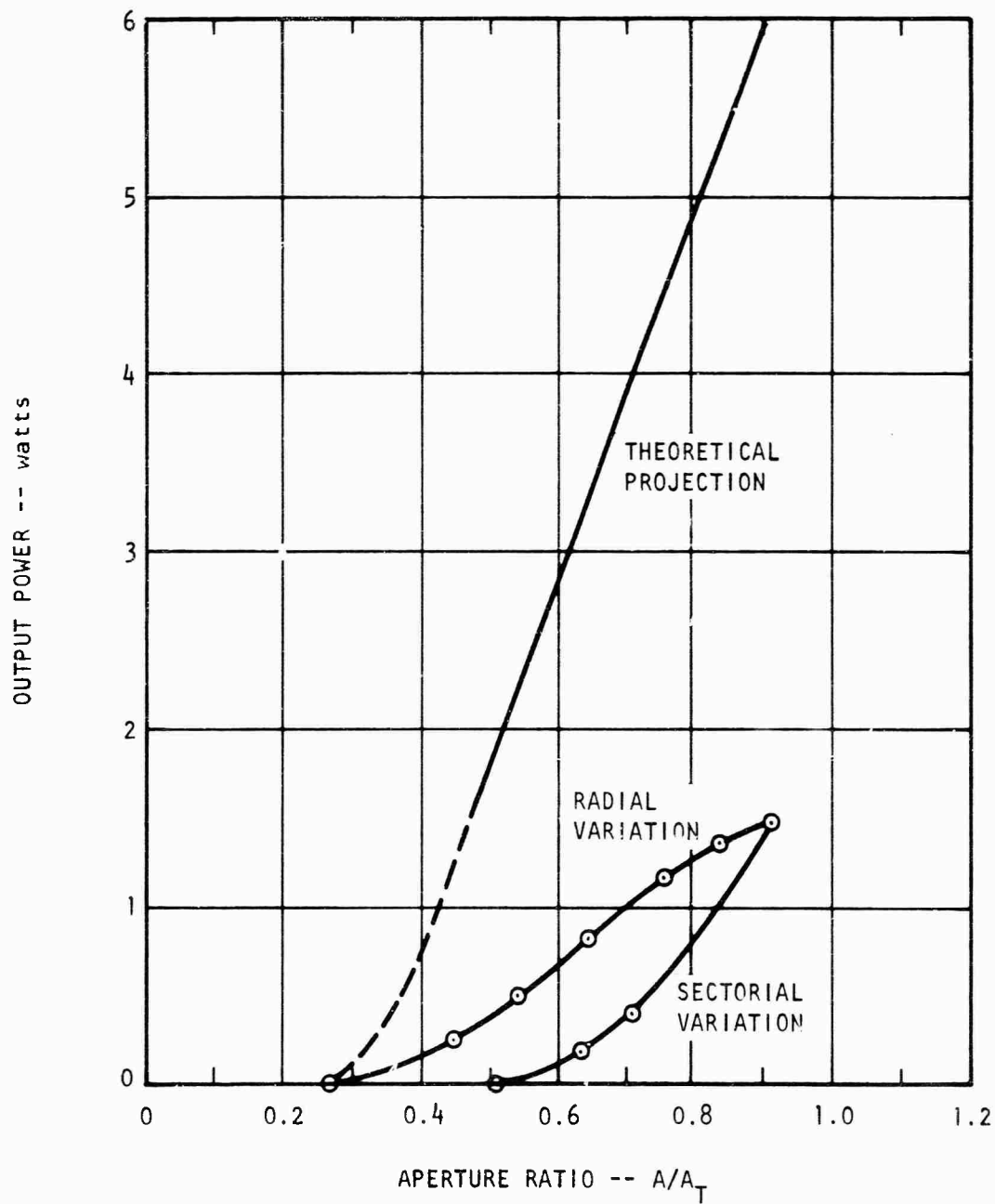
Figure 29 Sun Pumped Laser Output Power as a Function
of Telescope Aperture

order to evaluate the contribution of the chromium excitation. Figure 30 shows the laser performance with both the silver secondary mirror and the dielectric coated secondary. The experiments with the two mirrors were performed successively on the same day to minimize any variation due to change in the solar intensity. The laser rod temperature in both cases was maintained at about $100^{\circ}F$ for all values of A/A_T. The laser was not operated above $A/A_T = 0.45$ with the silver mirror because the rod temperature could not be maintained at $100^{\circ}F$ for telescope openings larger than this. Roughly, twice as much heat is dissipated by the rod heat sink with the silver mirror. Figure 30 shows that the laser performance with the silver mirror is significantly better than with the cold mirror indicating that a substantial portion of the light absorbed by the chromium ions is converted to 1.06μ fluorescence. Threshold with the silver mirror is about 35% lower than with the dielectric secondary; and an output of 1.2 watts is obtained with just under half the telescope area as opposed to 0.5 watts output with the cold mirror.

Modelocked operation of the sun pumped laser at a rate of 500 MHz was demonstrated using the modulator discussed in Section 1 and Appendix III. Insertion of the modulator in the laser cavity reduced the laser output to 0.35 watts. This decrease in output is attributed primarily to the polarization of the laser by the Brewster angle $LiNbO_3$ modulating crystal. The modelocked pulses were relatively long, about 1 nsec. and the operation was fairly unstable. A photograph of the oscilloscope trace showing the modelocked laser output as a function of time is shown in Figure 31. In these tests an RF power of 0.5 watts was required to drive the modulator. The long pulse length and instability are believed to be due mainly to the multimode operation of the laser and intra-cavity etalon effects caused by the etalons formed by the rod ends and the laser mirrors. These results indicate, however, that modelocked operation of the sun pumped laser is entirely feasible. Substantial improvements discussed in Section VII.

The time dependence of the CW laser output (modulator not in the laser cavity) was also observed by displaying the recorder output of the CRL Model 212 power meter on an oscilloscope. The oscilloscope trace shown in Figure 32 was taken with the laser operating at the 1.5 watt output level with the dielectric coated secondary. The laser output is predominantly continuous with a small intermittent ripple superimposed on the CW component. The ripple in Figure 32 is on the average about 0.1 volts peak to peak, and the zero of this ripple was 1.1 volt above the zero laser output base line. The ripple thus amounts to $\pm$ 5% of the laser output. The ripple was very sporadic, however, occurring in short bursts lasting less than a second. The laser ran several seconds at a time between bursts. Between ripple bursts the variation in the laser output was so small it could not be observed on the highest gain scale of the oscilloscope. This behavior may be due to mechanical instability but a definite cause was not isolated. The spiked laser output common to Nd:YAG laser rods co-doped with chromium was not observed, and this is probably due to the relatively low chromium doping level (0.1%) in our case. This is significant since spiking in the output would be detrimental in a PCM communication system.

With the 2% transmitting, 60 cm radius output mirror used to obtain the maximum power output of 1.6 watts the full angle divergence of the laser beam was measured to be about 6 mrad. The laser output is very high order

49
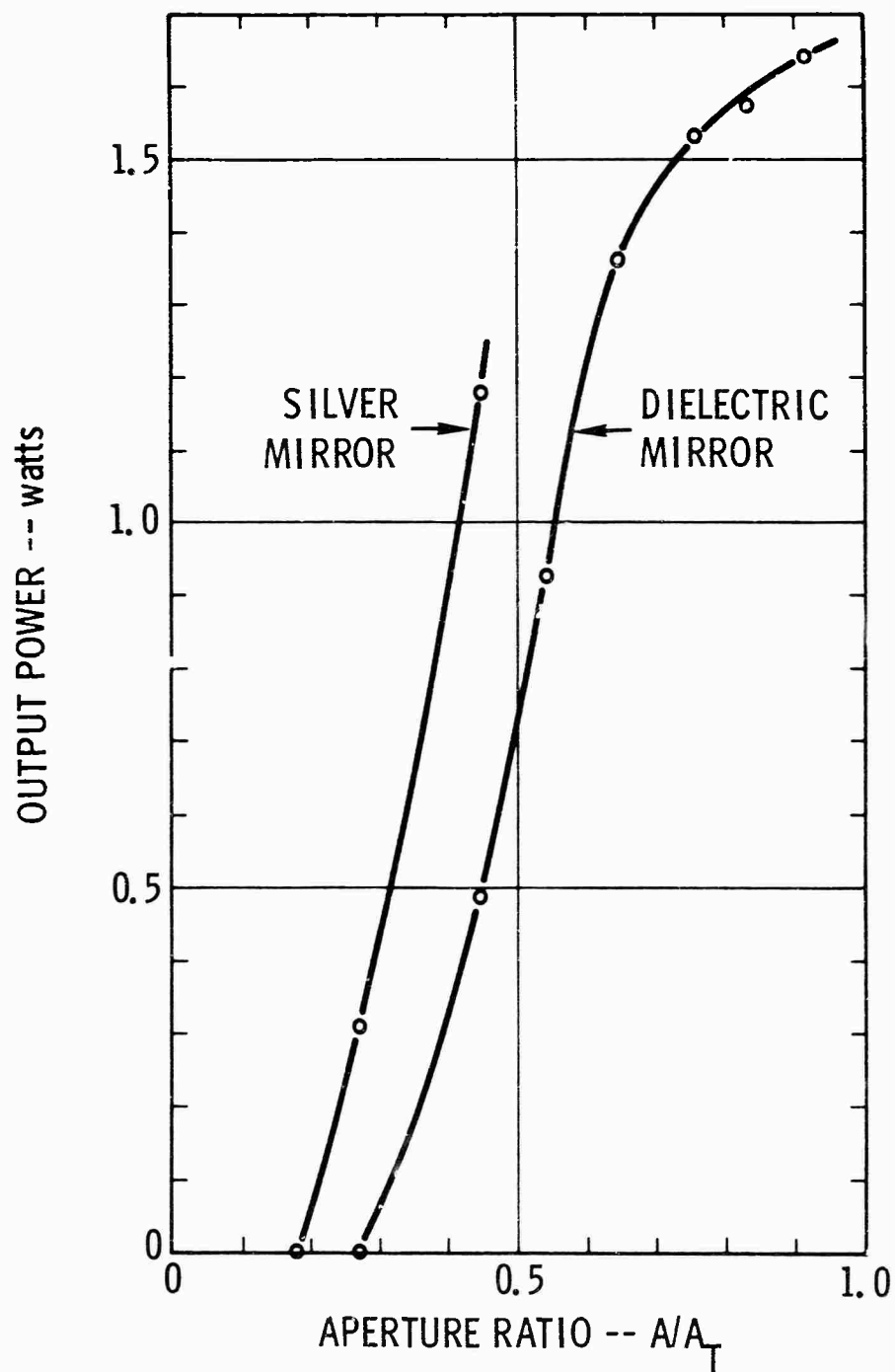
Figure 30   Sun Pumped Laser Performance with Silver
and Dielectric Coated Secondary Mirrors
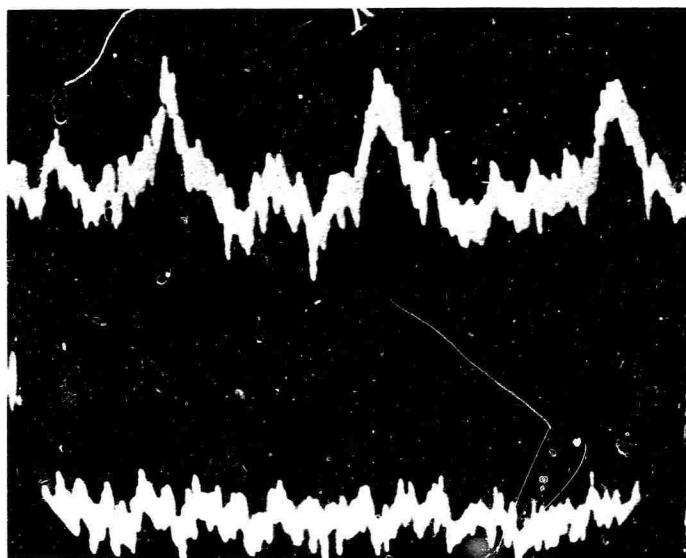
Figure 31.   Mode Locked Laser Output as a function
of Time (pulse rate is 500×10^6 pps)
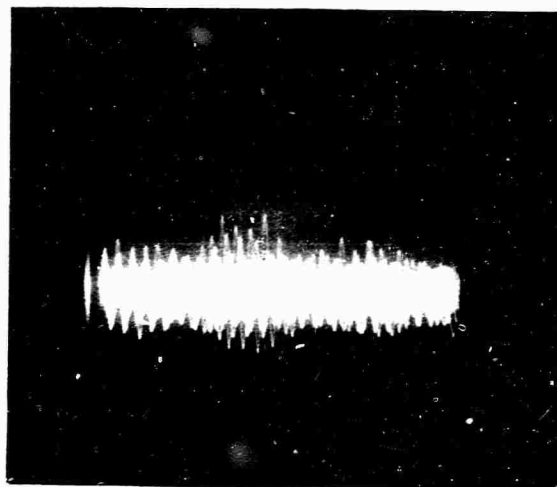
Figure 32.   Time Dependence of the CW Laser Output-
(Time scale 50 μ sec/div, vertical scale
0.05 volt/div ; ripple burst center line is
1.1 volt above laser output zero base line)

multimode with this mirror. Several attempts were made to operate the laser with a flat output mirror in order to increase the diameter of the fundamental mode and reduce the mode order. Lasing with a flat mirror could not be obtained. Using a 1.3% transmitting mirror with a 145 cm radius of curvature and a 0.060" dia. aperture in the laser cavity, 0.22 watts output was obtained in the TEM_{01} mode. The laser output with this mirror and no aperture in the cavity was 0.8 watts. Very unstable laser operation was briefly obtained with a 3% transmitting, 7 meter radius output mirror. A thorough study of the mode structure and beam divergence of the laser was not possible with this mirror because the operation was so unstable. However, the mode order of the beam was considerably lower than with the 60 cm radius mirror. Further study of the mode structure and beam divergence with output mirrors of varying radii of curvature and the optimum mirror transmission is required, in order to obtain low order mode operation of the laser.

Section V

THEORETICAL ANALYSIS OF SUN PUMPED LASER PERFORMANCE

Foster[10] developed a theoretical model of the CW Nd:YAG laser which predicts how the laser performance is related to and varies with the various physical parameters of the laser. The analysis is presented in Appendix IV. In this section we will apply this model to the experimental results and we will determine how the laser performance varies with two important parameters, the laser rod diameter and the intracavity loss.

The laser is characterized by the following equations:

$$P_{out} = \eta_d \, [P_{in} - P_{th}] \tag{1}$$

$$\eta_d = \frac{KT}{\alpha\beta} \tag{2}$$

$$P_{th} = P_o + \frac{\alpha}{K} \tag{3}$$

$$T_{op} = 2 \left(\sqrt{g_o \alpha_o} \right) - \alpha_o \tag{4}$$

$$\alpha = T/2 + \alpha_o \tag{5}$$

$$g_o = K(P_{in} - P_o) \tag{6}$$

where

T = total transmission through both laser mirrors

g_o = small signal gain

α_o = single pass dissipative loss

β = gain saturation parameter

In terms of basic physical quantities the parameters K for the two cases of side pumping and end pumping are given by

side pumping

$$k_{sp} = \frac{1}{d} \left(\frac{\beta A}{2} \right) \left(\frac{N_1 \sigma_p \eta}{2} \right) \left(\frac{\lambda p}{\lambda L} \right) \, k_p k_r \tag{7}$$

Preceding page blank

<u>end pumping</u>

$$k_{EP} = \left(\frac{\beta}{2}\right) \left(\frac{N_1 \sigma_p \eta}{2}\right) \left(\frac{\lambda p}{\lambda L}\right) k_p k_r L_M \left(1 - e^{-2/L_M}\right) \tag{8}$$

For the end pumping case L_M is the crystal length for which the pump light is attenuated by 1/e. Since $1/L_M = \sigma_p N_1$ we have

$$K_{EP} = \left(\frac{\beta\eta}{4}\right) \left(\frac{\lambda p}{\lambda L}\right) k_p k_r \left(1 - e^{-L/L_M}\right)$$

If the laser rod is much longer than L_M ($L \gg L_M$) we have

$$K_{EP} = \left(\frac{\beta\eta}{4}\right) \left(\frac{\lambda p}{\lambda L}\right) k_p k_r \tag{9}$$

This is a good assumption in our case as seen in Figure 17 since most of the incident useful pump light is absorbed in the first half of the crystal. It should be noted that this result for K_{EP} has been derived assuming the incident pump light is in a uniform collimated beam. This is, of course, not the case for the end solar pumped laser, but the formalism should still apply. The lamp conversion efficiency factor, k_r, does not apply for the sun pumping case since we are dealing with optical power at the outset. The efficiency factor k_p may be interpreted here as the fraction of sunlight incident on the telescope which enters the laser rod. For end pumping note that the slope efficiency is not dependent on the rod dimensions since

$$\frac{K_{EP}}{\beta} = \frac{\eta}{4} \left(\frac{\lambda p}{\lambda L}\right) k_p = K^* \tag{10}$$

This expression for K^* depends only on basic laser material properties and the optical collection and relay efficiency.

For the sun pumped laser case it is convenient to write the equations which describe the operation of the laser in terms of the telescope aperture instead

56

of input power. Therefore let

$$P_{in} = A_p A^r \tag{11}$$

$$P_{th} = A_p A^r_{th} \tag{12}$$

where $A^r = A/A_T$ is the telescope aperture area normalized to the area of the
24" collector. We then have

$$P_{out} = \eta_d \left(A^r - A^r_{th} \right) \tag{13}$$

$$\eta_d = \left(K^* A_p \right) \frac{I}{\alpha} \tag{14}$$

$$A^r_{th} = \frac{\alpha A}{2(K^* A_p)} \frac{2}{\beta A} \tag{15}$$

$$g_o = \frac{2}{A} \left(K^* A_p \right) \left(\frac{\beta A}{2} \right) A^r \tag{16}$$

For sun pumping P_o is of course equal to zero.

Let us apply the model to the experimental results obtained with the
silver secondary mirror shown in Figure 30. The model is not strictly valid
here because as we mentioned above the pump coupling efficiency varies as the
aperture is varied radially. For values of A/A_T from 0 to 0.4, however, this
variation should be small. This assumption is born out by the behavior of the
P_{out} vs A/A_T curves with radial aperture variation; the slope efficiency (de-
fined here as P_{out} divided by differential A/A_T) does not start to decrease
until $A/A_T \sim 0.6$. From the silver mirror data of Figure 30 we find that
$\eta_d = 5.3$ and $A^r_{th} = 0.22$. The output mirror transmission was $T = .02$ and the
diameter of the rod was 3 mm. From equation (14) we calculate

$$\frac{\alpha}{K^* A_p} = 3.78 \times 10^{-3} \tag{17}$$

57

Assuming an intracavity single pass dissipative loss, α_o, of 0.006 we then have

$$K*A_p = 4.25 \tag{18}$$

From equation (15) and the calculated value of $\alpha/K*A_p$ we find

$$\left(\frac{2}{\beta A}\right) = 1660 \text{ watts/cm}^2 \tag{19}$$

Applying this model to a variety of lamp pumped laser data, Foster calculated a value for $2/\beta A$ of 1500 watts/cm^2. Our result here is thus in good agreement with his.

From equation (16) and the calculated values of $K*A_p$ and $\left(\frac{2}{\beta A}\right)$ we find that for a value of $A/A_T = 0.4$ the small signal gain, g_o, is equal to 3%. The sun pumped laser at the one watt level is a low gain device.

Equations (14) and (15) show that the laser slope efficiency is independent of rod diameter but the threshold varies inversely with the cross sectional area of the rod. The gain also varies inversely with the cross sectional area. For any given intracavity loss substantial improvement in laser performance is obtained by using a smaller diameter laser rod. For example, from Figure 30 we note that a 1 watt laser output is obtained for a value of $A/A_T = 0.4$. Assuming the same α_o of 0.006 we find that the same laser output is obtained for $A/A_T = 0.29$ using a 2 mm diameter rod. Alternatively, an output of 1.6 watts is predicted at $A/A_T = 0.4$ with the 2 mm rod.

Figure 33 shows how the laser output power for $A/A_T = .5$ varies as a function of the single pass dissipative loss, α_o. A rod diameter of 3 mm was used in generating this curve and the optimum mirror transmission for each value of α_o was used in the calculation. This graph shows the striking dependence of low gain laser performance on the intra-cavity loss.

58
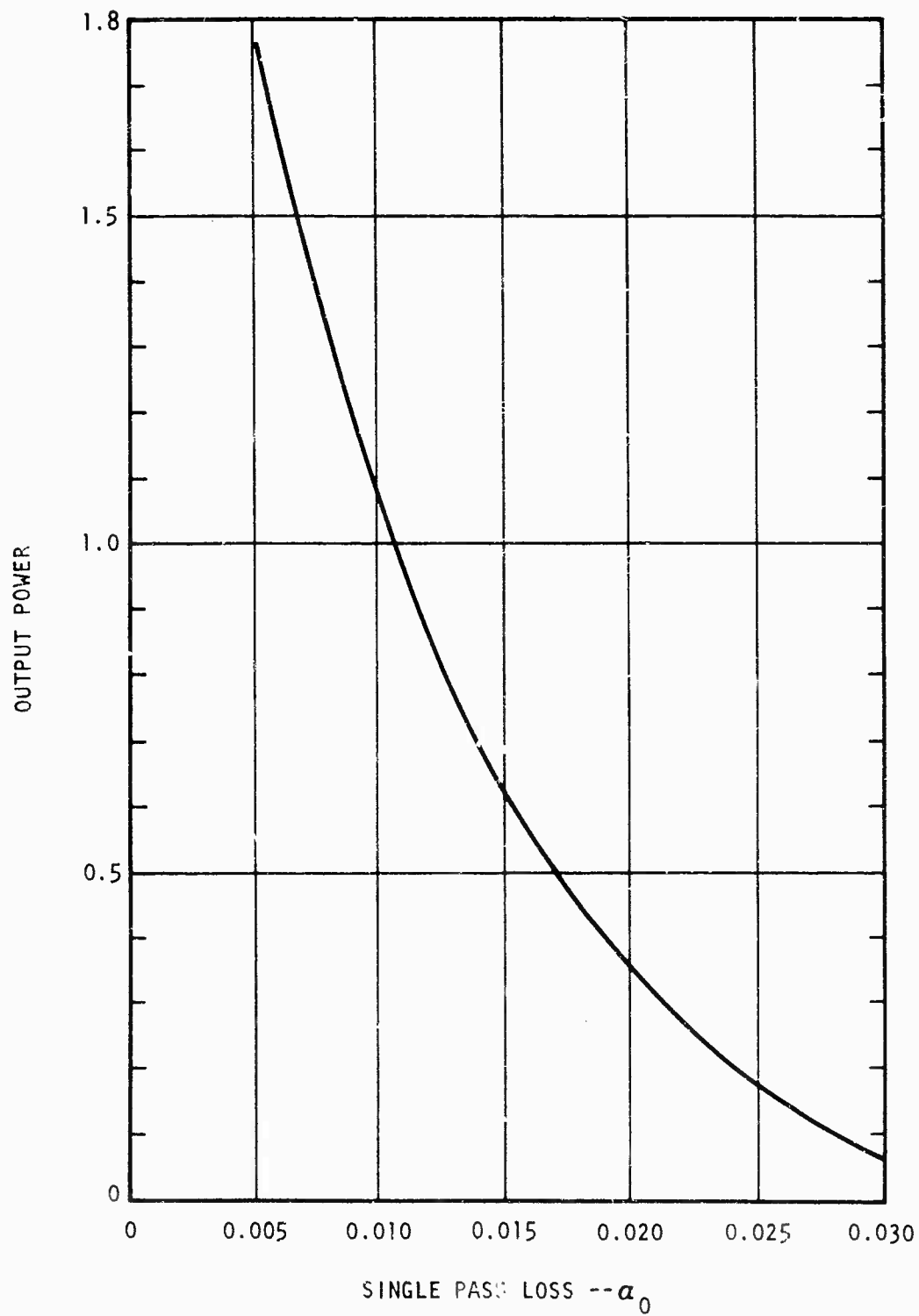
Figure 33 Calculated Sun Pumped Laser Output Power
as a Function of Intracavity Loss for $A/A_T = 0.5$

PREDICTED PERFORMANCE OF THE SUN PUMPED LASER
OUTSIDE THE EARTH'S ATMOSPHERE

We can use the present sun pumped laser performance data and the analytical results of Section V to predict what performance the laser will exhibit outside the earth's atmosphere. The laser output power is given by

$$P_{out} = \eta_d (A^r - A^r_{th})$$

For the silver mirror data of Figure 30 $\eta_d = 5.3$ and $A^r_{th} = 0.22$. This slope efficiency value is only valid for $A/A_T < 0.5$ since we know that the pump coupling efficiency decreases as the mirror diameter increases. Let us determine the laser output power in space for a mirror diameter of 12". Since the laser performance is improved with smaller rod diameters we will, of course, use a rod of less than 3 mm dia. with the 12" mirror. The smallest diameter rod we can consider, however, and use the data of Figure 30 to predict the laser performance is given by

$$d = 3 \left(\frac{12}{17} \right) = 2.1 \text{ mm}$$

We are making the reasonable assumption that the pump coupling efficiency of the optical system does not change if the ratio of the rod diameter and mirror diameter remains the same. With a 2 mm diameter laser rod, by equation the threshold is lower than that of the 3 mm rod by a factor of 2.25 and in space the sun intensity is greater than at sea level by a factor of $1/.63$; we will make the assumption that on the average, the spectral regions of the sun's radiation which pump the laser rod are enhanced by the same factor. Therefore, with a 2 mm diameter laser rod outside the earth's atmosphere, the data of Figure 30 predicts the performance of the laser will be given by

$$P_{out} = \frac{5.3}{0.63} \left[A^r - \left(\frac{.22}{2.25} \right) (0.63) \right]$$

For a mirror diameter of 12", $A^r = 0.25$ and P_{out} is calculated to be 1.6 watts.

It is important to recognize that this predicted power output of 1.6 watts is based on present sun pumped laser performance. Considerable improvement in the operation of the present device is expected to be obtained by better heat sinking resulting in lower temperature operation of the rod. Therefore, this prediction is a conservative one. Even when the losses

Preceding page blank

introduced with mode locked operation in the fundamental mode are considered,
it is still reasonable to expect that a laser output on the order of 1 watt
will be attainable outside the earth's atmosphere with a 12" diameter collector.

Section VII

DIRECTIONS FOR FURTHER WORK

In this section we consider the various areas where improvements can be made to enhance the sun pumped laser's performance. We have touched on some of the problems and shortcomings the present configuration exhibits in the above discussion and have indicated what can be done in some instances to improve the laser performance. In this section we will treat these design inadequacies in more detail and will indicate what effort can be spent toward refining the laser design.

1.   DUAL PUMPING

The laser cor ration using the open reflective cone which has demonstrated a power o of 1.5 watts cannot be simultaneously pumped by a lamp or diode array; tne heat sink entirely surrounds the laser rod. When this approach was implemented the effort was aimed exclusively at obtaining sun pumped laser performance since this was the basic objective of the program. There are two possible dual pumping configurations we have considered for use with end solar pumping. One is the design shown in Figure 11 in which a portion of the rod is completely surrounded by the heat sink and exclusively sun pumped and the remaining rod length is only partially contacted by the heat sink and lamp or diode pumped from the side in a reflective cavity. In the other design the rod is partially contacted by the heat sink its full length and the same portions are sun and lamp pumped. The second approach offers the advantage of utilizing a shorter laser rod. It also leads to an approximate cartesian rod thermal profile for both pumping situations which may have advantages in terms of mode control and depolarization losses.

Because of the importance of the dual pumping concept optimization of the sun pumped laser performance should proceed with the laser in a solar end pumping configuration which is compatible with lamp or diode pumping of the side of the laser rod. This approach is important because in most applications it is likely that the continuous operating capability afforded by dual pumping will be required. This can be accomplished with the present configuration by removing the heat sink cap which covers 2/3 of the rod circumference, removing the silver coating on the exposed portion of the rod and resoldering the rod into the 120° mounting groove. Sunlight entering the end of the rod at an angle to the rod axis and reflecting off the exposed portion of the rod is trapped inside the rod by total internal reflection since the bounce angle of the extreme ray (58.5°) is greater than the critical angle for YAG (33.5°). Solar end pumping experiments can then be performed with this configuration which is compatible with side lamp or diode pumping.

2.   CONDUCTIVE COOLING

It is fortuitous that the modification required to operate the laser in a dual pumped configuration should also allow the laser rod to operate at a lower temperature. With the heat sink cap removed only 1/3 of the previous

63

amount of power would be absorbed by the silver coating and dissipated by the rod heat sink. This assumes that the same silver coating is used; if the rod were resilvered with a higher reflectivity coating (which should be done) the heat dissipation would be still less. It is important to reduce the dissipation of waste heat by the rod heat sink in order to minimize the ΔT between the rod and the heat sink base thereby minimizing the operating rod temperature. It should be noted that this modification would result in better utilization of the useful pump energy in the solar spectrum as well. The sun rays reflecting off the exposed YAG-air interface would undergo only a small scattering loss instead of the 7% loss due to absorption by the silver coating. Improved laser performance should thus result from two effects: lower rod temperature and more efficient pumping.

The ΔT between the rod and heat sink base could also be lowered by reducing the thermal resistance between these two points. This could be done by reducing either the physical path length or increasing its thermal conductivity. Reducing the path length is a possibility in this case but the configuration should be compatible with dual pumping; placement of a reflective pump cavity over the rod and heat sink puts restraints on how close to the rod the cooling tube or heat pipe can be located. Increasing the thermal conductivity of the path could be accomplished by making the bulk of the heat sink out of a high thermal conductivity material such as copper and brazing a niobium rod mounting strip to the block. Consideration, however, would have to be given to the bi-metallic bending of this structure due to the expansion mismatch between the niobium strip and the block. It has been suggested that this effect may be relieved by slotting the copper block, a technique used in brazing metallic parts to ceramics.[14]

The thermal expansion match between niobium and YAG is excellent as pointed out above. The strain birefringence induced in the rod due to expansion difference between the heat sink and rod as the rod heats up should be negligible. The thermal expansion coefficient of indium which is used to solder the rod to the heat sink is about 6 times that of niobium and YAG, however. Since the rod and heat sink must be heated to the melting temperature of indium ($\sim 350°F$) in the soldering operation, residual-strain due to the expansion mismatch between the indium layer and the rod and heat sink may result after the structure is cooled. The sun pumped laser rod was examined between crossed polarizers after being soldered into its heat sink and did in fact reveal an irregular strain pattern. The magnitude of the birefringence was not determined, however, it is possible that this residual strain birefringence was responsible for most of the reduction in laser output when the mode locking modulator was inserted in the cavity. This residual strain problem should be examined more carefully in order to determine if it is important and if so what can be done to alleviate it. The laser rod's strain birefringence should be measured before and after the soldering operation. Also, the reduction of the laser output with the insertion of a polarizing Brewster plate should be determined. This should be done with the plate at various orientations since the strain will be angle dependent. These measurements should indicate the magnitude of this effect and how to reduce it.

64

3.   FUNDAMENTAL MODE OPERATION

In an optical communication system it is desirable for the laser transmitter to operate in the fundamental mode for several reasons. Smaller optics can be used to obtain a given beam width. A greater modulation depth can be achieved with an electro-optic modulator since the beam can be focused to a smaller size in the modulating crystal. A thinner crystal can thus be used which makes possible larger electric fields in the crystal. Shorter pulses with greater pulse to pulse amplitude stability can be obtained from a mode-locked laser. Finally, TEM_{oo} mode operation is required in a single frequency system with respect to modulation and demodulation of the carrier as well as obtaining single frequency operation of the laser.

Some work toward obtaining TEM_{oo} mode operation of the sun pumped laser has been done as discussed in Section IV above. Basically what is required is the determination of the radius of curvature of the output mirror and the diameter of the intracavity aperture necessary to obtain fundamental mode operation. Because of the influence of the rod cooling geometry on the mode properties of the laser this study should be performed with the laser in the dual pumping configuration. Thermal focusing is not expected to be important at the low power levels involved here; nonetheless, calculations should be made to determine if figuring the rod ends slightly would be expected to increase the fundamental mode volume in the rod and the TEM_{oo} output power. The method and geometry of the heat removal from the laser rod in the sun pumped laser should make TEM_{oo} mode operation more easily attainable than in conventional water-cooled lasers. Since heat is removed from one side of the rod in the conductive cooling scheme, the isotherms will be nearly linear with an approximately Cartesian temperature distribution. Depolarization of the TEM_{oo} mode and resultant conversion to higher order modes due to thermally-induced birefringence is not as severe in the Cartesian case[15]. Furthermore, conductive cooling is more uniform than fluid cooling through a jacket surrounding the rod. Random fluctuations in the temperature over the surface of the rod due to eddies in the fluid flow have been observed to impair TEM_{oo} mode operation in conventional lasers[16]. This effect is not present in a conductively cooled laser.

If we assume that focusing effects in the rod are small, the laser cavity design simply involves selection of the correct resonator mirror curvatures to produce a nearly collimated beam 1 to 2 mm in diameter inside the rod. A circular aperture stop placed inside the cavity produces selective loss for the higher order modes, which have larger diameters than the TEM_{oo} mode. Since the expected laser gain is only a few percent, there is no difficulty in producing sufficient loss to the higher order modes to prevent their oscillation. It should be noted, of course, that any aperture capable of suppressing the TEM_{01} mode, for example, will also produce some diffraction loss for the TEM_{oo} mode.[11]

Postulating a collimated gaussian beam of spot radius w_o and wavelength λ at the rod center, the beam radius w and wavefront radius R are

given by the equations

$$w(Z) = w_0 \sqrt{1 + \frac{\lambda Z}{\pi w_0^2}^2}$$

$$R(Z) = Z \sqrt{1 + \frac{\pi w_0^2}{\lambda Z}^2}$$

at any other point Z from the rod center. At the laser mirrors the wavefront must be tangent to the mirror surface; hence by evaluation of $R(Z_1)$ and $R(Z_2)$, where Z_1 and Z_2 are the distances from the rod center to the mirrors, one can readily design the resonator. A slight modification in $R(Z_1)$ and $R(Z_2)$ to include refraction out of the rod ends can easily be included in the calculation. Automatic design techniques for rapid digital computer calculation of spot sizes and wavefront radii even in the presence of distributed focusing by thermal effects in the laser rod are available. The losses imposed by the mode control requirement and the power attainable in the fundamental mode must be determined ultimately by experiments, however, because they depend critically on the gain and optical quality of the rod material.

4. MODE LOCKED OPERATION

Mode locked operation of the sun pumped laser was demonstrated with the electro-optic modulator discussed in the appendix, proving the feasibility of mode locking a low gain laser with this technique. The mode locked performance of the laser must be improved, however; shorter pulses with improved long term and pulse to pulse amplitude stability are required. There are three basic effects which are believed to have impaired the mode-locked operation of the laser: multimode operation intra-cavity etalons, and mechanical instabilities in the laser structure.

Since each transverse laser mode has its own set of longitudinal modes at a frequency slightly displaced from the frequency of any other set of longitudinal modes, phase locking the longitudinal modes of a multi-transverse-mode laser results in unstable operation and lengthened pulses. The mode-locking modulator cannot efficiently transfer energy from one set of longitudinal modes to another, and will only couple together well the longitudinal modes of one particular transverse mode. As a result the laser will operate with many modes oscillating, but the modes actually locked together will be few and constantly changing. The laser output under these circumstances will consist of an unstable pulse train of very long pulses.

Once a laser has been constrained to operate in only one transverse mode, shorter pulses are obtained by locking together as many longitudinal

66

modes as possible. In a well-mode-locked laser, the modulator actually trans-
fers enough energy to modes outside the normal oscillating line width to cause
them to oscillate in phase with the central modes. Any perturbation which favors
one longitudinal mode over another counteracts the effect of the mode-locking
modulator and degrades the quality of the mode locking. In particular, any
intra-cavity etalon discriminates markedly against some longitudinal modes and
makes it much more difficult to lock those modes. As a result only the favored
modes will be locked and the laser will produce much longer pulses than it would
in the absence of intra-cavity etalons. In some cases intra-cavity etalon ef-
fects are sufficient to prevent mode-locked operation entirely.

The mechanical stability of the laser cavity itself is very important
in a mode-locked laser. The mode-locking modulator transfers energy among the
longitudinal modes of the laser, and since the frequency spacing of these modes
is dependent on the length of the laser cavity, any instability in the cavity
length will produce an instability in the output pulse train.

The initial demonstration of mode locking the sun-pumped laser achieved
its objective of demonstrating the feasibility of mode locking a low-gain laser
with an electro-optic phase modulator. Subsequent work is necessary to improve
the quality of mode locking obtained in this laser by eliminating the three
deleterious effects discussed above. Specifically, single-transverse-mode
operation of the sun-pumped laser should be obtained in a mechanically stable
laser cavity. Any intra-cavity etalon effects should be eliminated by tilting
all surfaces, including the faces of the Nd:YAG laser rod, slightly off normal.
Under these circumstances the laser should be capable of producing very short
and stable pulses with the modulator which has already been demonstrated.

Section VIII

REFERENCES

(1)   D. F. Nelson and N. S. Boyle, "A Continuously Operating Ruby Optical Maser," Applied Optics, March 1962, Vol. 1, No. 2.

(2)   G. R. Simpson, "Continuous Sun-Pumped Room Temperature Glass Laser Operation," Applied Optics, June 1964, Vol. 3, No. 6.

(3)   C. G. Young, "A Sun Pumped CW One-Watt Laser," Applied Optics, June 1966, Vol. 5, No. 6.

(4)   "Solar-Pumped Laser," Final Technical Report, Contract NAS9-3671.

(5)   "Investigation and Development of a Sun-Powered Laser Transmitter," Final Technical Report, Contract AF33(616)-8025.

(6)   "Experimental Verification of Sun-Pumped Laser Transmitter," Final Technical Report, Contract AF33(657)-8619.

(7)   "Sun-Pumped Laser," Final Technical Report, Contract AF33(615)-1899.

(8)   J. L. Threlkeld Thermal Environmental Engineering, Prentice-Hall, Inc., Englewood Cliffs, N. J., Chapter 13.

(9)   See any basic geometrical optics text, for example, Optics, by F. W. Sears, Addison-Wesley Publishing Co. Inc., Cambridge, Mass.

(10)   Final Technical Report, "Space Qualified Nd:YAG Laser," by J. D. Foster and R. F. Kirk, NASA Contract No. NAS12-2160.

(11)   H. Kogelnik and T. Li, "Laser Beams and Resonators," Applied Optics, Vol. 5, pp 1550-1567, Oct. 1966.

(12)   M. E. Graham, et al., "Immersion Liquids for Ruby Lasers," Applied Optics, Vol. 4, No. 5, May 1965.

(13)   Final Technical Report, "Optical Pumps for Lasers," by L. Noble, J. Moffat, L. Reed and J. Richter, ECOM Contract DAAB07-70-C-0035.

(14)   L. Noble, private communication.

(15)   J. P. Segre, Journal of Quantum Electronics, QE-2, 6, 342, June 1969.

(16)   R. B. Chesler, "A Stabilizing Sleeve for the Nd:YAG Laser," Applied Optics Vol. 9, No. 9, Sept. 1970.

Preceding page blank

APPENDIX I

EVALUATION OF LASER ROD - TRUMPET BOND FAILURE

Verification that breakdown of the epoxy was responsible for the failure in the initial attempt to operate the laser with the YAG trumpet was accomplished in the following manner. The damaged small end of the trumpet was ground flat and polished. A polished piece of clear YAG was bonded to the trumpet using the Epo-Tek 301 epoxy and the assembly was placed at the focus of the telescope. The bond failed after about 5 minutes exposure to the focused solar radiation. The failure of the epoxy is believed to be due to thermal breakdown which begins as a slight discoloration of the epoxy layer. Once this discoloration begins the layer becomes very absorbing and heats quickly in a runaway manner which results in rapid disintegration of the layer.

Thermal breakdown of the epoxy can only occur through excessive heating of the bond layer caused by absorption of the incident sunlight. This was originally thought to be no problem since a thin layer of Epo-Tek 301 is essentially non-absorbing between 0.3 and 2.6μ as seen in Figure 34 and the amount of solar energy outside the spectral region where the thin epoxy layer absorbs is minimal. The absorption spectrum of a 1 cm length of the epoxy reveals, however, significant absorption in the short wavelength region of the visible and in the near IR (Figure 35). Thus, a layer that is not sufficiently thin could be expected to absorb enough solar energy to result in thermal breakdown under exposure to the focused sunlight.

In order to estimate the temperature rise of the rod-trumpet bond, a simple thermal analysis of the heating of an epoxy layer between two cover plates may be performed. The epoxy layer is assumed to be thin with no transverse temperature variation so that the temperature variation in the epoxy layer is determined by the one dimensional heat flow equation

$$\frac{d^2 T}{dX^2} + \frac{W}{k} = 0 \tag{1}$$

where W is the heat generation rate and k is the thermal conductivity. Heat is assumed to be generated uniformly in the layer through absorption of incident sunlight. Equation (1) may be solved for the temperature in the middle of the epoxy layer, T_e, to yield

$$T_e = T_s + \frac{Q}{A}\left[\frac{d}{2k_c} + \frac{t}{8k_e}\right] \tag{2}$$
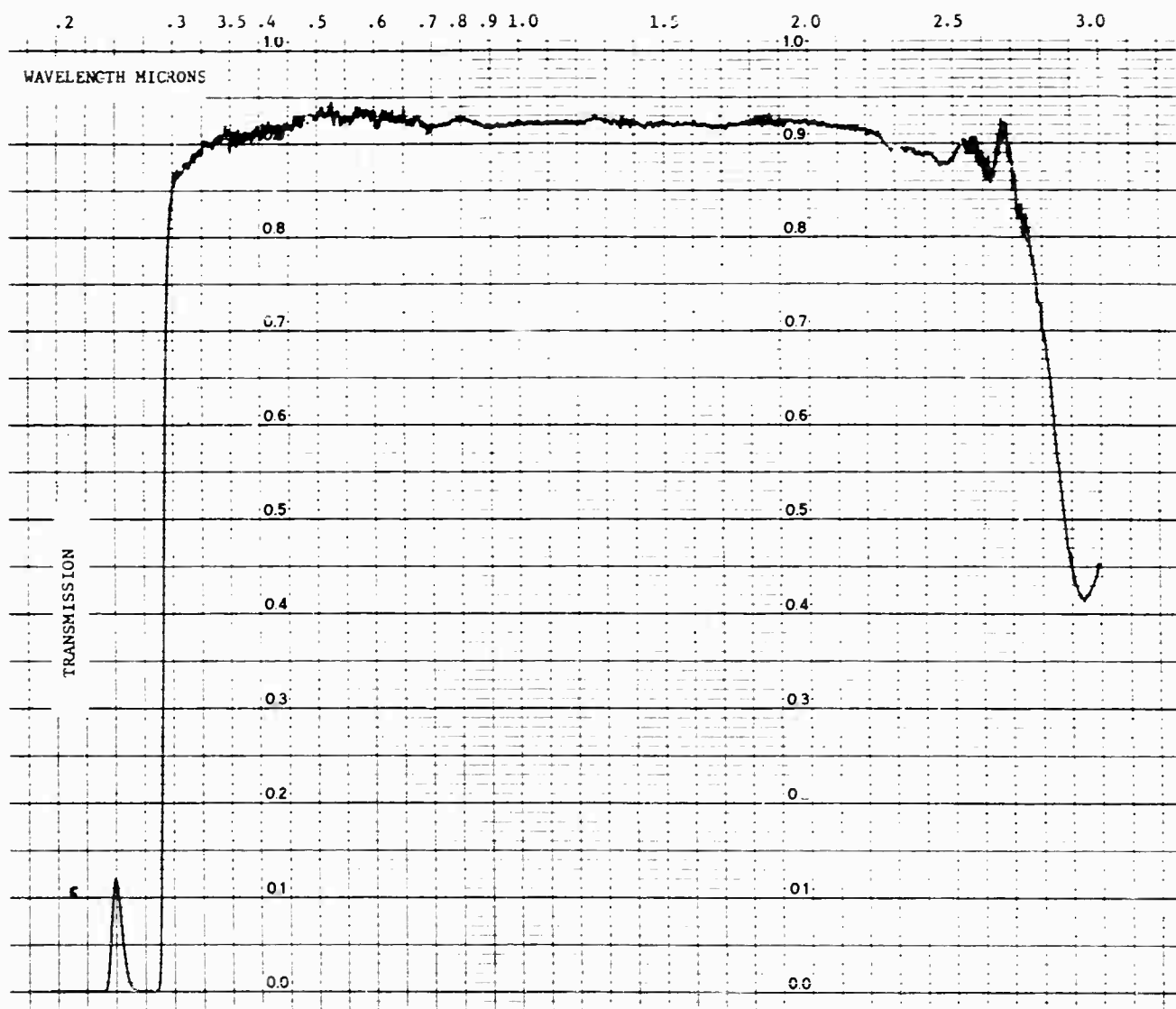
71

Figure 34   Transmission Spectrum of a Thin Layer of EPO-TEK 301
             Epoxy Between Quartz Plates (thickness = .0005")

Figure 35 Transmission Spectrum of a 1.0 cm Sample of Epo-Tek 301

where

T_s = outer surface temperature of the cover plates

Q = heat generated in the layer or the incident power absorbed

A = area of the layer

d = thickness of the cover plates

t = thickness of the epoxy layer

k_e = thermal conductivity of the epoxy.

The heat generated in the layer is given by

$$Q = t \int P_{in}(\lambda)\alpha(\lambda)d\lambda \tag{3}$$

where $\alpha(\lambda)$ is the absorption coefficient of the epoxy. We have made the approximation

$$1 - e^{-\alpha t} \approx \alpha t$$

which is true for small t. The integral in equation (3) was evaluated manually using the absorption spectrum of Epo-Tek 301 shown in Figure 35 and the exospheric solar spectrum, $P_{in}(\lambda)$. To account for atmospheric and collection losses $P_{in}(\lambda)$ was divided by a factor of 2. The result of this manual integration was

$$Q \approx 75 \cdot t \text{ watts} \tag{4}$$

Using this result for Q, the temperature T_e was calculated with values of $A = 0.0314$ cm^2 (2 mm diameter), $d = 1.0$ cm, $t = 1 \times 10^{-3}$ cm and $k_c = 0.14$ cm^{-1}°K^{-1} (the value for YAG). The model used with these values is representative of the rod-trumpet bond and thus should yield an approximation of its thermal behavior. The second term in the bracket in equation (2) was neglected since $t \ll d$. The value of T_e found from this calculation is

$$T_e = T_s + 10°C$$

where T_s is approximately room temperature. This quantitative result is not expected to be highly accurate because of the approximations made; however, it is evident that under the above conditions the temperature rise in a layer as thin as one hundredth of a mm can be significant. The conclusion to be made from this result is that the epoxy layer bonding the rod and trumpet was not sufficiently thin. Furthermore, the joint was surrounded by an internally silvered coupling sleeve. The thickness of the epoxy layer between the sleeve and the rod was on the order of 1 mil. Heating in this layer surrounding the

joint may have contributed to the failure. In any case the importance of making
the bond layer thin (with either an epoxy or an index matching fluid) is clearly
indicated. Furthermore, in bonding the trumpet to the rod, it is extremely im-
portant to remove all the excess epoxy surrounding the joint after the two are
pressed together. This excess epoxy spoils the total reflection inside the rod
and trumpet allowing substantial solar power to be transmitted through the excess
layer which is likely to be much thicker than the bond layer. This not only
reduces the amount of pump light which enters the rod, but can lead to failure
of the joint through heating in the thick excess layer.

These conclusions were substantiated by tests which were performed
to evaluate several epoxies and index matching fluids with respect to their
resistance to breakdown under exposure to focused sunlight. Thick and thin film
samples of both epoxies and fluids were tested by placing them at the 4 mm
diameter focal spot formed by the telescope mirror and an aspheric condensing
lens. This focal spot size resulted in a lower power density than would be
attained at the rod-trumpet bond; since the trumpet had been fractured in the
initial laser tests, it was not possible to achieve this solar power density.
Thin layers of the epoxies and fluids (t on the order of 0.1 mil) were sand-
wiched between quartz slides and placed at the focal spot. The following fluids
and epoxies were evaluated in this manner:

Fluids	Epoxies
Benzyl Benzoate	Epo-Tek 301
Glycerol	Stycast 1269A
$SnCl_2 \cdot 2H_2O$ in Glycerol	Stycast 1266
	Tra Cast 3010

All of these liquids and epoxies survived 10 minutes exposure to the focused
sunlight collected by the full telescope aperture except Benzyl Benzoate which
failed after two minutes exposure. This liquid, which is commonly used as
an index matching liquid in petrographic work, was therefore eliminated. The
solution of $SnCl_2 \cdot 2H_2O$ in Glycerol is useful because its refractive index
can be adjusted by changing the concentration of $SnCl_2 \cdot 2H_2O$.

Thick film samples of Epo-Tek 301 and Tra Cast 3010 were prepared
by spreading layers about 1 mm thick onto quartz slides with no top cover.
The Epo-Tek 301 sample failed immediately on exposure to 1/3 of the telescope
aperture. The Tra Cast 3010 sample survived five minutes at 1/3 aperture but
failed a few seconds after exposure to 2/3 aperture. These tests confirmed the
predicted importance of the layer thickness and suggest a method of more meaning-
ful evaluation of the samples with the reduced flux density. Since the tempera-
ture rise in the film is proportional to the incident light flux density and the
thickness of the layer, testing a 1 mm thick sample with a certain value of P_{in}/A
should be equivalent to testing a 0.01 mm sample with a flux density 100 times
greater. On this basis, the above results indicate that a thin film of Tra Cast
3010 should be able to withstand the full solar power collected by the telescope
concentrated into a 2 mm diameter area. This assumes, of course, that the break-
down of the epoxy is due to heating of the layer which is described qualitatively

75
.

by the simple analysis presented above. The equivalence would not apply if the failure mechanism were a process which depends only on the flux density or a combination of thermal breakdown and an intensity dependent phenomenon. UV degradation, for example, is a possibility; however, this is not likely since most of the UV energy was filtered out by the glass condensing lens. Further support of these conclusions were provided by the following series of tests.

Several thick film epoxy samples were prepared by sandwiching the epoxy between two glass microscope slides separated by a 0.015" thick teflon spacer. These samples were tested by placing them at the focal spot formed by the condensing lens and the telescope in the manner described above. Samples of Epo-Tek 301, Epo-Tek S-5, Tra Bond 2114 and Tra Cast 3010 all failed within a few seconds exposure of 1/3 of the telescope aperture. Since a thick layer of Tra Cast 3010 on a single quartz slide had previously withstood 5 minutes exposure at 1/3 aperture, it was concluded that the heat generated by the absorption of the glass slides was contributing to the failure of these samples. Filtering of the UV radiation was provided by the condensing lens; the additional heat generated in the slides was apparently due to the absorption of visible light (these particular microscope slides had a pale green tint).

Thick film samples were then prepared using quartz slides. Tests of several samples yielded the following results:

Stycast 1266	Failed 2 minutes after exposure of 1/3 aperture.
Tra Cast 3010	Withstood 5 minutes at 1/3 aperture. Failed after 1 minute exposure of 2/3 aperture.
Epo-Tek S-5	Failed 3-1/2 minutes after exposure of 1/3 aperture.
Tra Bond 2114	Withstood 5 minutes at 1/3 aperture. Failed a few seconds after exposure of 2/3 aperture.

These results with the quartz slides confirm the conclusion regarding the effect of the glass slides. The observations with both types of slides further indicate that the failure of the epoxy is due to thermal breakdown and not to UV degradation.

A 0.015" thick film sample of $SnCl_2 \cdot 2H_2O$ in Glycerol was also prepared in such a manner as to allow for expansion of the fluid. After a few seconds exposure of 1/3 of the telescope aperture, the liquid in the region of the focal spot boiled forming a bubble. The bubble was immediately replaced by cool liquid flowing into the region of the focal spot and in a few seconds the process repeated. No discoloration of the fluid was observed after this process was allowed to proceed several times. Since the amount of light absorbed by the epoxy films is comparable to that absorbed by the Glycerol solution, the boiling of the fluid indicates that quite high temperatures were attained in the focal

spot region of the thick film epoxy samples. Since the temperature rise in the thin epoxy film bonding the trumpet to the cooled laser rod will be much lower than in these thick film tests with samples cooled only by air convection, these tests indicate a high probability of success for either the epoxy bond or the use of the Glycerol solution as an index matching fluid in the end pumped laser configuration using the YAG cone.

Of the epoxies tested, Tra Cast 3010 and Tra Bond 2114 displayed the greatest resistance to failure in the focused sunlight. Tra Bond 2114 is the preferred epoxy because of its higher refractive index 1.554 as opposed to 1.476 for Tra Cast 3010. These refractive indices were determined by measuring the displacement of a Nd:YAG laser beam after passing through a wedge cell filled with the epoxies and are therefore the index values at 1.06μ. Transmission spectra of several of the fluids and epoxies tested are shown in Figures 36 through 40. These spectra are presented only to show the positions and relative strengths of the absorption bands and are not useful for determination of absolute absorption coefficients.

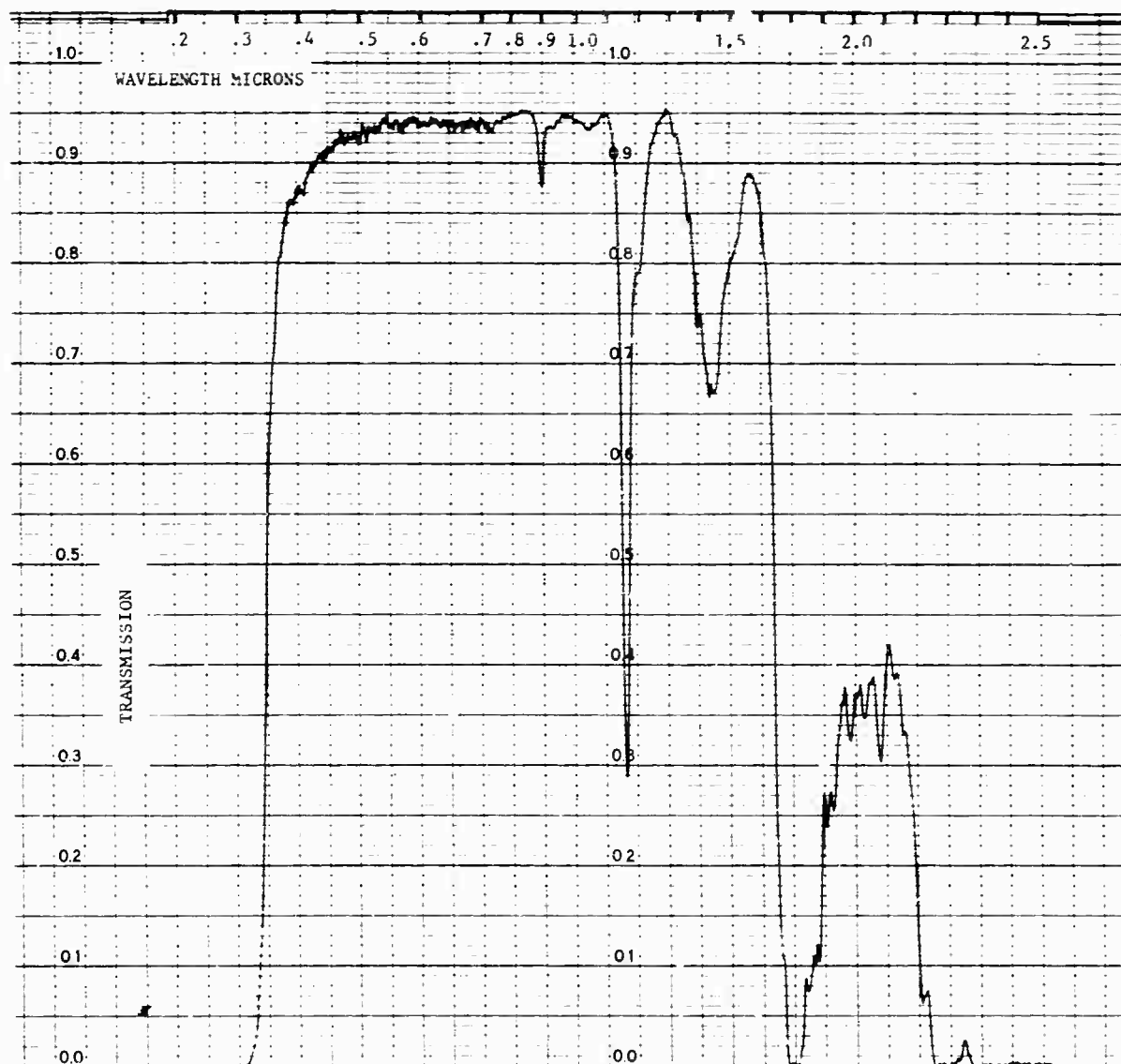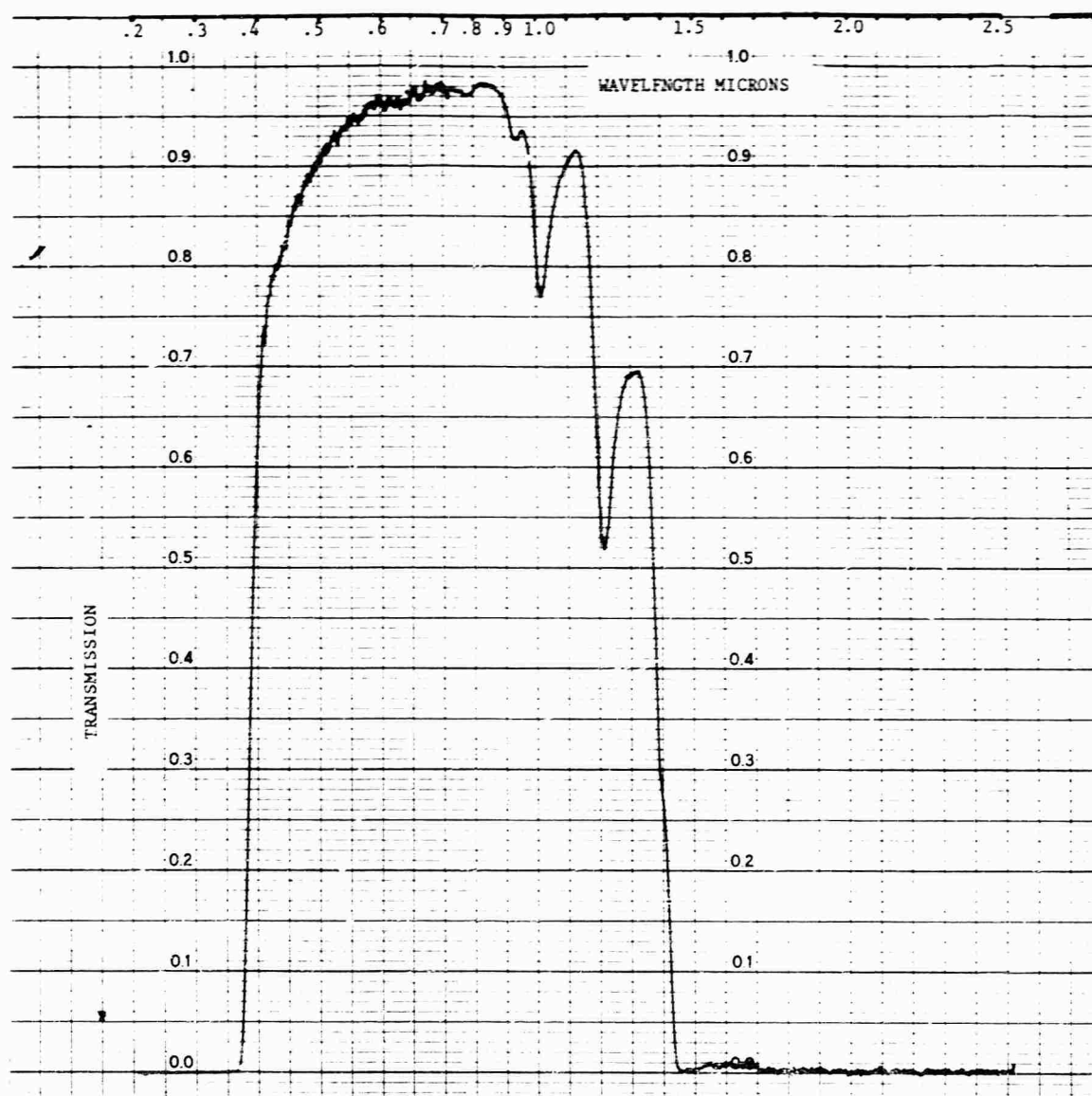Figure 36   Transmission Spectrum of Benzyl Benzoate (sample length = 1.0 cm)

Figure 37   Transmission Spectrum of $SnCl_2 \cdot 2H_2O$ in Glycerol (sample length = 1.0 cm)

79
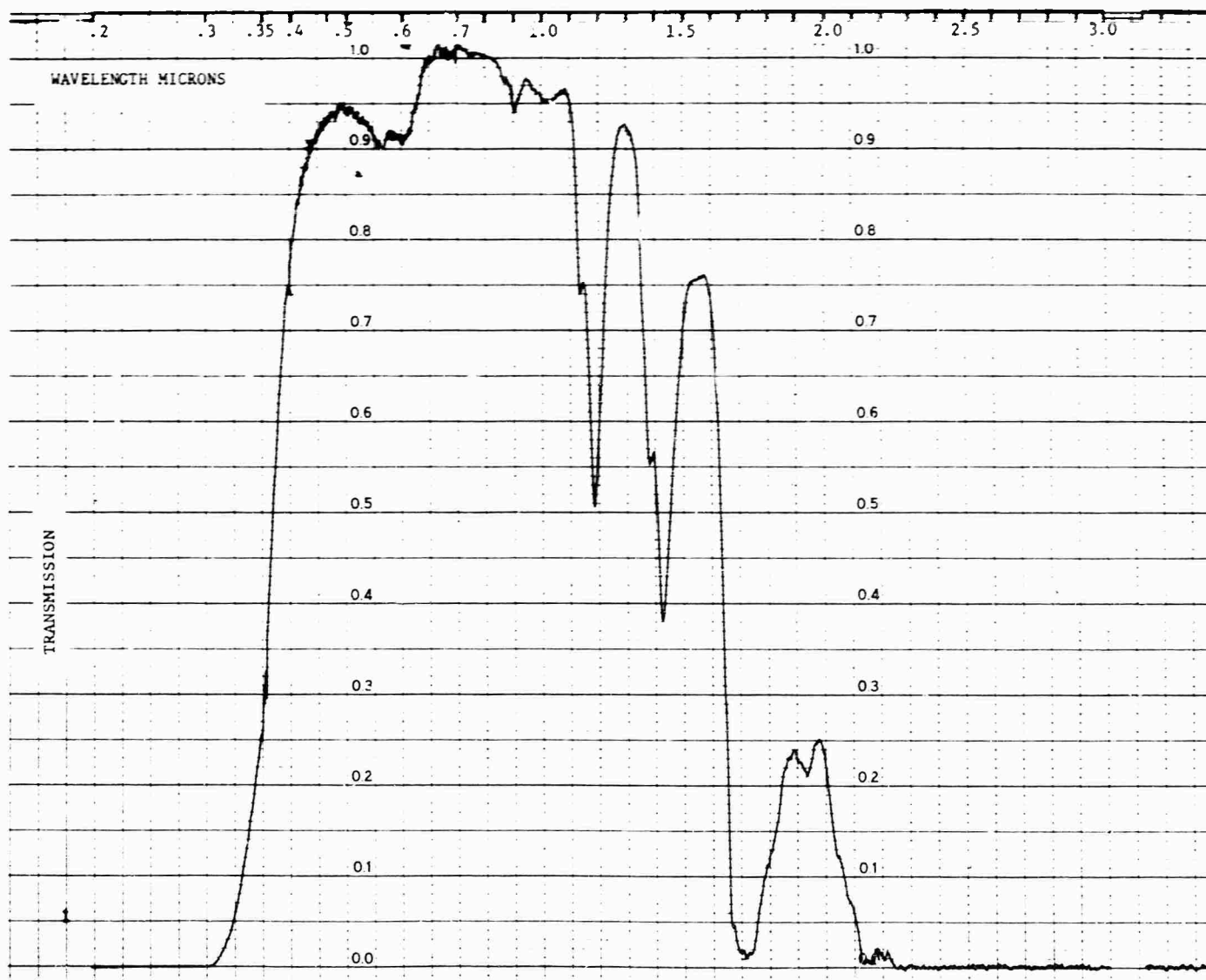
Figure 38 Transmission Spectrum of Stycast 1269A (sample length - 1 cm)

Figure 39   Transmission Spectrum of Tra Cast 3010 (Sample Length - 1 cm)
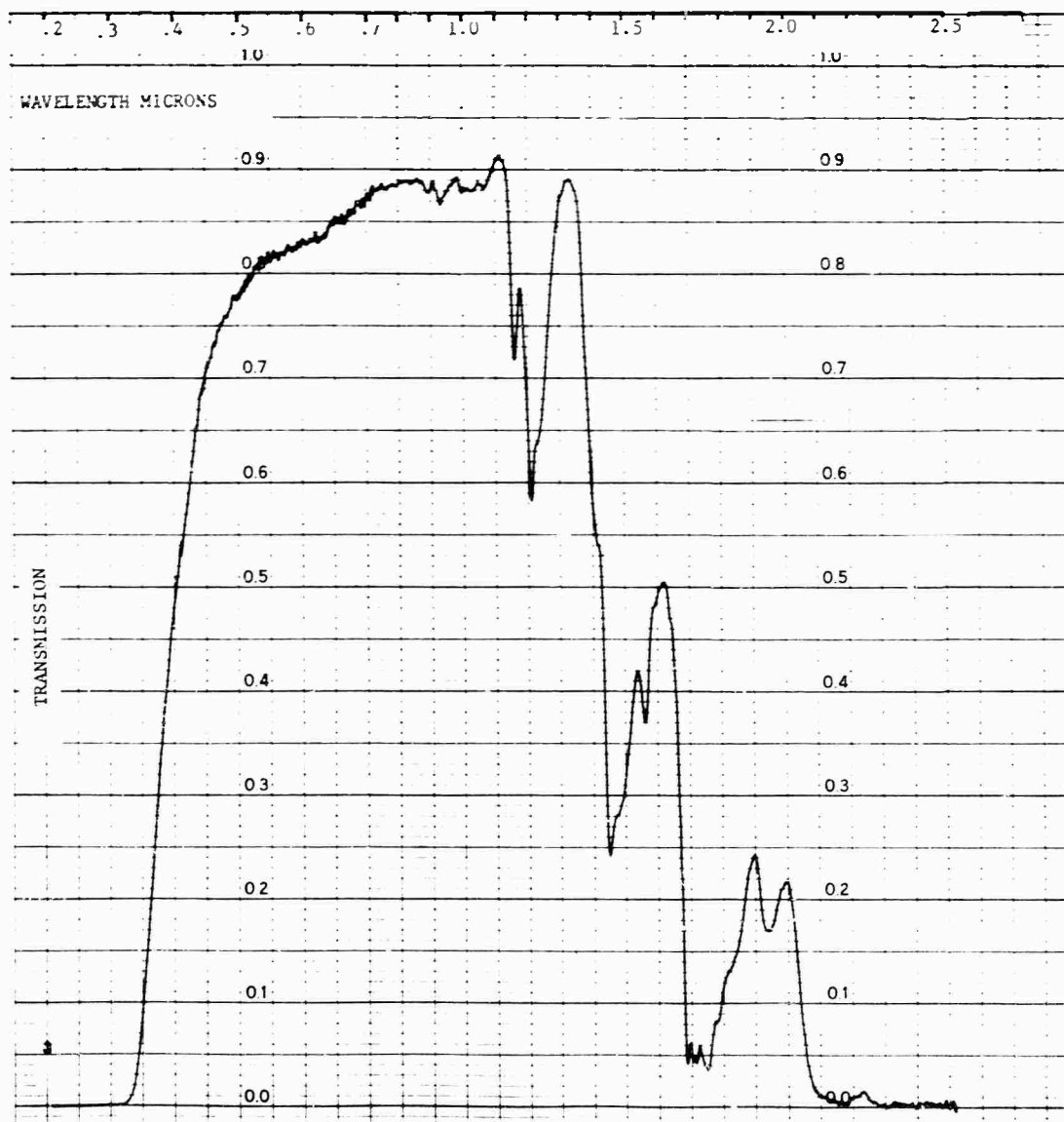
Figure 40   Transmission Spectrum of Tra Bond 2114 (sample length - 1 cm)

APPENDIX II

CONDENSING CONE DESIGN

The basic problem in the end pumping of a laser rod is how to concentrate the light from a source of finite extent (such as the sun) into the smallest possible area, or how to achieve the greatest reduction of the source image formed by the collection system. There is a fundamental limit to which the image formed by a collector of given diameter can be reduced. This limit is specified by the Abbe[1] sine condition which in a general sense is a manifest of the Second Law of Thermodynamics.[2] Referring to Figure 41, the Abbe sine condition may be written

$$D \ n \ \sin \phi \ = \ D' \ n' \ \sin \phi' \tag{1}$$

where D and D' are the diameters of the source and the image of the source, respectively. It is not necessary to know any of the details of the optical system to express this relation. If the optical system has an entrance pupil diameter (or collector diameter) d and the source distance u is much larger than d, then

$$\sin \phi \ \approx \ \tan \phi \ = \ \frac{d}{2u} \tag{2}$$

and we have

$$\frac{D}{u} \ n \ \frac{d}{2} \ = \ D' \ n' \ \sin \phi' \tag{3}$$

or

$$D' \ = \ \frac{D}{u} \left(\frac{n}{n'}\right) \frac{d}{2} \frac{1}{\sin \phi'} \tag{4}$$

Since $\sin \phi'$ must be less than or equal to one, we may write the inequality

$$D' \ \geq \ \frac{D}{u} \left(\frac{n}{n'}\right) \frac{d}{2} \tag{5}$$

For the sun $D/u = 9.3 \times 10^{-3}$. This result states that in air $(n/n' = 1)$ the smallest area into which the sunlight collected by a 24" diameter mirror can be focused is $D' = 0.1115"$ or 2.84 mm.

83

Figure 41   Geometry Used to Express the Abbe Sine Condition

84
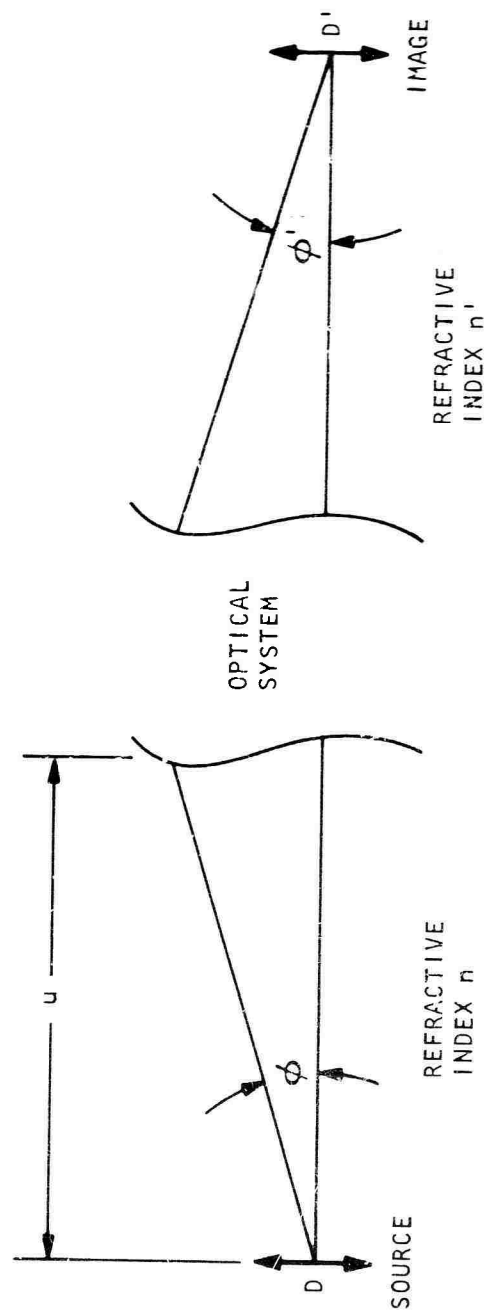
A condensing cone provides the best means of achieving the limit of the sine condition.[3] The cone is not capable of forming an image of the source; however, this is not necessary here. All we are interested in is concentrating the light collected by the primary system into the smallest possible area. A condensing cone placed at the focus of the primary system does this quite simply. The papers by Witte[3] and Williamson[4] provide descriptions of how the cone accomplishes this function and how the design of a cone may be performed.

Under what conditions a light ray entering a condensing cone will be transmitted through the exit opening can be simply visualized using the geometrical ray tracing of Williamson shown in Figure 42. In this tracing the figure defined by a plane bisecting the cone is rotated successively about its edges. As the figure is rotated each new figure generated is a mirror image of the previous one; therefore, a straight line drawn through this construction represents a light ray as it is reflected back and forth through the cone. If a particular ray is to exit from the small end of the cone, the line representing this ray in the trace must intersect the polygon formed by the small end of the rotating figure. Ray A in Figure 42 is transmitted through the cone, but ray B is incident at too steep an angle and is retro-reflected from the cone.

The geometry defined by this ray tracing construction may be used to solve for the dimensions of a cone which must transmit a ray at a given incident angle. In Figure 43 the polygon formed by rotating the cone is replaced by a reference circle of radius r. The image of the source, in our case the sun, is formed at the entrance of the cone and the extreme ray from the primary system is incident on the entrance of the cone at an angle V. The geometry may be solved to yield a relationship between the cone length and angle and the incident angle V

$$x = (1 - c/s) \left[\frac{s \cos V}{\left(\frac{\cos \phi}{\cos \alpha}\right) \frac{c}{s} - \sin V} \right] \tag{6}$$

For the steepest ray accepted by the cone $\phi = 0$ and for long cones $\cos \alpha \approx 1$. Under these conditions equation (6) reduces to Williamson's result which is missing the $\cos \phi / \cos \alpha$ factor. From equation (6) it is observed that the greatest image reduction or smallest value of c/s that can be obtained with the simple cone is given by $\sin V$ and this reduction is obtained only with a cone of infinite length. The limit of the sine condition can nearly be obtained with a cone of a finite practical length, however, with the use of a field lens which effectively reduces the angle V. The geometry with the field lens is shown in Figure 44. The relationship between the cone geometry and the incident angle given in equation (6) applies to this case with V replaced by V', and V and V' may be simply related by the magnifying power of the lens. Equation (6) may then be used to design the cone, but a much simpler technique is by construction using the geometry of Figure 44. Before proceeding to the cone design by either calculation or construction, however, it is well to note

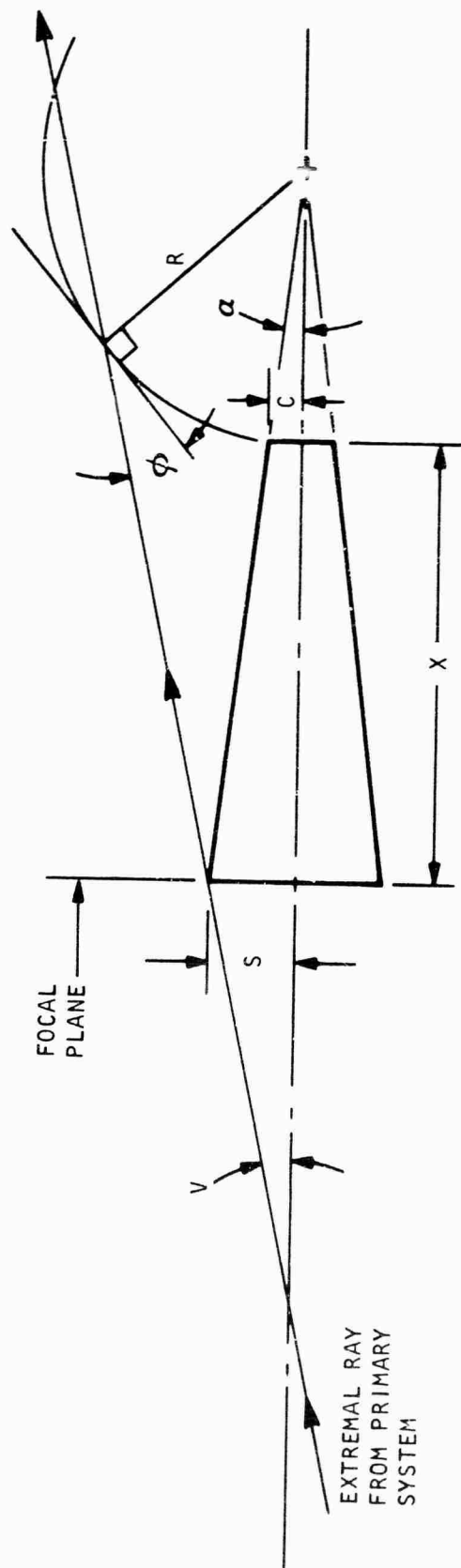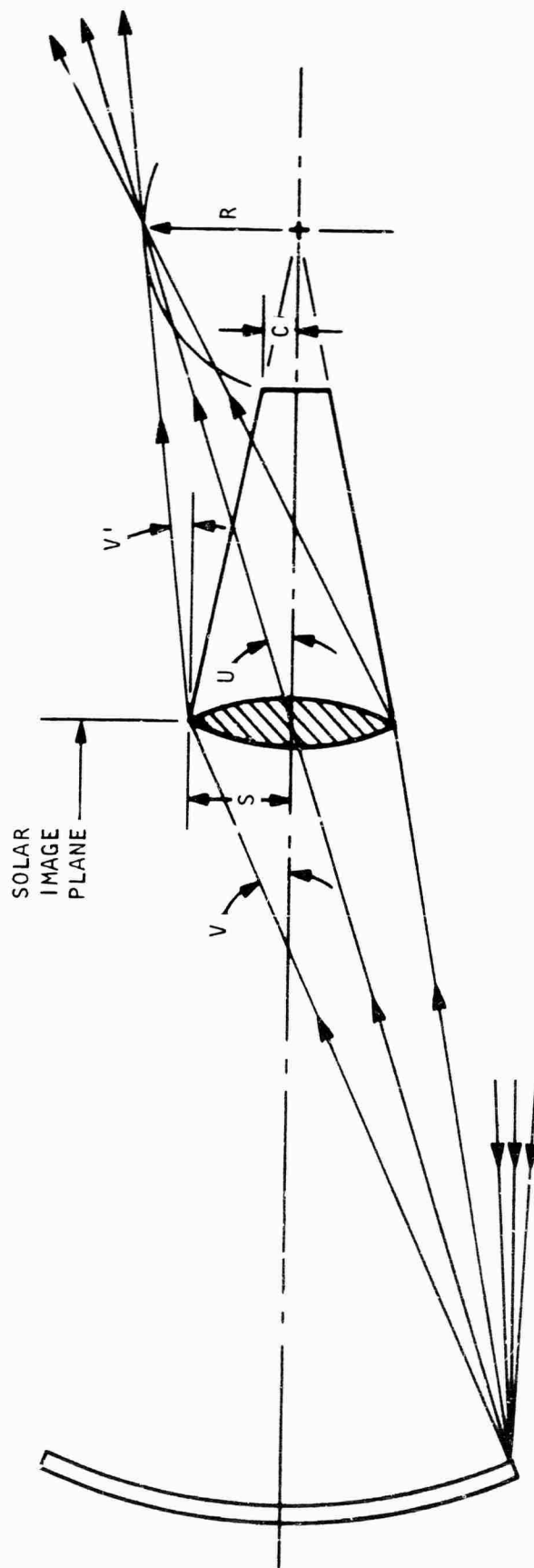Figure 42   Condensing Cone Ray Trace Construction
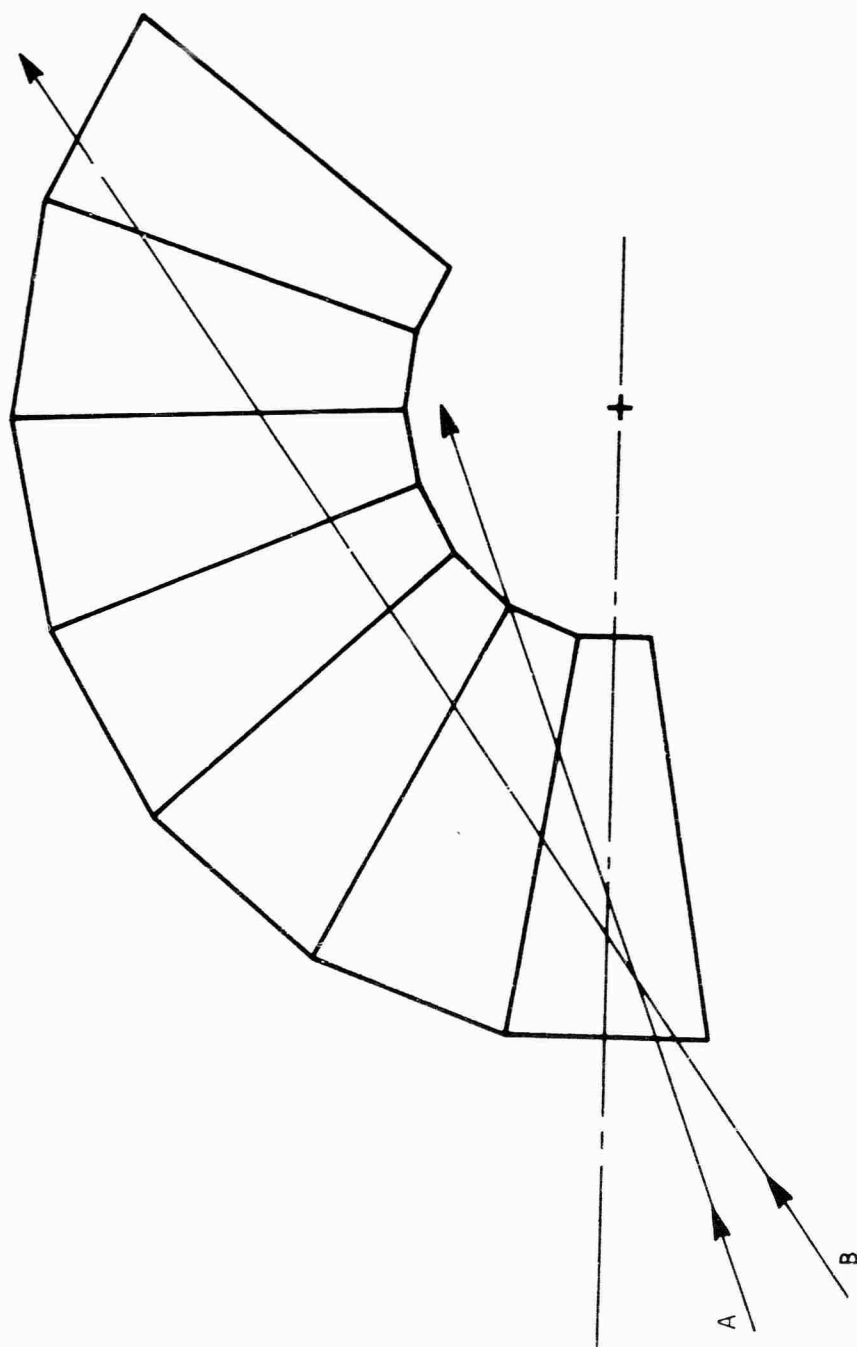
Figure 43 Geometry Used to Determine Dimensions of a Simple Cone

Figure 44 Geometry of Condensing Cone with Field Lens

two important characteristics of the cone with the field lens. In Figure 43 we drew only one extremal ray, the ray entering the top edge of the cone. Since all rays passing through the solar image are diverging, any reference circle intercepted by the top ray will be intercepted by all the rays. In the case of the cone with the field lens, this is not always true. Figure 44 shows extremal rays from opposite edges of the sun in addition to the ray from the center of the sun; these rays converge to a point in the image plane of the cone field lens. If the cone is made longer to increase the diameter of the reference circle, some of the rays passing through near the bottom of the cone entrance are rejected as shown in Figure 45. The relationship between the length of the cone and the focal length of the lens which is specified by equation (6) must be satisfied in order for all the rays to be passed by the cone.

The second important characteristic of the cone with the field lens is that the ratio of c/s is independent of cone length. This is shown by using the geometry of Figure 44 to derive the relationship $\sin V = c/s$. This relationship is an approximation as pointed out by Williamson,[4] but it is valid unless the cone is very short. Even though the c/s ratio is independent of cone length, the focal length of the field lens and the cone length are related as mentioned above; therefore, if the cone length is changed, the focal length of the field lens must be changed accordingly.

Choosing the length of the cone involves two considerations: (1) the number of reflective bounces the rays make passing through the cone decreases as the cone length decreases, and (2) a shorter cone requires shorter focal length lens with a larger radius of curvature. Since we want to minimize reflective losses, we should make the cone as short as possible; however, as the focal length of the lens decreases and the lens radius becomes larger the angle of incidence of extremal rays impinging on the lens increases. Since it is not possible to antireflection-coat a lens for a broad range of angles, the reflective loss at the lens increases as the focal length of the lens decreases. A computer ray trace analysis would be required to fully optimize the cone with respect to length, taking into account all the reflective losses as well as chromatic and spherical aberrations of the cone field lens. This was beyond the scope of this program; therefore, the cone length was determined by selecting a lens of practical (and available) focal length which appeared to result in a compromise between the number of cone reflections and the reflective loss at the lens.

The cone used with the 3 mm diameter laser rod was designed by construction as shown in Figure 46. The diameter of the entrance of the cone was determined by the diameter of the solar image formed by the optical system which in this case was 16 mm. A plano convex quartz lens with a focal length of 50 mm was chosen for the field lens. A point on the edge of the primary 24" diameter mirror is shown imaged by the lens at the point where the two extremal rays A and B converge. The center of the reference circle and hence the angle of the cone are defined by this image plane. The smallest cone exit diameter possible is determined by a reference circle of radius equal to the height of the image of the primary (0.36" for this case). This reference circle results in an exit diameter of 2.84 mm, the limit specified by the sine condition; a reference circle of radius 0.38" gives the desired 3.0 mm exit diameter. Using this latter reference circle the exit angle of the extremal ray is observed to be 27° (this is the angle between the exiting extremal ray and the normal to the cone surface).

89

Figure 45   Illustration of Improper Design of Cone with Field Lens

MIRROR
IMAGE
PLANE
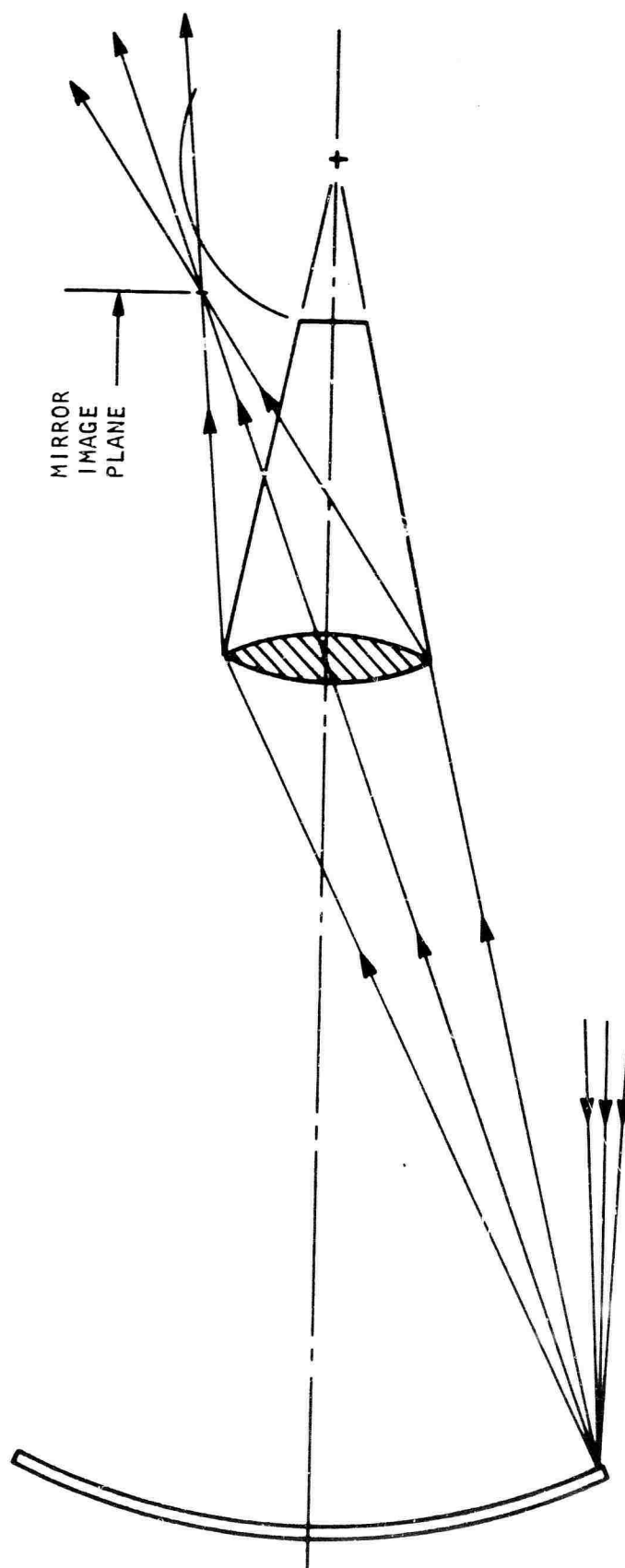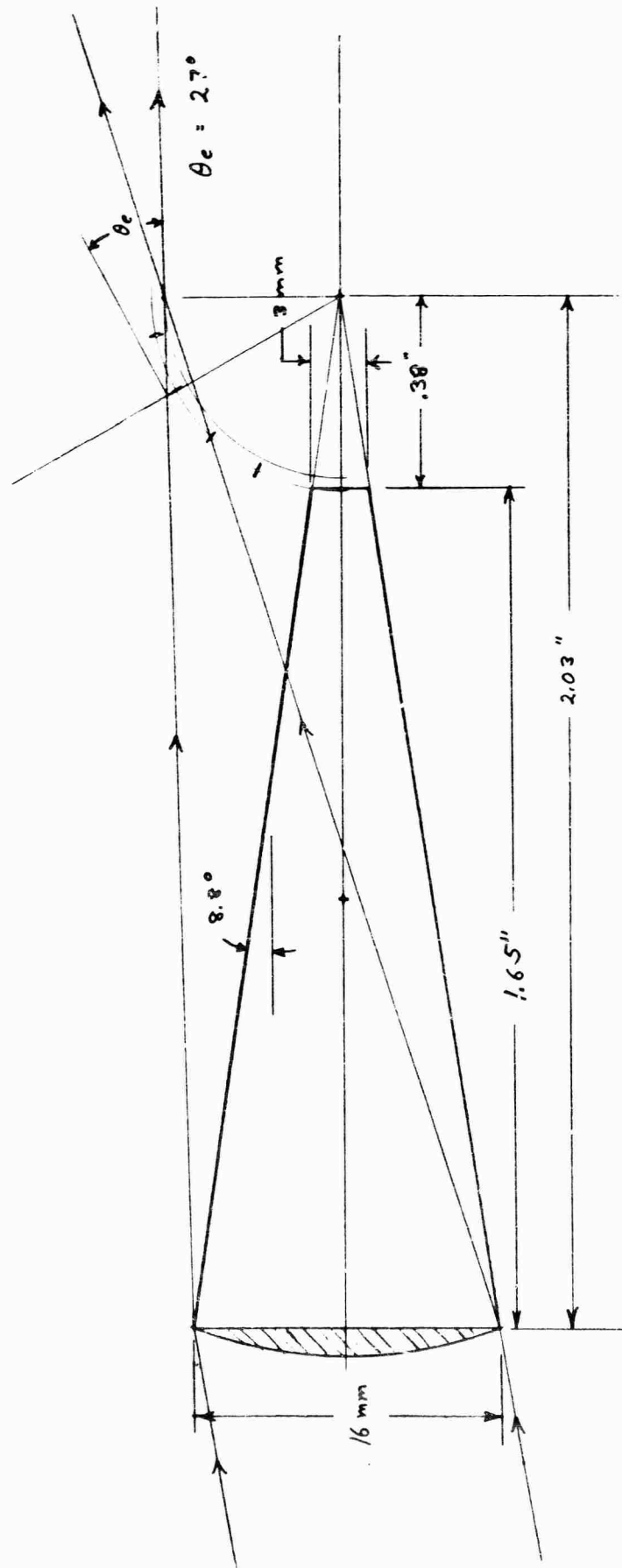
Figure 46 Geometric Constructional Design of Open Cone with Field Lens

91

The same construction technique was used to design the clear YAG cone. This construction is shown in Figure 47. With the solid cone a smaller exit diameter is possible because the refractive index of the material is greater than that of air. For YAG (n = 1.82) the smallest exit diameter is found from the relation

$$D' = \frac{D}{u}\left(\frac{n}{n'}\right)\frac{d}{2}$$

to be 1.56 mm. With an exit diameter of 2 mm the exit angle of the extremal ray for the YAG cone is 48°. Again, equation (6) is valid for the solid YAG cone with the relationship between V and V' given by

$$\sin[\sin^{-1}\left(\frac{S}{R}\right) + V] = n[\sin^{-1}\left(\frac{S}{R}\right) + V']$$

where R is the radius of curvature of the entrance face and n is the refractive index of the cone.
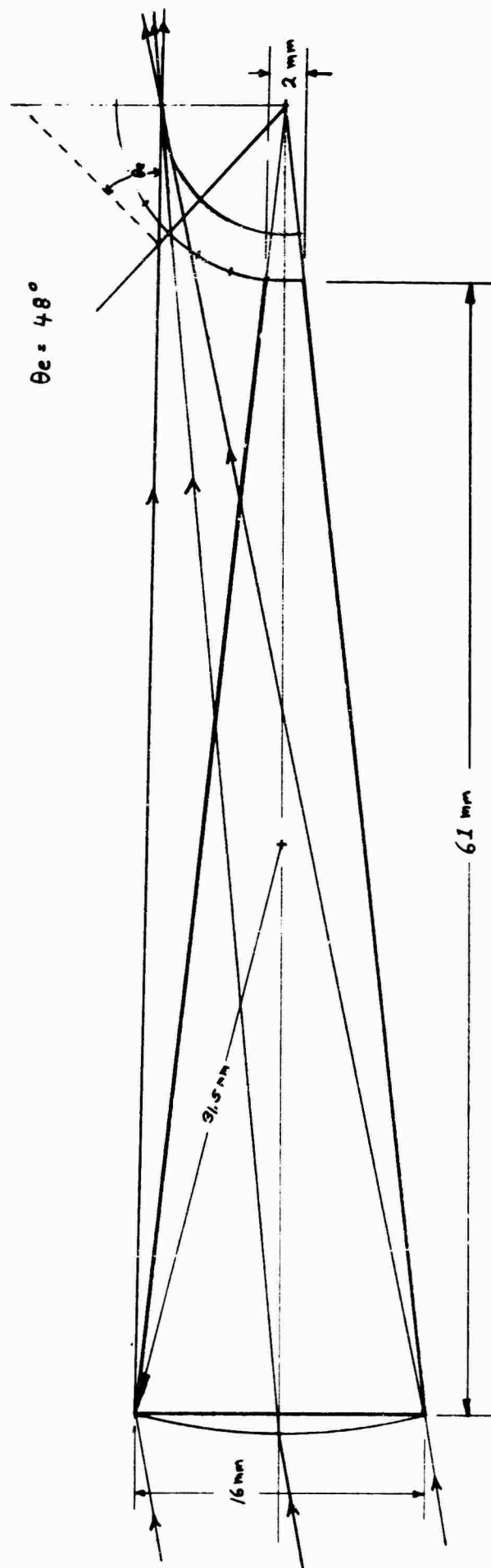
Figure 47 Geometric Constructional Design of Solid Clear YAG Condensing Cone

$\theta e = 48°$

2 mm

31.5 mm

61 mm

16 mm

SCALE - 5X

REFERENCES TO APPENDIX II

1. F. W. Sears, _Optics_, Addison-Wesley Publishing Co., Cambridge, Mass.

2. R. Clasius, _Mechanical Theory of Heat_, Macmillan Company, London, 1879.

3. W. Witte, "Cone Channel Optics," Infrared Physics, 1965, Vol. 5, pp. 179-185.

4. D. E. Williamson, "Cone Channel Condenser Optics," Journal of the Optical Society of America, Vol. 42, No. 10, Oct. 1952.

APPENDIX III

MODE LOCKING THE SUN PUMPED ND:YAG LASER

If the intracavity loss or phase of a laser is modulated at a frequency equal to the reciprocal of the round-trip transmit time, the axial modes are coupled together and forced to assume a definite amplitude and phase relation among themselves.[1,2] In particular, Nd:YAG lasers have been mode locked both by loss modulation[3] and by phase modulation.[4] A mode-locked laser is necessary as the transmitter of a pulse code modulation optical communication system.

In addition to providing short pulses for communication purposes, mode locking quiets competition between axial modes and thus effects a marked increase in amplitude stability of the laser. Pulsewidths of less than 30 picoseconds have been observed and SHG enhancements of nearly 30 have been induced by mode locking.[4] A study of the interaction between intracavity harmonic generation and mode locking[5,6], has shown that intracavity frequency doubling has a deleterious effect on mode locking.

Since the modulation frequencies in question are typically measured in hundreds of megacycles, electro-optic modulators are usually chosen to provide the required phase or loss modulation. In a material which displays the electro-optic effect the size, shape, and/or orientation of the optical indicatrix can be perturbed by the application of an electric field. This perturbation of the indicatrix of course, affects the phase of the light passing through the modulator, and the device may be utilized either as a phase modulator or a loss modulator by an appropriate choice of optical polarization and crystal orientation.

Mode locking the sun pumped laser presents a particularly interest-
ing problem since this laser operates with a low gain. Any additional loss to
the laser cavity caused by the inclusion of the mode-locking apparatus must be
strictly minimized or eliminated altogether, in order to minimize weight and/or
power consumption. This consideration makes the conventional electro-optic mod-
ulator appear somewhat unattractive because the insertion of a polarizer and an
electro-optic crystal into the laser cavity usually results in a severe increase
of intracavity loss. We will discuss several possible alternative techniques
of mode locking the sun pumped laser, and will conclude that the most promis-
ing technique is with a special intracavity electro-optic modulator.

One technique of mode locking a laser without placing a lossy modulator
inside the laser cavity is to place the modulator in a separate, coupled cavity.
This technique has been successfully employed with a He-Ne laser by several in-
vestigators, in one case using an electro-optic modulator,[7] and in another case
using an acousto-optic modulator.[8] The experimental arrangement is shown in
Figure 48. The idea can be viewed conceptually as an ordinary laser cavity in
which the common mirror, modulator, and second-cavity mirror act to form a time-
dependent mirror for the laser cavity.

It is important to realize, in considering techniques of mode locking
Nd:YAG lasers, the difference between inhomogenous lasers, such as He-Ne and
all other gas lasers, and homogenous lasers, such as Nd:YAG and all other solid-
state lasers. As a result of its inhomogenous broadening and hole-burning
phenomenon,[9] a He-Ne laser will oscillate in every longitudinal cavity resonance
that falls under the atomic gain line. The number of longitudinal modes oscil-
lating therefore depends only on cavity length and is typically around five or
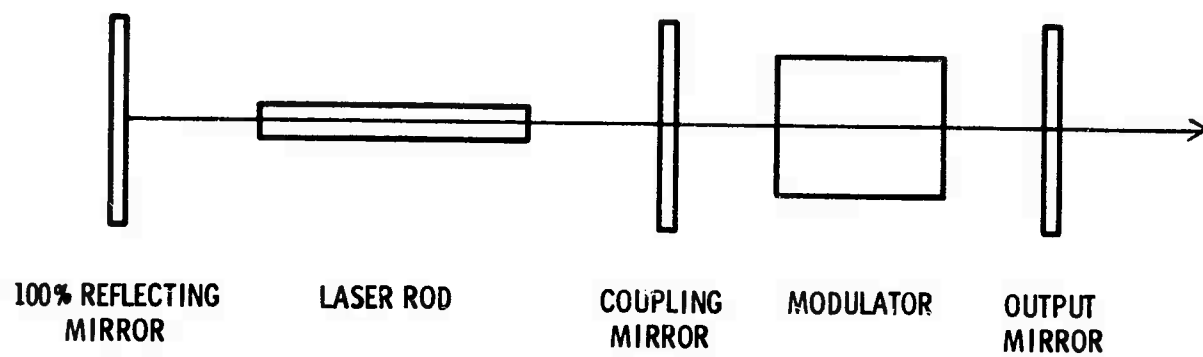
Figure 48.   Laser with Electro-Optic Modulator

six for a reasonably long laser. Since a Nd:YAG laser is homogenously broadened, on the other hand, the first longitudinal mode to reach threshold will use up all the population inversion itself and prevent any other modes from reaching threshold.[9] In practice the spatial differences of the standing waves may allow a second or third longitudinal mode to oscillate weakly in Nd:YAG.

Thus, in order to mode lock a Nd:YAG laser it is necessary to couple enough energy from the oscillating mode to the nonoscillating ones so that the gain in these modes is increased until it is equivalent to the gain of the oscillating mode. This is a much more difficult requirement than in a He-Ne laser, where it is theoretically possible, neglecting the effect of frequency pulling of the modes, to mode lock with zero-energy transfer. Another way to appreciate the difference between these two types of laser is to consider what happens when the mode-locking modulator is turned off. When a He-Ne modulator is turned off all the longitudinal modes continue to oscillate and they will remain mode locked until disturbed by an external perturbation (e.g., residual reflection from intracavity surfaces). When a Nd:YAG modulator is turned off, however, all but one or two of the longitudinal modes instantaneously cease to oscillate, and the laser is no longer mode locked.

The point of this discussion has been to establish that a greater modulation is necessary to mode lock Nd:YAG than He-Ne, and that successful operation of a particular technique with a He-Ne laser is not indicative that successful operation with Nd:YAG lasers will follow. In particular, the two-cavity technique of modelocking He-Ne lasers is not necessarily applicable to our Nd:YAG laser. We have carried on a theoretical analysis of the two-cavity mode-locking scheme which indicates that it is not applicable to Nd:YAG lasers. Both the

98
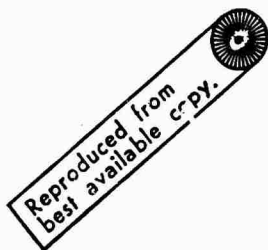
amount of modulation and the amount of crystal loss affecting the main laser
cavity depend on the coupling between the cavities, and if this coupling is
increased enough to provide adequate modulation for mode locking, the crystal
loss is increased to the point along where nothing has been gained by using
a second cavity. We have therefore eliminated this technique from the list
of possibilities.

A second possible arrangement is shown in Figure 49. In this case the
acousto-optic modulator frequency shifts the scattered light by ω_m on each
pass through the modulator, and ω_m is selected so that $\omega_m = 1/2 \; C/2L$ and the
light which is returned to the laser is shifted to a side band.[10] We can com-
pare this technique with an internal FM modulator by considering the amount of
field placed in the side bands by each type of modulator. For the internal
FM modulator, the functional amount of field present in each first side band
by each type of modulator after a double pass through the modulator is

$$\frac{E_n + 1}{E_n} = 2J_1(\delta) \approx \delta \tag{1}$$

where δ is the modulation depth of the modulator. Since modulation depths of
0.1 radian are easily achieved with electro-optic modulators, we have

$$\frac{E_n + 1}{E_n} \approx 0.1 \tag{2}$$

For the external acousto-optic modulator (Figure 49) the fractional amount of
field in the side band is

$$\frac{F_n + 1}{E_n} = t \; \eta \; r \; \eta \; t \tag{3}$$

99.
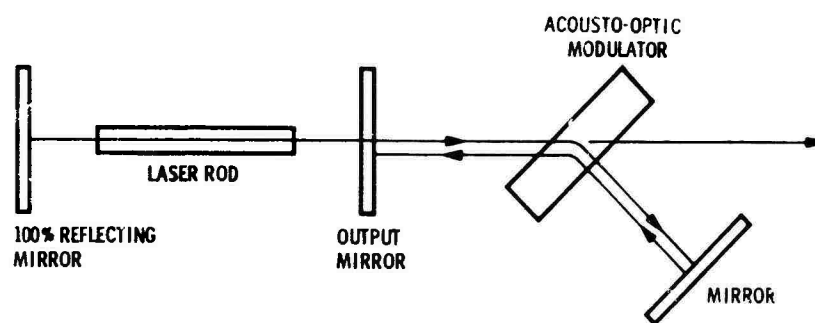
Figure 49.   Laser with Acousto-Optical Modulator

where t is the (field) transmission of the mirror, η is the (field) scatter-
ing efficiency in the modulator, and r is the (field) reflectivity of the second
mirror. The output mirror cannot have greater than about 10 percent (field)
transmission (or, if it does, the intracavity loss will be too high) and it is
not reasonable to expect the scattering efficiency to be greater than 10 percent
at these frequencies. If the second mirror is completely reflective, then the
fractional amount of field in the sideband is

$$\frac{E_n + 1}{E_n} = (.1)\ (.1)\ (1)\ (.1)\ (.1) = 10^{-4} \qquad (4)$$

This is three orders of magnitude less than for the internal electro-optic
modulator. We therefore also eliminate this technique from the list of pos-
sibilities.

Having eliminated all mode-locking techniques in which the modulator
is placed outside the laser cavity, we must examine very closely several types
of intracavity mode-locking modulators. The basic choice is between an internal
electro-optic modulator and an internal acousto-optic modulator.

An electro-optic modulator is far simpler to build and more reliable
in operation than an acousto-optic one. An acousto-optic modulator which
operates at the appropriate frequency for this application (500 Mhz) is a
state-of-the-art device, with all the problems and uncertainties of such a device.
The disadvantage of an electro-optic modulator, on the other hand, is the intra-
cavity loss which accompanies the insertion of a polarizer (a laser must be
polarized in order to operate with an electro-optic modulator) and the electro-
optic crystal into the laser cavity. It is important to remember, however,

that since the output of this laser will be modulated by a PCM modulator the laser will have to be polarized anyway, or half of the laser output will have to be rejected. Although there has been insufficient work done with conductively cooled lasers to make a positive assertion, we believe on the basis of previous work with low power lasers that the laser can be polarized with a small reduction of output power. Thus, it is actually desirable to use an intracavity polarizer regardless of what type of modulator is used, and the only advantage of an acousto-optic modulator is the lower insertion loss of quartz as compared with $LiNbO_3$. We therefore propose to use an intracavity $LiNbO_3$ modulator to mode-lock the sun pumped laser.

We will now discuss the design of this laser, and show that a 5-mm long $LiNbO_3$ crystal will provide enough modulation depth to mode-lock the laser. We propose to use a thin slab of $LiNbO_3$, positioned at Brewster's angle as shown in Figure 50 as the mode-locking modulator. Thus, the modulator will also serve as the polarizer and eliminate the need for any extra surfaces in the cavity. The electric field is applied along the Z axis, perpendicular to the plane of Figure 50. Following Yariv[11] we multiply the electro-optic tensor for $LiNbO_3$ by the vector which describes the applied field,

$$
\begin{pmatrix}
0 & -r_{22} & r_{13} \\
0 & r_{22} & r_{13} \\
0 & 0 & r_{13} \\
0 & r_{51} & 0 \\
r_{51} & 0 & 0 \\
-2r_{22} & 0 & 0
\end{pmatrix}
\begin{pmatrix}
0 \\
0 \\
E_z
\end{pmatrix}
=
\begin{pmatrix}
r_{13}\,E_z \\
r_{13}\,E_z \\
r_{33}\,E_z \\
0 \\
0 \\
0
\end{pmatrix}
\qquad (5)
$$
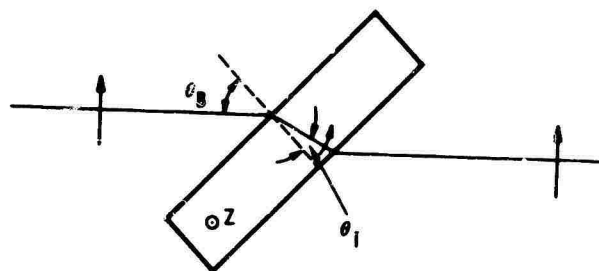
Figure 50. LiNbO$_3$ Slab Positioned at Brewster's Angle

Using the Voight notation[11] we add this electro-optic perturbation to the normal-impermeability tensor which describes the optical indicatrix

$$
B = \begin{pmatrix} 1/n_o^2 + r_{13}E_z & 0 & 0 \\ 0 & 1/n_o^2 + r_{13}E_z & 0 \\ 0 & 0 & 1/n_e + r_{33}E_z \end{pmatrix} \qquad (6)
$$

The matrix is diagonal, which means that the electro-optic effect changes the length of the axes; but not the orientation, of the optical indicatrix. Light whose polarization vector lies anywhere in the x-y plane sees an index of refraction given by $n_1 = [1/n_o^2 + r_{13}E_z]^{-\frac{1}{2}}$, while light whose polarization lies along the z direction will see index $n_{//} = [1/n_e^2 + r_{33}E_z]^{-\frac{1}{2}}$. It turns out that in LiNbO₃ the electro-optic coefficient r_{33} is about 2.5 times as large[12] as r_{13} and, therefore, a much larger modulation depth can be obtained by polarizing the laser along the z axis of the LiNbO₃ modulation. However, we have elected to polarize the laser in the x-y plane of the modulator and thereby utilize the smaller of the available electro-optic coefficients. There are two reasons for this decision. Extensive previous experience[13] with LiNbO₃ has convinced us that the higher loss for light polarized along the z direction negates the advantage of the greater electro-optic effect for this polarization. This consideration is especially valid for the space-qualified laser. Secondly, it is not possible to use the same crystal as modulator and polarizer if the polarization vector is oriented along the z direction.

We will now calculate the modulation depth that can be introduced by the modulator shown in Figure 48 and show that this modulation depth is adequate to mode-lock the laser.

The optical length of the LiNbO$_3$ crystal is, for light polarized in the x-y plane,

$$\ell = \ell_0 \left[\frac{1}{n_0^2} + r_{13}E_z \right]^{-1/2} \tag{7}$$

where ℓ_0 is the physical distance the light travels through the crystal. Differentiating, we obtain

$$\frac{d\ell}{dE_z} = \frac{\ell_0}{2} \left[\frac{1}{n_0^2} + r_{13}E_z \right]^{-3/2} r_{13} \approx \frac{\ell_0 r_{13}}{2} n_0^3 \tag{8}$$

or

$$\Delta \ell = \frac{r_{13} n_0^3}{2} \Delta E_z \ell_0 \tag{9}$$

Now the change in optical length is related to the phase change by

$$\frac{\Delta \ell}{\lambda} = \frac{\delta}{\pi} \tag{10}$$

so

$$\delta = \frac{\pi}{\lambda} \frac{r_{13} n_0^3}{2} V_0 \frac{\ell_0}{d} \tag{11}$$

where we have used the fact that the field inside the crystal is given by $\Delta E_z = \frac{V_0}{d}$ where V_0 is the voltage on the plates and d is crystal thickness between the plates. The experimentally observed quantity is usually the RF power input to the modulator, and not the voltage on the plates. These

105

quantities are related[14] by the RF cavity Q

$$Q = \omega_o \frac{\text{stored energy}}{P_{RF}} \tag{12}$$

The energy stored in a parallel-plate capacitor C at voltage V is $1/2\ CV^2$, so

$$V = \sqrt{\frac{2\ P_{RF}Q}{\omega_o C}} \tag{13}$$

Assuming a cavity Q of 170, capacitance of 10 pf, $\frac{c}{2L}$ frequency of 300 MHz, and RF input of 5 watts, the voltage on the plates is 756 volts. Substituting this value into Equation 11 results in a modulation depth of

$$\delta = .0975 \frac{\ell_o}{d} \approx 0.1 \frac{\ell_o}{d} \tag{14}$$

$\frac{\ell_o}{d}$ is the length-to-thickness ratio of the mode-locking crystal. In this computation we have used the published value[15] of r_{13} at 6328Å, corrected by the experimentally determined[16] correction factor for 1.06 microns.

Siegman and Kuizenga[17] have carried out an excellent analysis of the mode-locked Nd:YAG laser and conclude that the mode-locked pulse length is given by

$$\gamma_{FW} = \sqrt{\frac{2^{\ell}n2}{\pi}} \left(\frac{2\alpha}{\delta} \right) \left[\frac{1}{\Delta f_{axial} \Delta f_{atomic}} \right]^{1/2} \tag{15}$$

Here, α is the single-pass cavity loss, Δf_{axial} is the axial mode spacing, Δf_{atomic} is the atomic line width ($\approx$120 GHz for Nd:YAG) and δ is the modulation depth as in Equation 14. Excellent comparison between the equation and

experimental results have been obtained over a variation of four orders of magnitude of the modulation depth.[17] Figure 51 shows the pulse length of the sun pumped laser as a function of modulation depth as calculated from Equation 15. It can be seen from Figure 51 that very small modulation depth is required to produce pulse lengths on the order of 0.1 μs and referring back to Equation 14 we see that a very thin slice of $LiNbO_3$ will indeed provide adequate modulation depth to produce very effective modelocking.
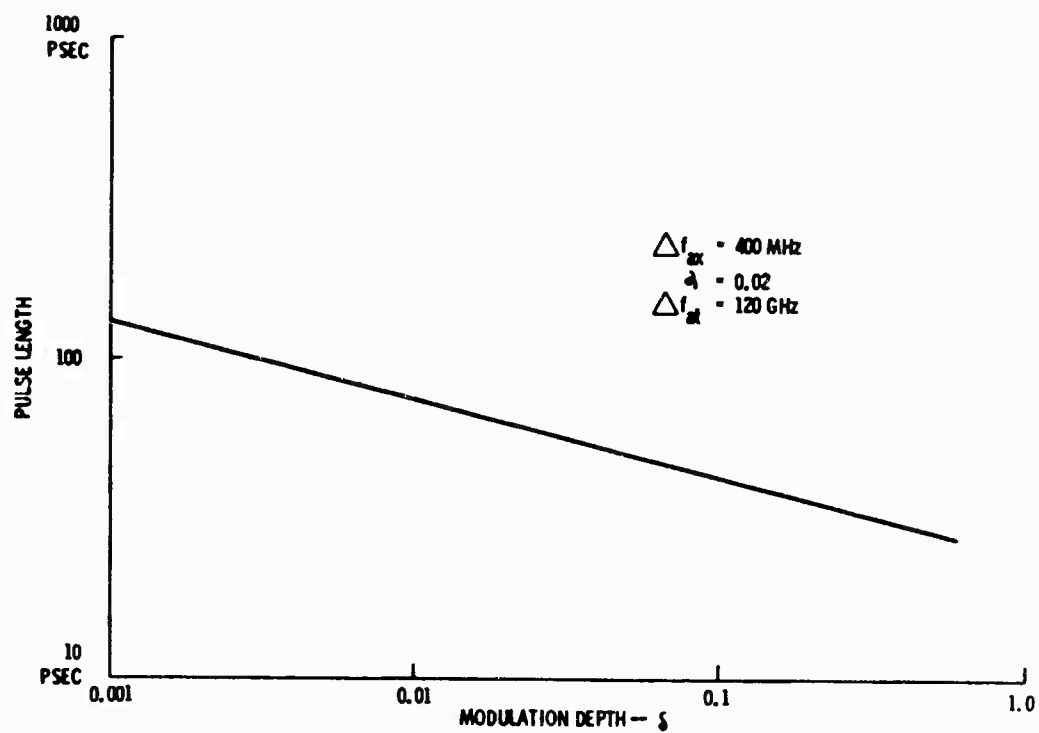
Figure 51. Pulse Length of Space-Qualified Laser
as a Function of Modulation Depth

References

1. P. J. Titterton, "Quantum Theory of an Internally Phase Modulated Laser", Journal of Quantum Electronics, QE-4, 85; 1968.

2. D. J. Kuizenga and A. E. Siegman, "FM and AM Modelocking of the Homogenous Laser," Applied Physics Letters, 14, 6, p 181; 15 March 1965.

3. M. DiDomenico, Jr., J. E. Geusic, H. M. Marcos, and R. G. Smith "Generation of Ultrashort Optical Pulses by Modelocking the Nd:YAG Laser, "Journal of Applied Physics 39, p 4163; 1968.

4. L. M. Osterink and J. D. Foster, "A Modelocked Nd:YAG Laser," Journal of Applied Physics 39, p 4163; 1968.

5. C. B. Hitz and L. M. Osterink, "Frequency-Doubled, Modelocked Nd:YAG Laser," final report, contract NAS 8-20967. NASA/MSFC; 27 July 1970.

6. C. B. Hitz and L. M. Osterink, "Simultaneous Intracavity Second Harmonic Generation and Modelocking," presented at 1970 Device Research Conference, Seattle, Washington; 1 July 1970.

7. L. B. Allen, R. R. Rice, and R. F. Matthews, "Two-Cavity Locking of a He-Ne Laser," Applied Physics Letters, 15, p 416; 15 December 1969.

8. M. DiDomenico, Jr. and V. Czerniewski, "Locking of He-Ne Laser Modes by Intracavity Acoustic Modulations in Coupled Interferometers," Applied Physics Letters, 6, p 150, 15 April 1965.

9. See, for example, A. Yariv, Quantum Electronics, p 263, John Wiley and Sons; 1967.

10. L. C. Foster, M. D. Ewy, and C. B. Crumly, "Laser Modelocking by an External Doppler Cell," Applied Physics Letters, 6, p. 6; 1 January 1965.

11. A. Yariv, ibid., chapters 18 and 19.

12. E. H. Turner, *Applied Physics Letters*, 8, 303; 1966. The electro-optic coefficients are given as $r_{13} = 8.6 \times 10^{-12}$ V/m, $r_{33} = 30.8 \times 10^{-12}$ V/m at 6328Å.

13. As reported by L. M. Osterink and J. D. Foster, "Laser Spectral Control Techniques," final report under Contract F30602-67-C-0173, Rome Air Development Center, Griffiss AFB, New York.

14. J. D. Jackson, *Classical Electrodynamics*, chapter 8, John Wiley and Sons; 1962.

15. D. J. Kuizenga, PhD disertation, Stanford University; 1970. The correction factor is given as $r_{13}(1.06\mu)/r_{13}(6328Å) = 0.905$.

16. A. E. Siegman and D. J. Kuizenga, "Modelocked Pulses in Homogeneous Lasers," *Applied Physics Letters*, 6, 181; 15 March 1970. See also reference 11.

17. A. E. Siegman, private communication.

APPENDIX IV

THEORETICAL MODEL OF THE CW ND:YAG LASER

1.   Introduction

In this Appendix we will develop a theoretical model of the Nd:YAG laser that includes as many of the laser design parameters as possible. The analysis will start from a set of four-level rate equations. Using proper simplifying assumptions, these equations will be reduced to a set of two rate equations---one for the inversion density, and one for the laser photon density. The steady state solution of these equations gives the desired theoretical model. The optical pumping parameters in this model will then be expressed in terms of the laser rod size and the input power to the pump lamps. We will then have a theoretical model containing most of the parameters at our disposal in designing a laser.

2.   Four-Level Rate Equation Analysis

Nd:YAG is an example of a 4-level laser material. Figure 52 depicts the various levels involved. The ground state has energy E_1, the lower laser level has energy F_2, and the pump bands have an energy distribution which we call E_4. In a good laser material such as Nd:YAG the following sequence is followed. The laser material is irradiated with pump light photons that result in a certain pumping rate W_{14} from level 1 to level 4. The laser ions in level 4
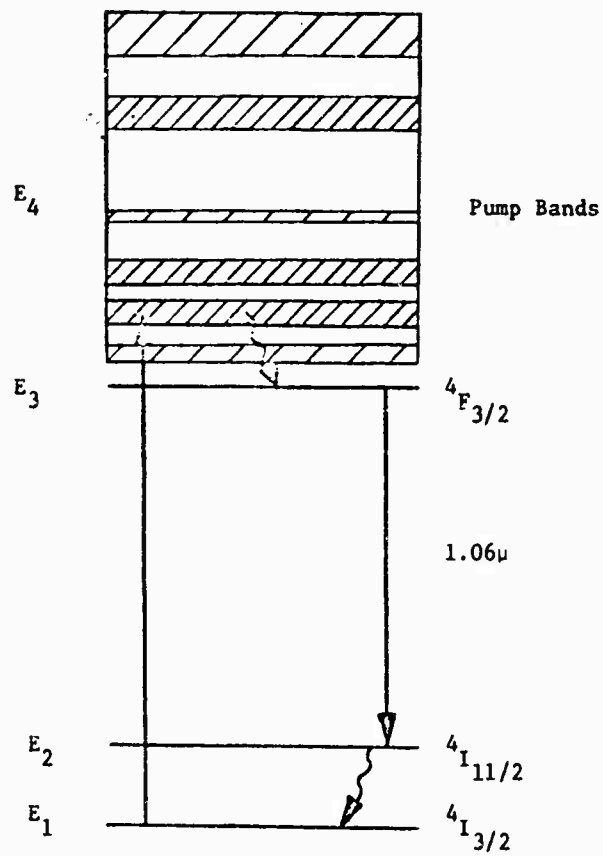
Figure 52. Energy Levels of Nd:YAG,
a Four Level Laser Material

spontaneously decay with various lifetimes τ_{4A} into the lower lying levels. The lifetime τ_{43} for decay into the upper laser level is ideally much shorter than any of the other decay times from level 4.

The upper laser level, E_3, is usually metastable with a long lifetime for decay into all its lower lying levels. The spontaneous decay from level 3 to level 2 of course produces the photons that initiate laser oscillation. An important consideration for initiation of laser oscillation is the total number, p, of resonant modes possible in the laser resonator volume, V_R, since in general only one of these modes is initiated into oscillation. This number is given by the familiar expression

$$p = \frac{8\pi \nu^2 \Delta\nu V_R}{c^2} \qquad (1)$$

where ν = the laser optical frequency

$\Delta\nu$ = the frequency width of the level 3 to level 2 spontaneous emission

V_R = the optical resonator volume

c = the speed of light

For successful laser operation the primary loss mechanism from level 3 is stim -lated emission with a transition rate W_{32}.

The lower laser level, E_2, should ideally have low population at all times. The decay lifetime τ_{21} should therefore be very fast and the pumping rate from the ground state W_{12} should be low.

113

We also have to consider the photons stored in the laser resonator cavity. The number stored per unit volume of resonator will be designated by ρ. Photons are lost from the resonator by transmission of the laser mirrors to produce the laser output power and by dissipative scattering and absorption losses in the optical cavity. The photon cavity lifetime, τ_c, is then given by

$$\tau_c = \frac{1}{(\text{loss per round trip})(\text{round trips per second})}$$

$$= \frac{1}{(2\alpha)(c/2L_R)} = \frac{L_R}{\alpha c} \tag{2}$$

where α = the average single pass loss

L_R = optical resonator length

c = speed of light

We may now write rate equations for the number of ions N_1, N_2, N_3, and N_4 per unit volume stored in the various laser ion levels.

$$\frac{dN_4}{dt} = W_{14}(N_1-N_4) - \frac{N_4}{\tau_{43}} - \frac{N_4}{\tau_{42}} - \frac{N_4}{\tau_{41}}$$

$$\frac{dN_3}{dt} = W_{13}(N_1-N_3) + \frac{N_4}{\tau_{43}} - \frac{N_3}{\tau_{32}} - \frac{N_3}{\tau_{31}} - W_{32}(N_3-N_2)$$

$$\frac{dN_2}{dt} = W_{12}(N_1-N_2) + W_{32}(N_3-N_2) + \frac{N_3}{\tau_{32}} + \frac{N_4}{\tau_{42}} - \frac{N_2}{\tau_{21}} \tag{3}$$

$$\frac{dN_1}{dt} = W_{14}(N_4-N_1) + W_{13}(N_3-N_1) + W_{12}(N_2-N_1) + \frac{N_4}{\tau_{41}} + \frac{N_3}{\tau_{31}} + \frac{N_2}{\tau_{21}}$$

$$\frac{d\rho}{dt} = W_{32}(N_3-N_2) + \frac{N_3}{\rho\tau_{32}} - \frac{\rho}{\tau_c}$$

114

Let us now simplify these equations. In the rate equation for level 4 let us account for the τ_{42} and τ_{41} terms by a quantum efficiency factor η'. Assume that $N_1 >> N_4$ so that we can replace $N_1 - N_4$ by N_1. The simplified rate equation for level 4 becomes

$$\frac{dN_4}{dt} = W_{14}N_1 - \frac{N_4}{\tau_{43}\eta} .$$ (4)

The lifetime of level 4 is in general very short so we can assume steady state conditions and $\frac{dN_4}{dt} = 0$. This assumption is of course exactly true in the continuous case. The population density N_4 is then

$$N_4 = \eta' N_1 W_{14} \tau_{43} .$$ (5)

We may now substitute for N_4 in the rate equation for level 3. Also assume $N_3 << N_1$ so that we can replace $N_1 - N_3$ by N_1. The simplified rate equation for level 3 becomes

$$\frac{dN_3}{dt} = W_{13}N_1 + \eta' W_{14}N_1 - W_{32}(N_3 - N_2) - \frac{N_3}{\tau_{32}} - \frac{N_3}{\tau_{31}}$$ (6)

Let us define the pumping rate W and the quantum efficiency η by

$$\eta W = W_{13} + \eta' W_{14}$$

Then,

$$\frac{dN_3}{dt} = \eta W N_1 - W_{32}(N_3 - N_2) - \frac{N_3}{\tau_{32}} - \frac{N_3}{\tau_{31}}$$ (7)

Assume that the terms in τ_{42} and W_{12} may be neglected in the rate equation for level 2. Then,

$$\frac{dN_2}{dt} = W_{32}(N_3 - N_2) + \frac{N_3}{\tau_{32}} - \frac{N_2}{\tau_{21}} \qquad (8)$$

Define the inversion density $N = N_3 - N_2$. Subtracting equation (8) from equation (7)

$$\frac{dN}{dt} = \eta W N_1 - 2W_{32}N - 2\frac{N_3}{\tau_{32}} - \frac{N_3}{\tau_{31}} + \frac{N_2}{\tau_{21}} \qquad (9)$$

Define,

$$\frac{2N}{\tau_T} = \frac{2N_3}{\tau_{32}} - \frac{N_3}{\tau_{31}} + \frac{N_2}{\tau_{21}}$$

$$= 2N\left[\frac{1}{\tau_{32}} + \frac{1}{2\tau_{31}} + \frac{N_2}{2N}\left(\frac{1}{\tau_{21}} + \frac{2}{\tau_{32}} - \frac{1}{\tau_{31}}\right)\right] \qquad (10)$$

where τ_T will be called the total lifetime of the inversion. In general $N_2 << N_3$ so that $N_2/N << 1$ and we may assume

$$\frac{1}{\tau_T} = \frac{1}{\tau_{32}} + \frac{1}{2\tau_{31}} \qquad (11)$$

This is slightly different than the total upper laser level lifetime which would be given by $\frac{1}{\tau_f} = \frac{1}{\tau_{32}} + \frac{1}{\tau_{31}}$. The upper laser level lifetime is easily measured by time observation of spontaneous fluorescence and is readily available in the literature. If the branching ratios r_{32} and r_{31} are known τ_T may be deter-

mined with the following equation

$$\frac{1}{\tau_T} = \frac{r_{32}}{\tau_f} + \frac{r_{31}}{2\tau_f} \tag{12}$$

Substituting τ_T into equation (2-9), we get our final rate equation for the inversion density

$$\frac{dN}{dt} = \eta W N_1 - 2W_{32}N - \frac{2N}{\tau_T} \tag{13}$$

The rate equation for the photon density in (3) is for the case where the laser material volume and the laser resonator volume are equal. We will generalize this to the external mirror case where the laser material volume, V_L, and the laser resonator volume, V_R, are different. Since in general $N_3 \gg N_2$, we will assume that $N_3 = N$ in the spontaneous emission term. We will also generalize to the multimode case where n modes of the laser can be excited. The photon density rate equation is then

$$\frac{d\rho}{dt} = W_{32}N + \frac{nN}{p\tau_{32}} - \frac{\rho}{\tau_c} \tag{14}$$

The stimulated emission rate W_{32} must be expressed in terms of parameters. The number of stimulated emissions, N_s, per unit time per unit volume is

$$N_s = W_{32}N = I_L \sigma N \tag{15}$$

117

where I_L = the laser light irradiance or photons per unit area per unit time

traversing the laser material.

σ = the stimulated emission cross section per inverted laser ion.

The photon intensity, I_L, considering those moving both directions in the laser resonator is

$$I_L = \rho c \qquad (16)$$

where c is the speed of light.

The pumping rate W must also be expressed in terms of parameters. The number of pump photon absorptions, N_p, per unit time per unit volume is

$$N_p = W N_1 = I_p \, \sigma_p N_1 \qquad (17)$$

where I_p = the pump light irradiance or photons per unit area per unit time

traversing the laser material.

σ_p = the average pump light absorption cross section per laser ion.

The pump photon intensity, I_p, depends on the size of the laser material and the pump lamp and pump cavity configuration. Let us assume that we have a well designed laser such that the pump light is imaged on the laser rod for each rod size we consider. With this assumption, the irradiance, I_p, is just the total number of pump photons, ϕ_p, emitted per unit time divided by the cross section of the laser rod presented to the pump light. Considering cylindrical laser rods for side pumping

$$I_p = \frac{\phi_p}{Ld} \quad \text{(side pumping)} \qquad (18)$$

118

where L = laser rod length

d = laser rod diameter

and we have assumed only one or two passes of the pump light through the laser rod.

For end pumping

$$I_p(\ell) = \frac{4\phi_p}{\pi d^2} e^{-\frac{\ell}{L_M}} \quad \text{(end pumping)}$$

(19)

where ℓ = the axial distance from the entrance end of the rod.

L_M = the axial distance at which the irradiance has decreased by e.

To simplify this case we will determine the average, $\overline{I}_p$, of $I_p(\ell)$ in an end pumped laser rod of length L.

$$\overline{I}_p = \frac{1}{L} \int_0^L I_p(\ell)dL$$

$$\overline{I}_p = \frac{4\phi_p}{\pi d^2} \frac{L_M}{L} (1-e^{-\frac{L}{L_M}})$$

(20)

Utilizing (2-2), (2-13), (2-14), (2-15), (2-16), and (2-17), we can write the two coupled rate equations that govern operation of the Nd:YAG laser

$$\frac{dN}{dt} = \eta N_p - 2c\sigma 3N - \frac{2N}{\tau_T}$$

(21)

$$\frac{d\rho}{dt} = \frac{V_L}{V_R} c\jmath\rho N + \frac{nN}{p\tau_{32}} - \frac{\rho\alpha c}{L_R}$$

119

Let us now consider the steady state solution of these coupled rate equations.
$$\frac{dN}{dt} = \frac{d\rho}{dt} = 0$$

$$c\sigma \rho N + \frac{N}{\tau_T} = \eta \frac{N_p}{2} \qquad (22)$$

$$c\sigma \rho N + \frac{V_R}{V_L} \frac{\eta N}{p\tau_{32}} - \frac{V_R}{V_L} \frac{\rho \alpha c}{L_R} = 0 \qquad (23)$$

Solving (2-22) for N, substituting into (2-23) and solving for ρ and assuming we can neglect the term containing p we get

$$\rho = \frac{L_R}{\alpha c} \frac{\eta N_p}{2} \frac{V_L}{V_R} - \frac{1}{c\sigma \tau_T} \qquad (24)$$

Using (2-16), the two way laser irradiance, I_L, is

$$I_L = \frac{L_R}{\alpha} \frac{\eta N_p}{2} \frac{V_L}{V_R} - \frac{1}{\sigma \tau_T} \qquad (25)$$

The one way laser irradiance will be half of I_L. If the area of the laser beam is A, the laser mirrors have a total output transmission, T, and we multiply by $h\nu_L$, the photon energy, the laser output power in watts is given by

$$P_{out} = \frac{I_L}{2} TA \, h\nu_L$$

$$= \frac{TA \, h\nu_L}{2} \left(\frac{L_R}{\alpha} \frac{nN_p}{2} \frac{V_L}{V_R} - \frac{1}{\sigma\tau_T} \right)$$

$$P_{out} = \frac{T}{\dfrac{2\sigma\tau_T}{Ah\nu_L}} \left[\frac{\dfrac{nN_p \sigma\tau_T L_R V_L}{2V_R}}{\alpha} - 1 \right] \qquad (26)$$

Let us define the following

$$g_o = \frac{nN_p \sigma\tau_T \, L_R \, V_L}{2V_R} \qquad (27)$$

$$\beta = \frac{2\sigma\tau_T}{A \, h\nu_L} \qquad (28)$$

Then, equation (2-25) becomes

$$P_{out} = \frac{T}{\beta} \left(\frac{g_o}{\alpha} - 1 \right) \qquad (29)'$$

Let us now determine the significance of each of the variables in equation (2-29). We have already defined the total mirror transmission, T, (the sum of T_1 and T_2), and the single pass loss, α. The transmission loss is of course included in α. Let's further define α as composed of half of the double pass transmission loss, T, and a single pass dissipative loss, α_o.

$$\alpha = \frac{T}{2} + \alpha_o \qquad (30)$$

121

Let us also define the one-way or circulating power P_c in the laser cavity.

$$P_c = \frac{I_L}{2} A \qquad (31)$$

The laser output power is then just the product of the transmission T and P_c.

$$P_{out} = T\, P_c \qquad (32)$$

Equating (2-29) and (2-32),

$$P_c = \frac{1}{\beta}\left(\frac{g_0}{\alpha} - 1\right)$$

$$\frac{g_0}{\alpha} = 1 + \beta P_c$$

$$\alpha = \frac{g_0}{1+\beta P_c} \qquad (33)$$

Now, in the steady state condition gain, g, must equal the loss α. The gain must, therefore, be expressed by

$$g = \frac{g_0}{1+\beta P_c} \qquad (34)$$

This is just the equation for saturated single pass gain in a homogeneous laser material.[1] Our formulation of the rate equations has assumed homogeneous broadening since we have assumed that any photon can stimulate any inverted ion. The homogeneous assumption is correct for Nd:YAG. It becomes somewhat incorrect for Nd:Glass.

The gain decreases or saturates with increasing circulating power, P_c. We see that g_0 is the single pass gain at zero circulating power and β is the saturation parameter. Specifically, $1/\beta$ is the value of P_c at which the gain saturates to half of the initial value. It should be noted that this definition of β is for oscillators and assumes that P_c traverses the laser material in two directions. For amplifier calculations a different quantity $\beta_a = \beta/2$ must be used. This formulation can also be used for oscillators if the total power $2P_c$ traversing the laser material is used.

It is useful before we leave this subject to consider the relationship of g_0 to the inversion density, N. Consider in (2-21) the rate equation for N for the steady state case, $dN/dt = 0$ and the unsaturated case $\rho = 0$. Then

$$N = \frac{\eta N_p \tau_T}{2} \qquad (35)$$

Using equation (27),

$$g_0 = \frac{\eta N_p \tau_T \sigma L_R V_L}{2 V_R}$$

123

Assuming the resonator and the laser material have the same diameter,
$V_R = \frac{\pi}{4} d^2 L_R$ and $V_L = \frac{\pi}{4} d^2 L$, and substituting from equation (2-35),

$$g_0 = \sigma L N \qquad\qquad (36)$$

3. Model for Radiation Emission from Pump Source

In this section we will introduce a model for the pump radiation emission from a pump source. As an example, let us consider a tungsten-iodine lamp with which we ran the experiment shown in Fig. 2-2. The output from the lamp is filtered by a narrow band filter that transmits energy only in the primary Nd:YAG laser pump band spectral range. The radiation transmitted is detected and a record is made of detected radiation as a function of input power to the pump lamp.

A graph of the data from such an experiment performed with a tungsten-iodine pump lamp is shown in Fig. 53. The graph starts from the coordinate origin which at first has a curved characteristic and then becomes linear. The linear portion of this graph can be accurately represented by a linear intercept equation.

$$P_r = k_r (P_{in} - P_o) \qquad\qquad (37)$$

where P_r = the power radiated into the desired spectral region

k_r = the slope representing the efficiency of converting input power into the desired radiation

P_{in} = the input power to the lamp

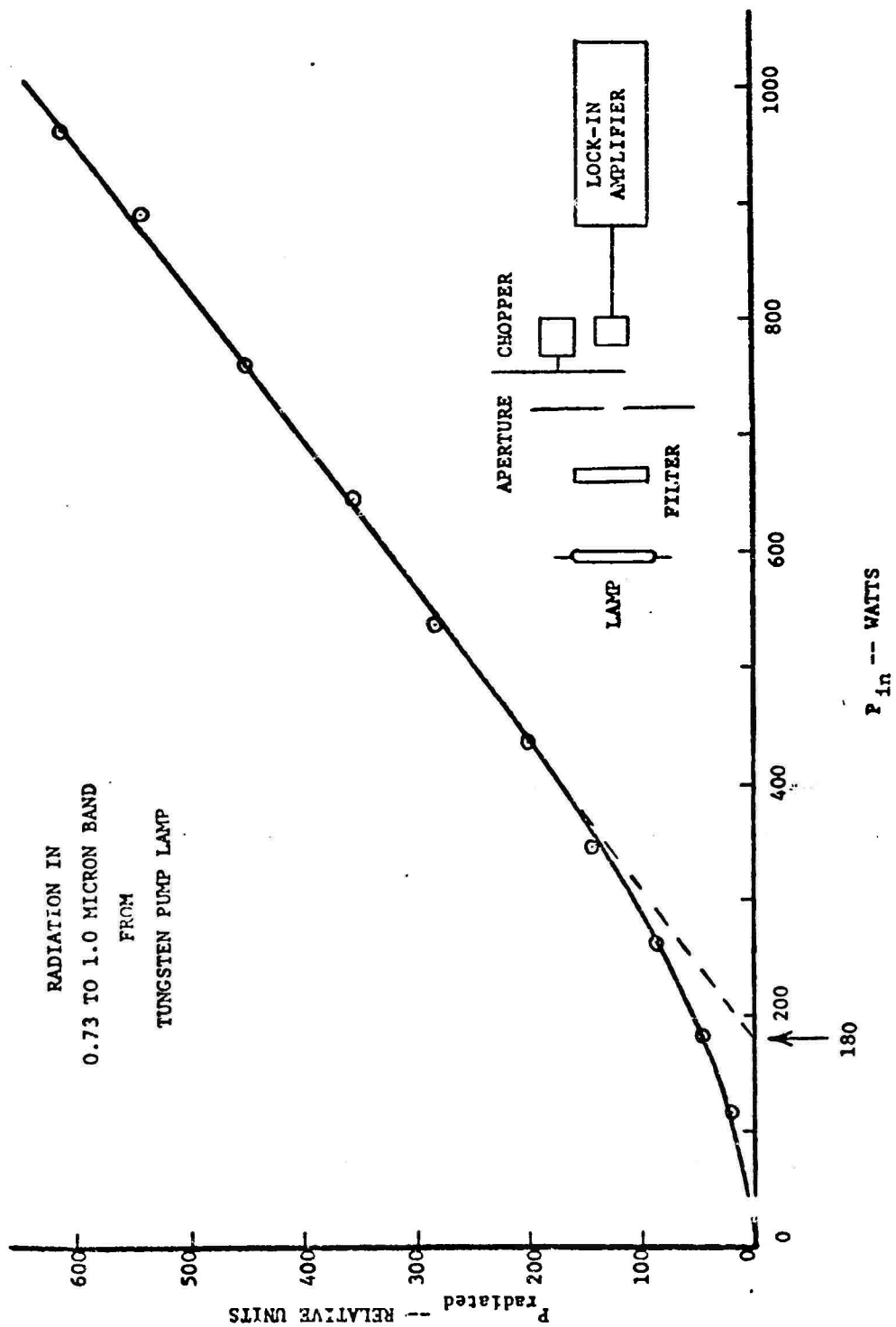P_o = the intercept of the linear curve with the P_{in} axis.

Figure 53 Narrow Band Radiation Output as a Function of Input
for the Tungsten-iodine Lamp

This model not only holds for the tungsten-iodine lamp shown in Fig. 53. It also applies to the Hg arc[2], and we have found it applies to the Kr arc, the K-Hg arc, and the RbI-Hg arc. With $P_o = 0$ it also applies to the ideal linear input-output characteristic which is approached by incoherent semiconductor diodes.

4. Theoretical Model for the Nd:YAG Laser

We can now formulate our theoretical model of the Nd:YAG laser. Because of the difference in the average pump light irradiance for the side pumped and the end pumped laser cases, we will have to have a model for each. We will show all details for development of the side pumped theoretical model but will only give the final results for the end pumped case.

5. Side Pumped Laser

Consider that we have a side pumped Nd:YAG laser of the type shown in Fig. 54.

The power radiated into the laser pump bands is given by equation(37)

$$P_r = k_r (P_{in} - P_o)$$

The total number of pump photons, ϕ_p, reaching the laser rod is

$$\phi_p = k_p \frac{P_r}{h\nu_p} \tag{38}$$

where k_p = the pump cavity transfer efficiency. (This constant includes the effect of multiple reflections in the pump cavity.)
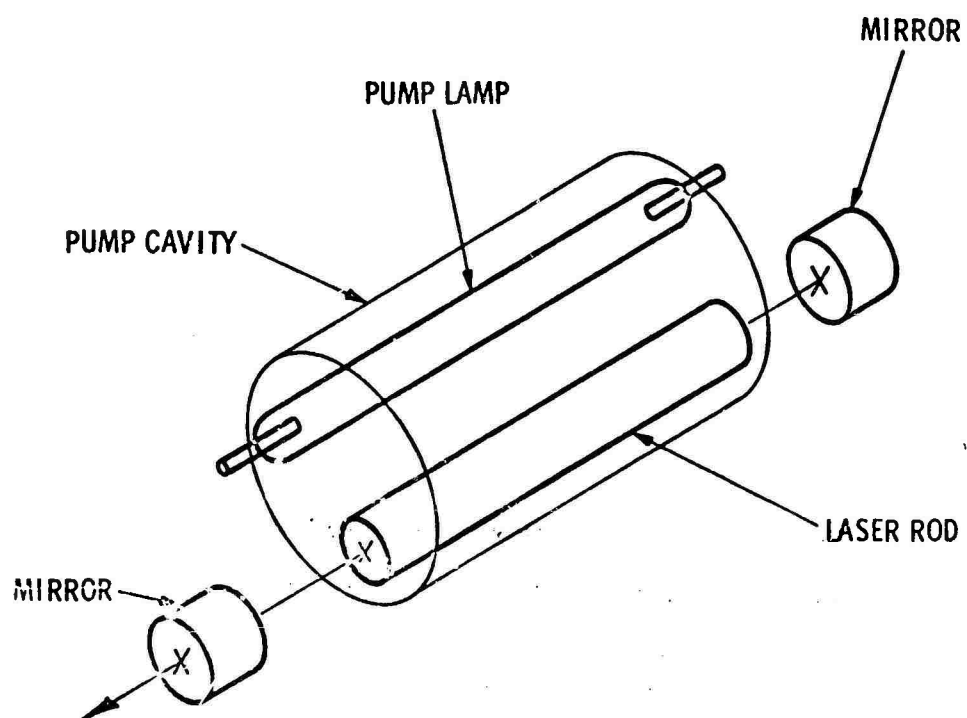
$h\nu_p$ = the average pump photon energy.

126

MIRROR

PUMP LAMP

PUMP CAVITY

LASER ROD

MIRROR

Figure 54.   Optically Side Pumped Laser

The pump light irradiance in the laser rod is then from equation (18)

$$I_p = \frac{k_p k_r \left(P_{in} - P_o \right)}{h \nu_p L d}$$

(39)

where   L = the laser rod length

d = the laser rod diameter

The pump photon absorptions per unit time, per unit volume is then from equa tion 17.

$$N_p = \frac{\sigma_p k_p k_r N_1}{h \nu_p L d} \left(P_{in} - P_o \right)$$

(40)

where again

σ_p = the average pump light absorption cross section per laser ion.

N_1 = the ground state laser ion density ions per unit volume.

Using equation (2-27), and assuming the diameter, d, of the laser rod and the laser resonator are the same, the single pass unsaturated gain, g_o, is

$$g_o = \frac{\sigma_p k_p k_r \, \eta \, N_1 \sigma \tau_T}{2 h \nu_p d} \left(P_{in} - P_o \right)$$

(41)

where σ = the stimulated emission cross section per inverted laser ion.

τ_T = the total inversion lifetime.

128.

Let us define,

$$K = \frac{\sigma_p k_p k_r nN_1 \sigma \tau_T}{2h\nu_p d} (P_{in} - P_o)$$ (42)

Then,

$$g_o = K (P_{in} - P_o)$$ (43)

To complete our model of the side pumped Nd:YAG laser we need to repeat equations (2-28) and (2-29).

$$\beta = \frac{2\sigma\tau_T}{Ah\nu_L}.$$

where $A = \pi/4 \, d^2$ the laser rod cross sectional area,

$h\nu_L$ = the laser photon energy,

and

$$P_{out} = \frac{T}{\beta} \left(\frac{g_o}{\alpha} - 1 \right)$$

where again,

$T = T_1 + T_2$, the sum of the two laser mirror output transmissions

$\alpha = \frac{T}{2} + \alpha_o$, the total single pass loss

α_o = the single pass dissipative loss.

129

Substituting (43) into (29) and rearranging, we get

$$P_{out} = \frac{KT}{\alpha \beta} \left[P_{in} - \left(P_o + \frac{\alpha}{k} \right) \right]$$ (44)

Define,

$$\eta_d = \frac{KT}{\alpha \beta},$$ (45)

and $$P_{th} = P_o + \frac{\alpha}{K}$$ (46)

Then,

$$P_{out} = \eta_d (P_{in} - P_{th})$$ (47)

This is the familiar linearized laser input-output equation with slope efficiency, η_d, and threshold, P_{th}. We have, therefore, developed a theoretical model for the parameters that affect the experimentally observable laser performance.

6.   End Pumped Laser

Following the same procedure as for the side pumped case we develop the following equations for the end pumped case:

$$\bar{I}_p = \frac{4k_p k_r}{\pi h \nu_p d^2} \frac{L_M}{L} (1 - e^{\frac{-L}{L_M}}) (P_{in} - P_o) \tag{48}$$

$$N_p = \sigma_p N_1 \bar{I}_p \tag{49}$$

$$g_o = K (P_{in} - P_o) \tag{50}$$

$$K = \frac{2\sigma_p k_p k_r \eta N_1 \sigma \tau_T}{\pi h \nu_p d^2} L_M \left(1 - e^{\frac{-L}{L_M}}\right)$$

The following equations are the same for both cases

$$\beta = \frac{2\sigma \tau_T}{A h \nu_L}$$

$$P_{out} = \frac{T}{\beta} \left(\frac{g_o}{\alpha} - 1 \right)$$

$$\eta_d = \frac{KT}{\alpha \beta}$$

$$P_{th} = P_o + \frac{\alpha}{K}$$

$$P_{out} = \eta_d (P_{in} - P_{th})$$

131

7.   Discussion of the Theoretical Model

8.   Material Constants and Their Experimental Determination

Material parameters can be lumped into a single constant for a given material in a given experimental configuration. We can determine the value of this lumped material constant experimentally. We will restrict ourselves to consideration of the side pumped case.

Rearranging equation (2-42)

$$dK = \frac{\sigma_p k_p k_r \eta N_1 \sigma \tau_T}{2h\nu_p} = \left(\frac{\beta A}{2}\right) \left(\frac{N_1 \sigma_p \eta}{2}\right) \left(\frac{\lambda_p}{\lambda_L}\right) \; k_p k_r \tag{51}$$

All parameters on the right are dependent upon the laser material or the pump lamp with the exception of k_p, the pump cavity efficiency. We can assume that in all cases we will maximize k_p such that it will always have very close to the same value. We, therefore, conclude that for a particular laser material and pump lamp in a good pump cavity the quantity dK is a constant.

$$dK = constant \tag{52}$$

Rearranging equation (2-28)

$$\frac{2}{\beta A} = \frac{h\nu_L}{\sigma \tau_T} \tag{53}$$

All parameters on the right are dependent only upon the laser material. We can

assume they are constant for a given laser material.

$$\frac{2}{\beta A} = \text{constant} \tag{54}$$

This quantity is the total laser power density at which the laser gain is reduced by a factor of 2.

Equation (2-52) represents gain characteristics of a given laser material-pump lamp combination. Equation (2-54) represents the saturation characteristics of a given laser material. These two characteristics will have important bearing on design of a space qualified Nd:YAG laser.

Let us now consider how we determine these constants. Consider that we have a laser and that we have a set of mirrors with several different transmissions, T, but <u>with constant total single pass dissipative loss</u>, α_o. Let us plot laser output power versus input power for each total mirror transmission combination. From these plots we determine the threshold, P_{th}, and the slope efficiency, η_d, for each mirror transmission, T.

Consider equations (2-46) and (2-30)

$$P_{th} = P_o + \frac{\alpha}{K}$$

$$\alpha = \frac{T}{2} + \alpha_o$$

Combining these,

$$P_{th} = (P_o + \frac{\alpha_o}{K}) + \frac{1}{2K} (T) \tag{55}$$

We have several experimental values of P_{th} as a function of T. If we draw a graph of P_{th} versus T, the ordinate intercept is $(P_o + \frac{\alpha_o}{K})$ and the slope is $(1/2K)$.

Consider equations (2-45) and (2-30)

$$\eta_d = \frac{KT}{\alpha\beta}$$

Combining,

$$\frac{1}{\eta_d} = \frac{\beta}{2K} + \frac{\beta\alpha_o}{K} (\frac{1}{T}) \tag{56}$$

Again, we have several experimental values of η_d versus T. If we draw a graph of $1/\eta_d$ versus $1/T$, the ordinate intercept is $\frac{\beta}{2K}$ and the slope is $\frac{\beta\alpha_o}{K}$. The two intercepts and the two slopes from equations (2-55) and (2-56) allow determination of K, α_o, β and P_o. From these and the known laser rod diameter, we can determine dK and $2/\beta A$.

We should emphasize that a number of different mirror transmissions must be used for this experiment and that the plots of P_{th} versus T, and $1/\eta_d$ versus $1/T$ must form straight lines. If α_o is different for the various mirrors or if α_o is a function of circulating laser power, the data will not form straight lines and this method cannot be used. Intracavity nonlinear crystals will

134

sometimes produce such effects even when the nonlinear process is not phase-matched.

9. Optimum Output Coupling

Consider that we have a laser with a pump lamp having a certain operating point that produces an unsaturated single pass laser gain, g_o. We will now determine the laser mirror transmission, T, that produces the optimum amount of laser output power. Consider equations (2-29) and (2-30).

$$P_{out} = \frac{T}{\beta} \left(\frac{g_o}{\alpha} - 1 \right)$$

$$\alpha = \alpha_o + \frac{T}{2}$$

Combining,

$$P_{out} = \frac{T}{\beta} \left[\frac{g_o}{\alpha_o + T/2} - 1 \right]$$

Differentiating twice with respect to T,

$$\frac{dP_{out}}{dT} = \frac{g_o\, T}{2\beta(\alpha_o + T/2)^2} + \frac{g_o}{\beta(\alpha_o + T/2)} - \frac{1}{\beta}$$

$$\frac{d^2 P_{out}}{dT^2} = \frac{-g_o}{2\beta(\alpha_o + T/2)^2}$$

135

Setting the first derivative equal to zero to find extremum and solving for the second derivative of this extremum.

$$\frac{dP_{out}}{dT} = 0 = g_o \alpha_o - (\alpha_o + T/2)^2$$

$$T = 2 (\sqrt{g_o \alpha_o} - \alpha_o)$$

$$\frac{d^2 P_{out}}{dT^2} < 0$$

The extremum is, therefore, a maximum and the optimum laser output transmission, T_{op}, is

$$T_{op} = 2 (\sqrt{g_o \alpha_o} - \alpha_o) \tag{57}$$

1.   W. W. Rigrod, "Gain Saturation and Output Power of Optical Masers",
        J. Appl. Phys. 34, 2602, Sept. 1963.

2.   W. Elinbaas, "The High Pressure Mercury Vapor Discharge", Interscience
        Publishers Inc., New York, 1951, pp. 18-31.